2016-11-01

A CryAB Interactome Reveals Clientele Specificity and Dysfunction of Mutants Associated with Human Disease

Whitney Katherine Hoopes
Brigham Young University

A CryAB Interactome Reveals Clientele Specificity and Dysfunction of Mutants Associated with Human Disease

Whitney Katherine Hoopes

A thesis submitted to the faculty of
Brigham Young University
in partial fulfillment of the requirements for the degree of

Master of Science

Julianne House Grose, Chair
Kelly Scott Weber
John Sai Keong Kauwe

Department of Microbiology and Molecular Biology

Brigham Young University

ABSTRACT

A CryAB Interactome Reveals Clientele Specificity
and Dysfunction of Mutants Associated
with Human Disease

Whitney Katherine Hoopes
Department of Microbiology and Molecular Biology, BYU
Master of Science

Small Heat Shock Proteins (sHSP) are critical molecular chaperones that function to maintain protein homeostasis (proteostasis) and prevent the aggregation of other proteins during cellular stress. Any disruption in the process of proteostasis can lead to prevalent diseases ranging from cancer and cataract to cardiovascular and Alzheimer's disease. CryAB (αB-crystallin, HspB5) is one of ten known human sHSP that is abundant in the lens, skeletal, and cardiac muscle. This protein is required for cardiac function and muscle cell integrity. When the cell experiences physiological stress, including heat shock, CryAB moves to the cytoskeleton to act as a chaperone and prevent aggregation of its protein clientele. This research is designed to investigate the molecular role of CryAB in cell proteostasis through the identification of putative protein clientele and chaperone activity analysis. We have identified over twenty CryAB-binding partners through combined yeast two-hybrid (Y2H) and co-purification approaches, including interactions with myofibril proteins. Previously reported disease-associated CryAB missense variants were analyzed in comparison to wild type CryAB through Y2H binding assays. The characterization of the similarities and differences in binding specificities of these variants provide a foundation to better understand the chaperone pathways of CryAB and how these changes in molecular function result in the development of disparate diseases such as cataract, cancer, and various myopathies.

Keywords: small Heat Shock Proteins (sHSP), HspB5 (αB-crystallin, CryAB), molecular chaperones, proteostasis, R120G, HspB2

TABLE OF CONTENTS

LIST OF TABLES

LIST OF FIGURES

SPECIFIC AIMS

CryAB (αB-crystallin, HspB5) is a small Heat Shock Protein (sHSP) expressed in various tissues and is critical in maintaining cellular homeostasis. CryAB is one of ten human sHSP that respond to cellular stress (e.g. heat, cold, oxidative, reductive, etc.) These chaperones function as anti-apoptotic proteins and help protect the cell from accumulating protein aggregates. Altered proteostasis is a critical event in the development of neurodegenerative, cardiac, and other various myopathy diseases resulting in the formation of protein aggregates. R120G-CryAB is a highly studied variant that has been shown to be a direct cause of protein misfolding and the growing accumulation of cytoplasmic aggregates that can lead to the development of cardiomyopathy. These aggregates propagate the enlargement of the heart, resulting in physiological changes including preventing efficient heart contraction and the inability to adequately deliver oxygen throughout the cardiovascular system. A key to understanding this disease is to elucidate the mechanisms of protein misfolding within cardiomyocytes. These studies examine the basic pathways involved in proteostasis and provide a foundation to further understand the molecular pathophysiology of cardiomyopathy and other associated diseases.

In addition to its expression in cardiomyocytes, the CryAB protein is also a primary cause of cataract, breast cancer, other myopathies, and Alzheimer's disease. Studies that investigate the molecular role of CryAB suggest that this protein functions as a diverse chaperone to suppress the formation of cytoplasmic aggregates of particular protein clientele. Although studies have shown this protein to be multifunctional, little is known why various mutations in CryAB cause such disparate disease states.

We hypothesized that CryAB will interact with a diverse variety of human proteins, including myofibril and regulatory proteins. CryAB has been shown to localize to the cytoplasm, and upon exposure to stress conditions, translocate to the cytoskeleton. Our preliminary data indicated that wild type CryAB and R120G-CryAB chaperones have altered protein-binding clientele, demonstrating a compromised cardiac protein maintenance environment in the presence of the missense R120G mutation. These findings suggest that studying the binding clientele of the various reported CryAB mutants could help explain their functional differences and molecular dysfunction.

Specific Aim I: Identify novel protein clientele of CryAB through yeast two-hybrid screening.

Specific Aim II: Contrast the binding affinities of CryAB including wild type, truncations, and reported disease-causing variants using yeast-two hybrid approaches.

CHAPTER ONE: CryAB Molecular Chaperone Activity

INTRODUCTION

Protein homeostasis, termed "proteostasis" is a critical process to maintain optimal cellular health conditions. The pathways of proteostasis require molecular chaperones to help maintain the central dogma in regulating protein synthesis, protein folding, and protecting cells from the accumulation of misfolded protein aggregates both under normal and stressed conditions [1-2]. When cells are subjected to various forms of physiological stress (e.g. heat shock, ischemia, exercise, etc.), these molecular chaperones are critical to help the cell maintain proteostasis and maintain the clearance of unfolded proteins [3-4]. When cells experience such stress, many proteins begin to denature and form cytoplasmic aggregates. These physiological stress conditions elicit the role of small heat shock proteins, including CryAB (αB-crystallin, HspB5) to maintain proteostasis. This introduction will provide information regarding CryAB and highlight its diverse molecular role as a chaperone to maintain overall cellular and protein clientele health.

SMALL HEAT SHOCK PROTEINS

There are ten small Heat Shock Proteins (sHSP) that are expressed throughout the human body (HspB1-HspB10) that prevent the formation of denatured protein aggregates. These proteins share a highly conserved alpha-crystallin domain and range in size from 12-43 kDa [3, 5]. Many proteins require molecular chaperones to properly fold and require the aid of sHSP chaperones to help facilitate this process under homeostatic conditions. Some molecular chaperones are known to be constitutively expressed throughout the body while the expression of others are tissue restricted and

specifically induced during the exposure of physiological stress conditions. These sHSP act as the first line of defense and possess chaperone activity to bind to denatured protein clientele and prevent their aggregation, and function as anti-apoptotic proteins to protect the cell from accumulating misfolded protein aggregates [6]. These sHSP can either bind their specific clientele in an ATP-independent process, or transfer denatured proteins to larger ATP-dependent heat shock proteins to either recover or degrade the protein clientele [5]. To aid in this process, these chaperones have the ability to form both homo- and heteromeric structures with other sHSP monomers. The formations of these complexes allow specific substrate binding, and are regulated by various events including phosphorylation and hydrophobic associations [7-9]. Interestingly, the protective role of these molecular chaperones is only elicited by specific interactions with particular protein-protein interactions. Studies suggest that the oligomers of sHSP contain multiple substrate binding sites, and therefore, multiple sHSP specific clientele [10].

THE ALPHA-BETA CRYSTALLIN PROTEIN CRYAB

Protein Features and Expression

CryAB is ubiquitously expressed throughout the body and due to this characteristic, remains of clinical importance. CryAB is a 175 amino acid protein with a molecular mass of ~20,159 Da. It is located on human chromosome 11 and uniquely shares an intergenic promoter with a closely related sHSP, Heat Shock Protein Beta 2 (HspB2), suggesting they share physiological, structural, and regulatory elements [11]. The close proximity of CryAB and HspB2 has interfered with the independent characterization of these chaperones. These two genes are oriented in a head-to-head position and are only 958 base pairs apart from transcriptional start sites. Although

CryAB and HspB2 share common regulatory elements, the varying levels of expression within tissues suggest they have unique and separate roles. CryAB expression has been shown to be induced following heat shock, while HspB2 expression remains unaffected by this physiological stress [12].

In the process of characterizing these individual chaperone functions, CryAB knock-out (KO) mice unintentionally removed regulatory elements that were also required for HspB2 expression, an inadvertent result of their close proximity. Double KO mice of both CryAB and HspB2 were characterized by lower cardiac respiration rates, lower ATP, and reduced glutathione levels (a compromised ability to reduce reactive oxygen species (ROS)) compared to wild type mice [11]. The absence of either sHSP results in vulnerability of cardiomyocytes to incur severe damage post-ischemia. To better characterize the specific and unique cardioprotective role of CryAB, the CryAB gene was transgenically expressed in the double KO mice. The protection of cardiac diastolic contractile performance was dependent on the expression of CryAB. HspB2 contributed to the quality of recovery for systolic performance and cardiac energetics, including ATP recovery [11]. In addition, the unique roles of CryAB and HspB2 were evaluated through comparing and contrasting their cellular binding partners. Identification of the HspB2 interactome revealed a role for this chaperone in mitochondrial function [13].

CryAB is constitutively expressed throughout the body but has been predominantly known as a structural protein of the lens. This protein is also highly expressed in tissues with high oxidative capacity including both cardiac and skeletal muscles [14]. The highest levels of CryAB expression in non-ocular tissue occurs in the heart, where it can consist of 1-3% total soluble protein [15]. CryAB was first found to harbor chaperone activity in its ability to suppress the thermally induced aggregation of

several enzymes [16]. Specifically within cardiomyocytes, this sHSP functions to protect cytoskeletal organization and intermediate filament assembly [11, 17]. Heat shock can increase the expression of CryAB and promote interactions with its protein clientele to prevent the formation of stress-induced protein aggregation. This sHSP has the capability to assemble into large oligomers and form multimeric cytosolic complexes with other sHSP to prevent protein denaturation [18]. The overexpression of CryAB in mouse hearts, demonstrated the cytoprotective role of this sHSP protecting cardiomyocytes from ischemic damage [19]. CryAB is a very critical protein in a variety of tissues, given that several reported mutations have shown diminished chaperone activity, and therefore, result in pathophysiological development.

Molecular Properties

CryAB expression has been previously localized to the I-bands of myofibrils, supporting a role of muscle maintenance and stress tolerance [20]. Due to the highly soluble properties of CryAB, this chaperone remains within the cytosol. Physiological stressors including heat and ischemia will induce its translocation to the I-band to facilitate specific interactions with other proteins including actin, desmin and titin [21]. Several heat shock proteins have been reported to interact directly with proteins involved in apoptosis pathways and interfere with the activation of programmed cell death function [22]. CryAB has been characterized as an anti-apoptotic protein as it functions to inhibit initiation of apoptotic pathways. Studies have shown this protein to inhibit the activation of both the mitochondrial and death receptor pathways. Interestingly, both of these pathways involve the activation of procaspase-3, suggesting this chaperone negatively regulates the activation of downstream pathways through the inhibition of caspase-3 [23].

THE R120G-CRYAB VARIANT

It is important to understand the molecular roles of CryAB in maintaining cellular health and to characterize the mechanisms of action that are affected in reported CryAB alleles. The exploration of these pathways provides insight to the development of associated diseases. R120G-CryAB, a highly studied variant of the CryAB protein, has been shown to induce the development of a life-threatening disease, protein aggregation cardiomyopathy, in both humans and mice [20, 24-25]. This pathophysiology is characterized by the upregulation and accumulation of R120G-CryAB protein. The R120G-CryAB mutant was first identified as a mutation inherited in desmin-related myopathies. The R120G mutation is an autosomal dominant mutation that results in the amino acid change from A → G in CRYAB, a residue that is highly conserved and required for functional protein structure [20].

Several studies have shown that CryAB variants, including R120G-CryAB, acquire altered chaperone activity and protein function [26-28]. Using real-time spectroscopy, the ability of R120G-CryAB to stabilize alpha-lactalbumin was significantly compromised compared to wild type CryAB, supporting a compromised chaperone activity [29]. The cardiomyopathy that results from this missense mutation is due to a toxic gain-of-function property and is dependent on the overexpression and altered metabolism of glucose-6-phosphate dehydrogenase (G6PD). Analysis of R120G cardiac tissue revealed protein aggregate formation and the upregulation of G6PD, a key supplier of NADPH [30]. This upregulation of G6PD is novel to the development of desmin-related cardiomyopathy, but the precise molecular pathway remains to be discovered. These changes result in the development of protein aggregates, including CryAB and protein clientele, and altered redox stasis of cardiomyocytes. Interestingly,

the protein aggregation formation has been shown to be reversible when R120G expression is suppressed [30]. The characterization of CryAB and its role to maintain structure and reductive homeostasis is necessary to further understand how this missense mutation interferes with proteostasis.

Several human diseases are characterized by the increased expression of this mutant chaperone. The specific mechanisms in which this mutant protein contributes to disease remain to be elucidated. Depending on the location of the mutation, different variants of CryAB result in different pathologies. Interestingly, HspB1 co-aggregated with R120G-CryAB in the hearts of myopathic mice. The knockdown of HspB1 resulted in an increase in protein aggregation of several CryAB mutants, including R120G, 450delA, and 464delCT mutants, suggesting a cytoprotective role of HspB1 in preventing the accumulation of CryAB protein aggregates [31]. The R120G-CryAB variant has been shown to be a direct cause of both cataract and cardiomyopathy, however most other variants of the CryAB protein result in only one phenotype, either cardiomyopathy or cataract. Each CryAB variant harbors a different mechanism in which it elicits a specific pathophysiology. R120G-CryAB remains the most extensively studied variant of CryAB so far, both in protein structure and mechanism of action. This compromised chaperone activity results in aggregate formation of mutant CryAB and other clientele proteins including desmin [25].

Phenotypes Associated with R120G-CryAB

Oxidative stress is characteristic to many cardiac diseases including a decrease in GSH (reduced Glutathione) to GSSG (oxidized Glutathione) ratio. Reductive stress (an increased GSH to GSSG ratio) may also have negative implications when it comes to cardiac disease and chaperone function. The overexpression of R120G-CryAB results in

cardiac hypertrophy, heart failure and ultimately early onset of death. Several transgenic mouse lines were created to determine if the R120G-CryAB mutant was a direct cause of desmin-related myopathy (DRM). In comparison to wild type CryAB, R120G-CryAB directly led to aberrant CryAB and desmin protein aggregates, compromising overall cardiac muscle function [25]. Transgenic mice that harbor the R120G-CryAB mutation had an increase in the reduced form of GSH and interestingly an increase in Hsp25 expression, a redox-dependent heat shock protein [30]. This study also found increased levels of glucose-6-phosphate dehydrogenase (G6PD), glutathione reductase, peroxidase, and catalase in a dose-dependent manner with R120G-CryAB expression [30, 32]. Increased molecular interactions between CryAB, Hsp25, and G6PD with heart specific R120G-CryAB expression were also noted. When G6PD-deficient mice were crossed with R120G-CryAB transgenic mice, no chaperone dysfunction or consequences occurred, thus providing evidence that the reductive stress was a direct mechanism of action for R120G-CryAB induced cardiomyopathy [30].

Desmin-related cardiomyopathy is characterized by the formation of intracellular aggregates containing both CryAB and desmin. Studies have shown that this mutation results in a dysfunction of cardiac chaperone activity resulting in altered contractile capabilities and disrupted mitochondrial function [33]. Ultimately this can lead to an increase in apoptotic activity and overall heart failure. Wild type CryAB functions to maintain cytoskeletal integrity and protect protein clientele by binding unfolded proteins and preventing their denaturation and aggregation. A key aspect to understand these pathophysiologies is to understand the clientele and pathways that are affected by R120G-CryAB altered chaperone activity.

OTHER DISEASE-ASSOCIATED ALLELES

Several reports of CryAB mutants have been linked to a variety of human diseases. These include both skeletal and cardiac myofibrillar myopathies, and cataract. R120G-CryAB mutant knock-in mice develop cardiomyopathy and cataract similar to that of humans, defined by the characteristic accumulation of CryAB-desmin aggregates within the lens and muscle cells [30]. Several other missense CryAB mutants were identified including R11H, P20S, R56W, D109H, D140N, G154S, R157H, and A171T [34-41]. All of these mutations have been reported to contribute to the development of cataract and/or cardiomyopathy. The anti-apoptotic characteristic of CryAB remains of high interest in the study of several forms of cancer (e.g. ovarian, breast, etc.) [42-44]. An increase in apoptotic activity has been reported for the R120G, D109H, and A171T mutants [33, 45]. This data suggest that these mutations disrupt the anti-apoptotic function of wild type CryAB.

In support of HspB1 function to suppress the formation of protein aggregates resulting from the R120G variant, another study provided supporting evidence that the overexpression of HspB1 inhibits the protein aggregation that results as a consequence of mutated CryAB protein [45]. The mechanisms in which these mutations alter chaperone activity and protein clientele remains to be elucidated. R157H-CryAB is a missense mutation found in inheritable Dilated Cardiomyopathy (DCM). This mutation affects a highly conserved amino acid within the alpha-crystallin family. The resulting mutation did not affect the cellular distribution of crystallin protein but resulted in a decreased binding affinity to the titin-connectin heart-specific N2B domain [40]. The R157H-CryAB variant is better characterized as a loss-of-function mutation in contrast to the gain-of-function associated with R120G-CryAB.

CONCLUSION

The cell can experience many physiological stressors that range from myocardial ischemia to heat shock. The cell responds to stress and initiates critical downstream pathways to protect protein structure and function. Molecular chaperones, including sHSP, are key players in these protective processes. The proper protein folding processes of many cellular proteins require the function of molecular chaperones, and their ability to promote protein degradation following a physiological stress. During basal conditions, these molecular chaperones behave in a cytoprotective manner, however heterogeneous dominant gene mutations can compromise normal chaperone activity and produce subsequent pathophysiologies.

The results of these aims will provide direct insight to the molecular mechanisms of CryAB and its chaperone activity of protein interactors. These studies will increase our knowledge of sHSP function and how disease-causing alleles result in the dysfunction of their chaperone activity and protein clientele that can ultimately, lead to the disruption of proteostasis.

CHAPTER TWO: A CryAB Interactome Reveals Clientele Specificity and Dysfunction of Mutants Associated with Human Disease

Whitney Hoopes[1], Nick Nielson[1], Rachel Farnsworth[1], Kent Jarvis[1], John Kauwe[2], Ivor J. Benjamin[3], and Julianne H. Grose[1]

[1]Microbiology and Molecular Biology Department, Brigham Young University, Provo, UT, [2]Biology Department, Brigham Young University, Provo, UT, [3]Division of Cardiovascular Medicine and Cardiovascular Center, Froedtert and Medical College of Wisconsin, Milwaukee, WI

ABSTRACT

Small Heat Shock Proteins (sHSP) are molecular chaperones critical in maintaining proper protein synthesis, function and degradation within cells. The sHSP CryAB (αB-crystallin, HspB5) has been implicated as an antioxidant protein essential to maintain proper cytoskeletal organization and myofibril function. More than nine autosomal dominant and recessive human mutations in CryAB have been associated with various human diseases including cardiomyopathy and cataract. Despite the clear importance of CryAB function, the precise molecular pathways and protein clientele are poorly understood, with few characterized clientele (e.g. BAG family molecular chaperone regulator 3 and several myofibril proteins including titin, actin, and desmin). Herein, we provide the first large-scale protein interactome for human CryAB identified through both yeast two-hybrid (Y2H) and co-purification studies, and report the identification of several putative myofibril clientele as well as putative clientele involved in central metabolism. The CryAB interactome is compared with the recently published interactome of the ohnologous chaperone HspB2, with little (33%) overlap, suggesting some differences in chaperone function for these sHSP. In addition to the wild type CryAB interactome, Y2H screens were performed for several disease-causing variants, allowing comparison of binding partners to identify changes in molecular function associated with several of the reported missense mutations. This study helps provide a basis for further work in understanding the novel molecular functions of CryAB through the identification of putative *in vivo* clientele. In addition, it provides methods for analyzing the chaperone dysfunction of CryAB variants to help elucidate the molecular mechanisms for prevalent diseases.

INTRODUCTION

Heat Shock Proteins (HSP) are ATP-independent molecular chaperones that help proteins retain their functional structure, deliver misfolded proteins for degradation, and prevent partially unfolded proteins from forming cytoplasmic aggregates [1-2]. They are conserved in all cellular organisms where they function in a variety of essential processes including cell cycle control, apoptosis, autophagy, myogenesis, and muscle structure maintenance [3-6]. The principal Heat Shock Proteins are divided into subgroups based on their molecular mass and function. There are ten known Small Heat Shock Proteins (sHSP) encoded in the human genome that are defined by their size (15-30 kDa) and the presence of a highly conserved, C-terminal alpha-crystallin domain [7-8]. Although they have variable expression patterns, they are thought to share overlapping roles including protein clientele.

CryAB (αB-crystallin, HspB5) is a sHSP that was first known for its structural role as a lens crystallin and has since been shown to function in cytoskeletal maintenance, apoptosis, cell cycle regulation, intracellular protein transport, stress and hormone signaling, Golgi architecture, and immune response (for a recent review see [9]). CryAB is ubiquitously expressed throughout the human body with the highest expression in mammalian tissues that are characterized by increased rates of oxidative metabolism including the heart, skeletal muscle, kidney, brain, and ocular lens [7, 10]. Specifically within cardiomyocytes, CryAB plays a cytoprotective role in maintaining cytoskeleton remodeling and diastolic contractile performance including cellular redox state [4, 10]. This role in muscle maintenance is supported by the functional interaction of CryAB with desmin intermediate filaments [5, 11]. Fitting with its expression

patterns, several human CryAB alleles have been reported that cause a variety of protein aggregation diseases including cardiomyopathy and cataract [12-20].

More than nine autosomal dominant and recessive mutations in the CryAB coding region have been linked to human disease including five that cause cataract disease, two that cause myofibrillar myopathies, and two variants that result in both pathophysiologies (see Table 2.4.) [12-20]. Although these CryAB variants have been reported, the molecular basis for these missense mutations causing a wide variety of disparate diseases remains to be discovered. The R120G-CryAB variant, named for the single missense amino acid substitution (Arginine to Glycine at codon 120), is the best-studied variant and is known to cause inheritable protein aggregation cardiomyopathy through the initiation of oxido-reductive stress [21]. This R120G-induced cardiomyopathy is due to an increase in glutathione recycling, an overexpression of glucose-6-phosphate dehydrogenase (G6PD), a key supplier of NADPH, and a related increase in reduced glutathione [21]. Accordingly, the repression of G6PD overexpression rescues R120G-mutant mice from the development of this phenotype as well as the subsequent reductive stress [21]. In support of this antioxidant role, the R120G mutation enhances the phosphorylation of CryAB during oxidative conditions, which under homeostatic conditions has been shown to stimulate the translocation of CryAB to myofibrillar Z-discs to maintain muscle structure and function following heat shock [9, 11]. The R120G mutant protein also displays greater binding affinity for desmin and is found in aggresomes that contain both misfolded desmin [22] and a toxic amyloid oligomer, linking cardiomyopathy-associated chaperone dysfunction to a variety of neurodegenerative phenotypes including Alzheimer's disease [23].

Despite its clear importance, the precise molecular pathways of CryAB function in the heart and skeletal muscle are poorly understood. Only a handful of protein

substrates have been characterized for CryAB, including BAG family molecular chaperone regulator 3 (BAG3), F-actin, titin and desmin [22, 29]. Herein, we provide the first large-scale protein interactome for CryAB identified through both yeast two-hybrid (Y2H) screens and co-purification methods and report the identification of twenty-four binding partners in total, including several myofibril clientele. The CryAB interactome also provides support for non-redundant sHSP clientele as it is compared to the recently reported HspB2 interactome [24], in that only a subset of the proteins in the smaller CryAB interactome overlap with the HspB2 interactome or interact with both CryAB and HspB2 when directly tested in the Y2H system. In addition to understanding wild type CryAB function, this interactome provides a basis for identifying the dysfunction of reported disease alleles, and was used to test the function of eight other variants, with several displaying altered binding specificity (either gain- or loss-of-function). Thus, this study not only establishes a basis for identifying the overlapping yet unique roles of the ten human sHSP, but also allows for the further characterization of CryAB disease-causing alleles, including R120G-CryAB.

MATERIALS AND METHODS

Plasmids, Primers, and Allele Construction

A list of plasmids and primers are provided in Supplementary Table 2.1. & 2.2. Wild type CryAB was cloned into the Y2H bait plasmid pGBKT7 (Clontech) using primers JG2609 and JG2461 and standard polymerase chain reaction (PCR)-based cloning methods. The resulting plasmid of wild type CryAB (pJG736) was used as the parent plasmid for all subsequent mutant allele and truncation construction. Mutant alleles were made using Strategene's QuikChange Lightning Site-directed Mutagenesis Kit (Agilent Technologies, Santa Clara, CA) and method, with primers outlined in Supplementary Table 2.2. All plasmids were sequenced (BYU DNA Sequencing Center) to verify correct truncation and/or base pair change. CryAB truncations and alleles were cloned into Clontech's prey (pGADT7) plasmid using standard cloning techniques. All restriction enzymes were purchased from New England BioLabs (NEB, Ipswich, MA).

Y2H Screens

Protein clientele for the wild type and R120G-CryAB chaperones were identified using the Y2H Matchmaker Gold protocol (Clontech). The Y2H Gold yeast strain (Clontech) expressing R120G-CryAB (pJG581) was mated with yeast expressing either the Human ORFome cDNA library (Clontech) or Human Cardiac cDNA library (Clontech). Yeast colonies that grew on the Y2H selection plates (SD-Trp-Leu-His-Ade) were patched to confirm their phenotype and subjected to colony PCR (using oligos JG2761 and JG2762) and verified through DNA sequencing (BYU DNA Sequencing Center) for identification of the library plasmid insert. In total for the R120G Y2H screens, over 130 million matings were performed with a total of approximately 1,500

transformations. Sequences were reported for e-values greater than e^{-50}. Y2H screens were performed with the Human Cardiac cDNA library (Clontech) for CryAB variants outlined in Table 2.4. as previously outlined for R120G-CryAB. To verify positive protein-protein interactions, the library plasmids were purified from yeast and re-transformed into naïve yeast (Y2H Gold, Clontech) harboring R120G-CryAB (pJG581), wild type CryAB (pJG736) or the empty vector bait plasmids (pJG485, pGBKT7, Clontech). The resulting yeast colonies were selected on SD-Trp-Leu plates, and streaked onto SD-Trp-Leu-His-Ade to determine reporter gene expression dependency with either R120G-CryAB or wild type CryAB. Dependency tests were performed in triplicate.

Y2H Allele Interactions and Growth Assays

Both CryAB truncations and missense variants expressed in the Y2H bait pGBKT7 vector were co-transformed into Y2H Gold yeast cells with either ALDOA (pJG774) or PGM1 (pJG1159), protein clientele identified from the R120G-CryAB Y2H screen. The resulting yeast colonies were selected on SD-Trp-Leu plates and streaked onto SD-Trp-Leu-His-Ade to determine interaction strength in comparison to wild type, R120G-CryAB, and empty vector bait plasmids. For Y2H growth assays, saturated overnights were grown in SD-Trp-Leu media for 48 hours at 30°C to select for bait and prey plasmids, followed by a 1:5 serial dilution in water and spotted onto medium lacking the appropriate amino acids (SD-Trp-Leu-His-Ade) Y2H interaction selection plates, as well as SD-Trp-Leu control plates to ensure plasmid selection and equal dilution. Plates were incubated at 30°C for 2-3 days until colonies were apparent. Growth assays were performed in triplicate.

Mammalian Heat Shock and Mass Spectrometry

C2C12 mouse myoblast cells were cultured in Dulbecco's modified Eagle's medium (DMEM) and supplemented with 10% fetal bovine serum (GE Healthcare Life Sciences). C2C12 cells were plated at 150,000 cells per well and transfected with 1.5 μg plasmid DNA, 3.5 μl LTX-plus reagent and 5 μl lipofectamine (Invitrogen Life Technologies) according to standard cell transfection protocol. Transfected plasmids expressed human CryAB fused to Myc peptide (pJG483) [25] or empty plasmid pCMV-Myc vector (pJG906, Clontech). C2C12 myoblast cells were heat shocked 48 hours post-transfection at 45°C for 30 minutes, followed by a 4 hour recovery at 37°C. The cells were resuspended and lysed in 300 μl mammalian lysis buffer (20 mM HEPES pH 7.8, 10 mM KCl, 100mM NaCl, 1mM EDTA, 1mM EGTA, 1% NP-40, 10% Glycerol, 1mM DTT, mammalian PICs) and homogenized on ice. The cell lysates were centrifuged for 5 minutes at 13,000 rpm. Both the supernate and pellet were analyzed on 12% SDS-PAGE and proteins transferred to nitrocellulose blot paper. Myc-tagged CryAB co-purification samples were prepared for mass spectrometry (MS). MS analysis was performed in duplicate. Heat shock assays were analyzed on 12% SDS-PAGE, transferred to nitrocellulose paper, and visualized with appropriate antibodies including anti-ALDOA (Proteintech Group) and anti-beta Tubulin (Cell Signaling Technologies).

RESULTS

Selection of CryAB Constructs for Yeast Two-Hybrid Screening

To test the functionality of wild type CryAB in yeast prior to large scale screening, we constructed various CryAB truncations designed to strengthen or weaken self-oligomerization based on the findings of Laganowsky et al. [8]. This study reported the CryAB truncation (aa 68-162) to maintain chaperone activity for target proteins, while the further truncation of CryAB (aa 68-157) resulted in a loss of chaperone function [8]. As predicted, the C-terminal truncation from amino acid 164 on strengthened self-oligomerization as this domain is known to contribute to chaperone function and oligomerization, while the larger C-terminal truncation from amino acid 160 on weakened it (Figure 2.1. and Table 2.1.). These results suggest that CryAB folds in a similar manner in yeast cells and can function and self-oligomerize as predicted.

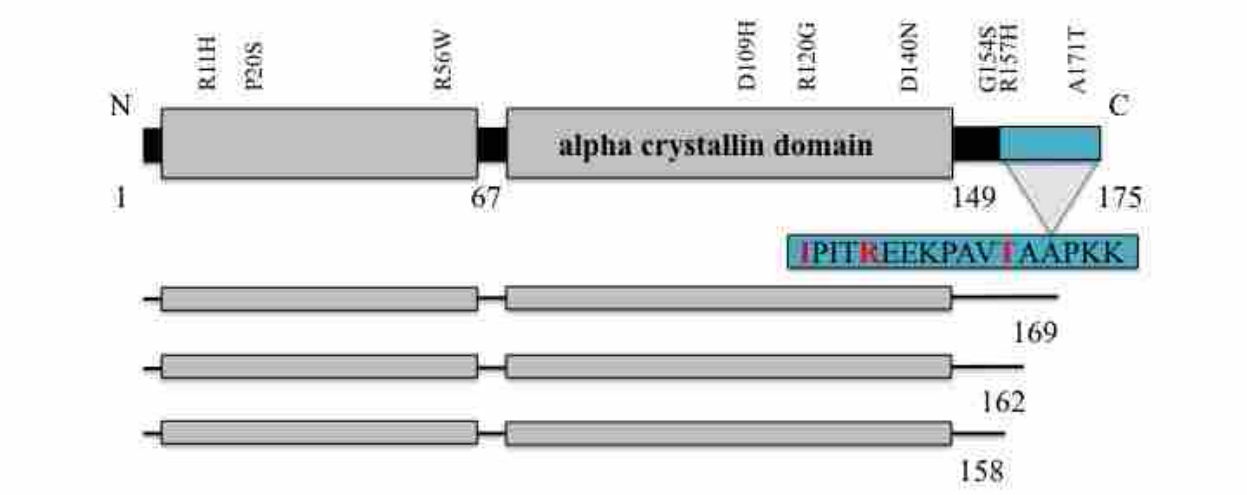

Figure 2.1.

A diagram of CryAB alleles and truncations analyzed in this study to evaluate their ability to maintain self-oligomerization and chaperone activity. Each truncation is represented, with the terminal amino acid of that truncation highlighted in red.

Table 2.1.

Behavior of full-length and truncated CryAB and R120G-CryAB in the yeast two-hybrid system suggests the constructs of CryAB function similarly to the native protein when using *S. cerevisiae* as a model organism. Yeast two-hybrid interactions of various CryAB truncations were assayed for self-oligomerization. Y2H Gold cells (Clontech) containing either empty vector, full-length, or truncated forms of CryAB and R120G-CryAB proteins in both bait and prey plasmid backbones were co-transformed and streaked onto Y2H selective media (SD-Trp-Leu-His-Ade) to determine interaction strength. Plates were incubated at 30°C for 3-4 days until growth was apparent. Growth was scored as weak, moderate, or strong according to colony size.

CryAB Construct	pJG#s	Self-Oligomerization Strength
Full-length WT CryAB	736/576	Moderate
CryAB aa1-169	577/578	Weak
CryAB aa1-162	1554/1555	Moderate
CryAB aa1-158	580/583	No Growth
Full-length R120G-CryAB	581/1292	Moderate
R120G-CryAB aa1-169	587/588	Moderate/Strong
R120G-CryAB aa1-162	589/590	No Growth
R120G-CryAB aa1-158	584/582	No Growth

Y2H Screen with CryAB Reveals Expanded Binding Partners for the R120G Variant

The molecular mechanisms of CryAB were explored through the identification of CryAB clientele in yeast. The initial Y2H screens for CryAB binding partners were performed with the full-length, wild type CryAB bait (pJG736) and the Clontech Human Heart cDNA library as prey. However, these screens yielded extremely low mating rates and efficiencies, making it difficult to identify clientele. Alternatively, when the R120G-CryAB variant was used as bait (pJG581), yeast mating was restored and an approximate 1,500 putative interactions were retrieved from over 130 million matings total with two, independent Y2H libraries. The Human Heart cDNA library (Clontech) and Human ORFome cDNA library (Clontech) were each used to screen for putative binding partners. A majority (>90%) of the resulting interactions yielded CryAB encoded in the prey plasmid as determined by colony PCR with CryAB-specific forward and prey plasmid-specific reverse primers (JG2461 and JG2762 respectively).

Colonies with prey plasmids not encoding CryAB were sequenced, purified from yeast, and amplified using *E. coli*. In order to verify R120G-CryAB protein dependency as well as to test its interaction with wild type CryAB, each putative binding partner was reintroduced into naïve yeast containing the Y2H empty vector (pJG485), wild type CryAB (pJG736), or the R120G-CryAB (pJG581) bait plasmids. The resulting transformants were streaked onto yeast two-hybrid selective media (SD-Trp-Leu-His-Ade) to determine the presence of a protein-protein interaction (see Figure 2.2.). The eighteen prey plasmids identified from both Y2H libraries in total, that were also verified to be CryAB or R120G-CryAB dependent are provided in Table 2.2.

The yeast two-hybrid identified unique clientele for R120G-CryAB, including proteins involved in a variety of cellular processes. A majority of the proteins (~39 %) localize to the cytoskeleton, consistent with the reported localization of CryAB (see

Table 2.2. and Figure 2.3.). Several of the protein clientele (~33%) are known to be involved in muscle structure and regulation, which is consistent with the muscle maintenance role previously reported for CryAB [10]. In addition to myofibril putative clientele, we identified several binding partners involved in central metabolic processes (~17%), including the Fructose-Bisphosphate Aldolase A (ALDOA, pJG774) and Phosphoglucomutase 1 (PGM1, pG1159).

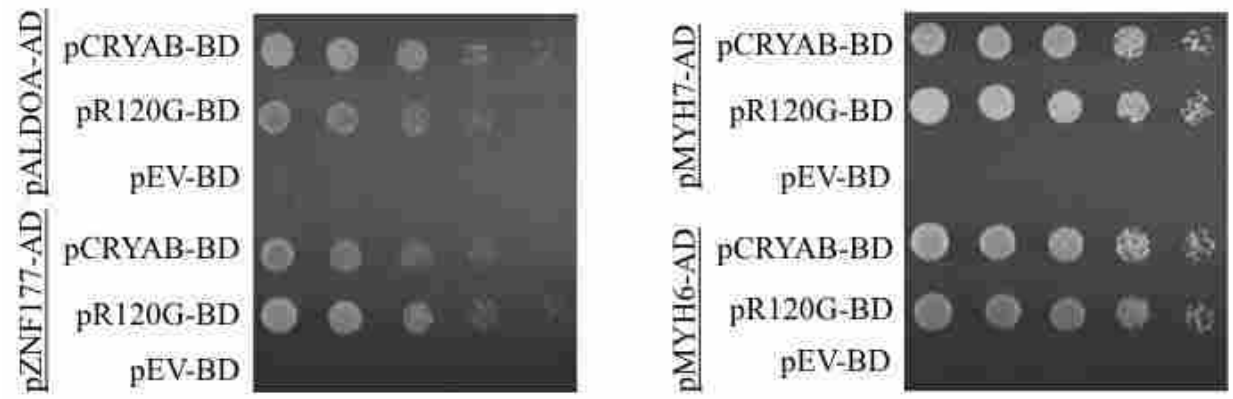

Figure 2.2.

Comparison of CryAB and R120G-CryAB reveal unique and expanded binding partners for R120G. Provided are examples of differential clientele binding of the CryAB and R120G-CryAB proteins via yeast two-hybrid methods. Y2H Gold cells (Clontech) were co-transformed with bait plasmid (BD, pGBKT7, Clontech) and prey plasmids (AD, pGADT7, Clontech). Overnights were grown in SD-Trp-Leu for plasmid maintenance, diluted 5-fold serially, and plated on Y2H selective media (SD-Trp-Leu-His-Ade) including control plates (SD-Trp-Leu). Plates were incubated at 30°C for 2-3 days until colonies were apparent.

Table 2.2.

CryAB binding partners retrieved from yeast two-hybrids screens. R120G-CryAB was used as bait in yeast two-hybrid screens with two, different prey libraries including a Human Heart cDNA library (Clontech) and a Human ORFome cDNA library (Clontech). Proteins encoded by the plasmids retrieved from the Y2H screen are provided with protein name, UniProt accession #, gene symbol, cellular localization, and amino acid truncation found in the construct. Only putative clientele that were verified as positive Y2H interactions are listed. Gene symbols indicated with an asterisk are R120G-CryAB dependent only and do not interact with wild type CryAB in our assay.

Protein Name	Uniprot Accession	Gene Symbol	Cellular Localization	aa Construct
Myofibril or Cytoskeleton Structure/Regulation				
Microtubule-associated protein 1B	P46821	MAP1B	Cytoskeleton	2114 - 2343
Myomesin-1	P52179	MYOM1	Cytoskeleton	1020 - 1289
Myosin-6	P13533	MYH6	Cytoskeleton	1655 - 1855
Myosin-7	P12883	MYH7	Cytoskeleton	1701 - 1859
Titin	Q8WZ42	TTN	Cytoskeleton	20056 - 20305
Xin actin-binding repeat-containing protein 1	Q702N8	XIRP1	Cytoskeleton	1629 - 1844
Fermentation/Respiration				
Fructose-bisphosphate aldolase A	P04075	ALDOA	Cytoplasm	108 - 365
Cytochrome b	P00156	MT-CYB*	Mito IM	-1 - 263
Phosphoglucomutase 1	P36871	PGM1*	Cytoplasm	177 - 366
Signal Transduction				
Macrophage receptor MARCO	Q9UEW3	MARCO	PM	118 - 323
Roundabout homolog 2	Q9HCK4	ROBO2	PM	498 - 744
Gene/Protein Expression				
AT-rich interactive domain-containing protein 2	Q68CP9	ARID2	Nucleus	1351 - 1692
DDB1- and CUL4-associated factor 6	Q58WW2	DCAF6	Nucleus	422 - 627
Histone-lysine N-methyltransferase 2C	Q8NEZ4	KMT2C	Nucleus	2452 - 2790

Zinc finger protein 177	Q13360	ZNF177	Nucleus	76 - 425
Chaperone				
Alpha-crystallin B chain	P02511	CRYAB	Cytoskeleton	-3 - 175
Cell Repair				
Nibrin	O60934	NBN*	Nucleus	201 - 462
Intracellular Trafficking				
Golgi SNAP receptor complex member 1	O95249	GOSR1	Golgi	-4 - 251

*Abbreviations include Mitochondrial Inner Membrane (Mito IM) and Plasma Membrane (PM).

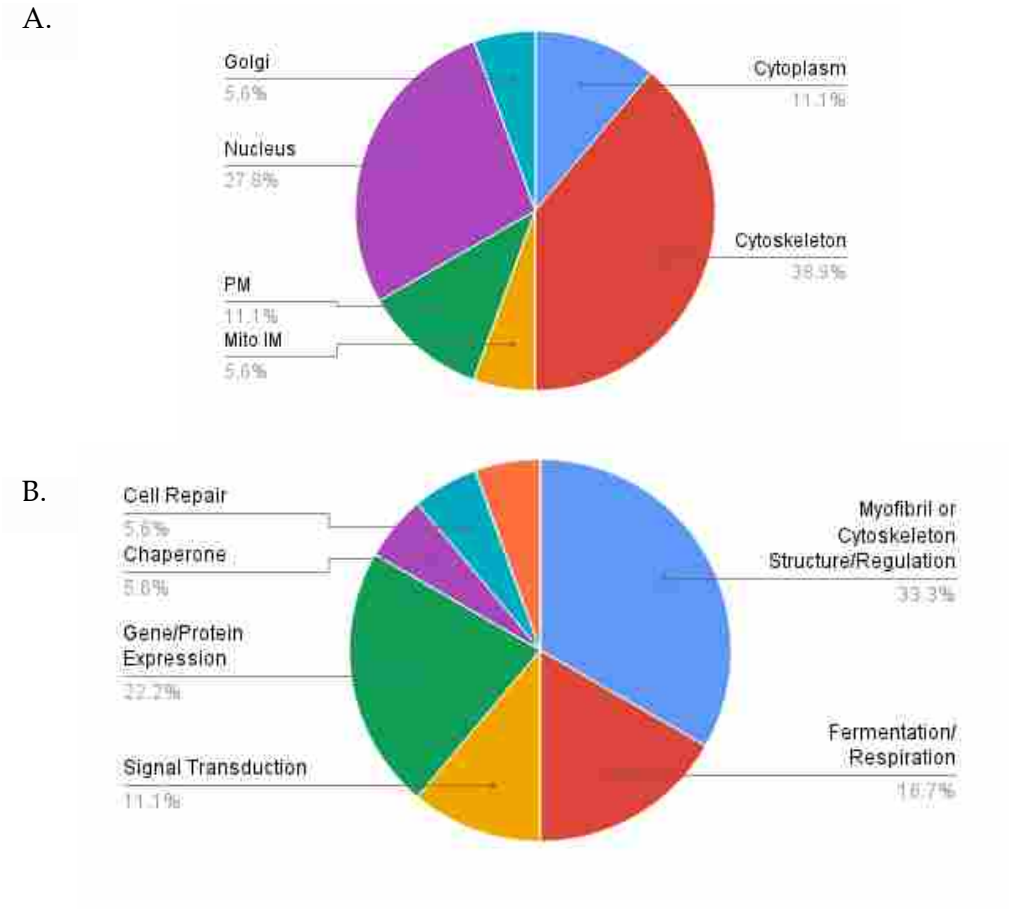

Figure 2.3.

Putative binding partners for CryAB revealed by Y2H confirm a role in myofibril maintenance and suggest roles in metabolism. A) A pie chart of the localization of putative R120G-CryAB binding partners. B) A pie chart of the reported functions for the putative R120G-CryAB binding partners.

There were several proteins isolated from the Y2H screens that were CryAB and R120G-CryAB dependent, but either out of frame or nonfunctional when verified by sequence analysis. We propose that CryAB and R120G-CryAB were able to interact with these clientele, despite being nonfunctional, due to a possibly altered protein structure as a result of being out of frame (see Supplementary Table 2.3.). Further analysis is required to explore these interactions and is outside the scope of this study.

As hypothesized from the wild type CryAB and R120G-CryAB Y2H screening results, we identified an expanded set of protein clientele for the R120G variant when compared to wild type CryAB. Of the eighteen putative protein clientele identified from the Y2H screens using R120G-CryAB as bait, three proteins were determined to be unique binding partners to this variant, consistent with the predicted gain-of-function associated with R120G [26] (see Table 2.2.), while other clientele revealed differences in binding affinity/strength interaction between the wild type and variant. These expanded clientele included Mitochondrially Encoded Cytochome B (MT-CYB), Phosphoglucomutase 1 (PGM1), and Nibrin (NBN), demonstrating specificity for R120G-CryAB, and possibly revealing critical proteins that aggregate with this variant and result in various human disease phenotypes. These results are consistent with previous hypotheses that due to a novel ability to bind a wider array of proteins, this variant possibly causes direct aggregation of otherwise partially functional proteins, disrupting proteostasis and ultimately resulting in disease including cataract and cardiomyopathy [21, 26-28].

The recently published HspB2 interactome [24] revealed the specificity in which HspB2 binds its targets by comparing interactions with CryAB and demonstrating unique clientele for each chaperone. For twelve binding partners isolated from the HspB2 Y2H screen, wild type CryAB only interacted with four HspB2 clientele (33%)

[24]. Of these four putative clientele, CryAB and ALDOA were both identified from the CryAB Y2H screens. Also, the comparison of localization for the putative protein clientele of both CryAB and HspB2 reveal interesting differences (see Figure 2.4.). For HspB2, 19% of putative protein clientele localized to the mitochondria, whereas only ~6% for CryAB clientele did. In addition, 7% of HspB2 clientele localized to the nucleus in comparison to ~28% for CryAB partners. These findings support a role of non-redundant function and specificity in sHSP protein interactions for both CryAB and HspB2.

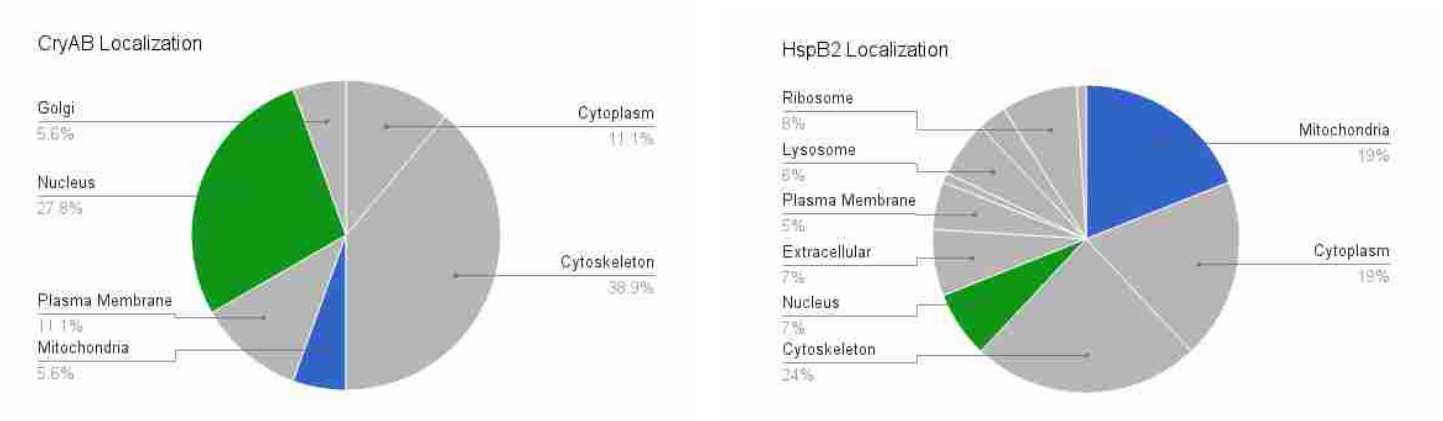

Figure 2.4.

Analysis of localization for putative protein clientele for both CryAB and HspB2 support a role of non-redundancy and specificity.

Co-purification Identifies Additional Putative Binding Partners

Co-purification of overexpressed CryAB in the undifferentiated mouse myoblasts cell line C2C12, followed by mass spectrometry (MS) of wild type CryAB (pJG483) [25] identified only six putative protein clientele (see Table 2.3.) Full-length CryAB fused to Myc was purified in triplicate and subjected to mass spectrometry. The six reported binding partners were identified only in the CryAB samples and not empty vector control. Interestingly, Eukaryotic translation elongation factor 1 alpha 1 (EEF1A1), identified from the wild type CryAB MS, was also determined to be a binding partner of HspB2 via Y2H [24]. However, we could not detect an interaction between EEF1A1 and CryAB in our Y2H assay. The association of CryAB with EEF1A1 may be through its binding to HspB2, as the advantage of co-purification is that it isolates large protein complexes

Despite the identification of six putative clientele through co-purification approaches, we obtained a much lower yield of protein interactions than we expected for the CryAB interactome. We propose that the pCMV-Myc construct of CryAB results in the expression of a partially functional protein. Previous use of this plasmid in other published studies have not directly explored the functionality or chaperone activity of CryAB in this construct. In support of this prediction, heat shock chaperone assays were designed to demonstrate the rescue function of CryAB. Using ALDOA as a substrate, a clientele identified from the Y2H interactome, no difference was observed between C2C12 cells overexpressing wild type CryAB (pJG483) in comparison to empty vector (pJG906). Due to the expression of a partially functional CryAB protein, there was no rescue of ALDOA from aggregating out into the pellet, following a thirty-minute heat shock (see Figure 2.5.). Troponin was used as a negative control, in which we predict no

protein-protein interaction, to demonstrate the inability of CryAB to interact and rescue this protein from aggregating into the pellet.

Table 2.3.

CryAB binding partners identified by co-purification and subsequent mass spectrometry. Myc-tagged full-length CryAB (pJG483) [25] was purified in triplicate and analyzed for protein-protein interactions by quantitative mass spectrometry. Associated proteins were analyzed in both CryAB (pJG483) and empty vector control (pJG906) independent samples. The reported proteins were present only in the wild type CryAB samples. Columns indicate the protein name, NCBI accession number, gene symbol, and number of times retrieved from a total of three samples (none were retrieved from all three).

Protein Name	NCBI Accession	Gene Symbol	# Hits
Hypothetical protein	149250554	N/A	2
Chromodomain helicase DNA binding protein 3	124358950	CHD3	1
Caseinolytic protease x isoform 1	113205071	CLPX	1
Eukaryotic translation elongation factor 1 alpha 1	126032329	EEF1A1	1
Eukaryotic translation elongation factor 1 alpha 2	6681273	EEF1A2	1
Annexin A11	7304885	ANXA11	2

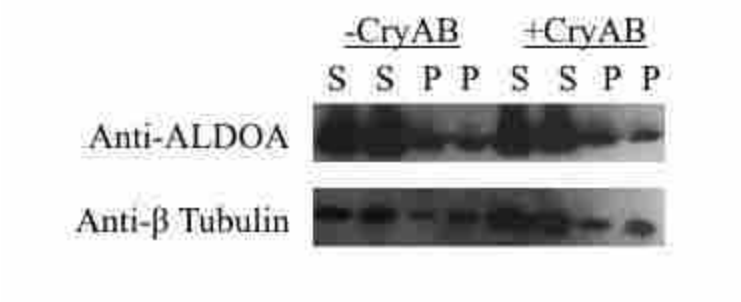

Figure 2.5.

Mammalian construct of CryAB results in a partially functional protein and fails to rescue the precipitation of identified putative clientele. Overexpression of CryAB fails to rescue ALDOA from denaturation in mammalian cells following a thirty-minute heat shock. Lysates were analyzed by 12% SDS-PAGE, transferred to nitrocellulose, and imaged with anti-ALDOA (Proteintech Group). Anti-beta Tubulin was used as a loading control (Cell Signaling Technologies).

Analysis of CryAB Mutants Reveals Altered Chaperone Function

As has been previously reported in the literature, mutations in the human CryAB gene result in distinct, yet disparate phenotypes for each variant including cataract, muscle, and heart myopathies. Only two variants, D109H and R120G, have been reported to cause multisystemic disease, which is characterized by multiple pathogenic phenotypes [15, 20]. Sacconi et al. used molecular modeling to demonstrate that the mutated amino acids of the D109H variant are involved in self-oligomerization, suggesting that the impairment of CryAB dimerization is important in its disease mechanism and may explain the differential phenotype of various mutants [15]. Mutations may also impair clientele binding as is reported by Inagaki et al. for both the R120G and R157H mutations [18]. In their study, mammalian-two-hybrid assays were performed by co-transfecting wild type CryAB, R120G and R157H with a plasmid

containing a specific titin cDNA domain known to associate with CryAB. Decreased binding was observed in cells expressing either mutant as indicated by a decrease in luciferase activity [18]. In support of this claim, the 68-162 amino acid truncation of R157H-CryAB by Laganowsky et al. demonstrated a loss of chaperone activity for target proteins, while the wild type form of this truncation maintained chaperone binding [8].

To test previously reported disease-associated mutations for alterations in self-oligomerization and/or clientele binding, the wild type CryAB bait plasmid pGBKT7 (Clontech) was mutated to produce nice of the reported variants as outlined in Table 2.4. To test for loss or maintenance of chaperone function, each plasmid construct was then further sub-cloned into the prey pGADT7 (Clontech) plasmid to test for oligomerization against itself, as well as one R120G-specific and one shared protein clientele (PGM1 and ALDOA, respectively).

Interestingly, both the R11H and D140N mutants interfered with self-oligomerization when tested via the yeast two-hybrid system, while none of the other mutants impaired self-oligomerization (see Table 2.5.). Several of the reported variants reside in the C-terminal extension that has been shown to house chaperone function, predicting they abolish chaperone function. Lie et al. characterized the D140N variant as a dominant negative sHSP through its loss of chaperone activity and reduced thermal stability, proposing this may be the direct cause of cataract [38]. Our results support the same loss of chaperone activity demonstrated by its inability to bind wild type CryAB clientele using the yeast two-hybrid system (see Table 2.7.).

Table 2.4.

Previously reported CryAB missense mutations and human disease phenotypes. Nine variants were identified from previously published studies for their role in the development of cardiomyopathy and cataract and chosen for further study herein. The mutant, amino acid change, base pair change, pathophysiological phenotype, and study reference are provided.

Mutant	aa Change	bp Change	Phenotypes	Study Reference
R11H	Arg →His	G → A	Cataract	Chen et al. 2009
P20S	Pro → Ser	C → T	Cataract	Liu et al. 2006
R56W	Arg → Trp	C → T	Cataract	Safieh et al. 2009
D109H	Asp → His	G → C	Cardiomyopathy & Cataract	Sacconi et al. 2011
R120G	Arg → Gly	A → G	Cardiomyopathy & Cataract	Vicart et al. 1998
D140N	Asp → Asn	G → A	Cataract	Liu et al. 2006
G154S	Gly → Ser	G → A	Cardiomyopathy	Pilotto et al. 2006
R157H	Arg → His	G → A	Cardiomyopathy	Inagaki et al. 2006
A171T	Ala → Thr	G → A	Cataract	Devi et al. 2008

In studies performed by Lie et al., the D140N mutation did not appear to be involved in self-interaction even though it's located in the same ACD region as D109H and R120G. Instead, the D140N missense mutation results in a loss of chaperone activity, in support of our Y2H findings, indicated by its inability to prevent the aggregation of insulin *in vitro*. In addition, this variant was also found to be more susceptible to heat denaturation and resulted in the formation of larger oligomers than wild type CryAB, altering both the tertiary and quaternary structure of alpha-crystallin [38].

Table 2.5.

Yeast two-hybrid self-oligomerization assays for wild type CryAB and nine reported CryAB alleles. Changes in self-oligomerization were analyzed using the Y2H system for nine reported CryAB variants. Y2H Gold cells (Clontech) containing either empty vector, full-length or CryAB alleles in both bait and prey constructs were co-transformed and streaked onto Y2H selective media (SD-Trp-Leu-His-Ade) to determine interaction strength and/or altered binding affinity. Plates were incubated at 30°C for 3-4 days until growth was apparent.

CryAB Construct	pJG#s	Strength
Full-length WT CryAB	736/576	Moderate/Strong
R11H-CryAB	1337/1339	No Growth/Weak
P20S-CryAB	1269/1585	Moderate/Strong
R56W-CryAB	1268/1293	Moderate/Strong
D109H-CryAB	1280/1295	Moderate/Strong
R120G-CryAB	581/1292	Moderate/Strong
D140N-CryAB	1296/1526	Very Weak
G154S-CryAB	1363/1364	Moderate
R157H-CryAB	1307/1308	Moderate/Strong
A171T-CryAB	1602/--	--

In contrast to self-oligomerization, several mutants displayed altered putative binding of CryAB clientele. While wild type CryAB was able to interact with ALDOA indicated by a weak/moderate binding affinity via Y2H, all other variants except R120G and P20S were unable to interact with this putative clientele suggesting a loss of wild type function. Interestingly, PGM1 was identified as a unique substrate for the R120G variant. P20S was the only variant that was able to weakly interact with this clientele, whereas the other variants behaved similarly to wild type for this particular clientele.

This may suggest that P20S-CryAB also acts through a gain-of-function mechanism similar to R120G.

Table 2.6.

Binding partners identified from the CryAB interactome are compared to CryAB truncations. Comparison of CryAB truncations using the yeast two-hybrid system to test for clientele binding of PGM1 and ALDOA revealed altered binding protein and interaction strengths. Y2H Gold cells (Clontech) containing either empty vector or CryAB (including full-length and truncations) were transformed and streaked onto Y2H selective media (SD-Trp-Leu-His-Ade) to determine interaction strength and/or altered binding affinity. Plates were incubated at 30°C for 3-4 days until growth was apparent.

Y2H Bait CryAB Construct	pJG#	Interaction Strength with PGM1 (pJG1159)	Interaction Strength with ALDOA (pJG774)
Full-length WT CryAB	736	No Growth	Weak/Moderate
CryAB aa1-169	577	No Growth	No Growth
CryAB aa1-162	1554	No Growth	No Growth
CryAB aa1-158	583	Weak/Moderate	Moderate
Full-length R120G-CryAB	581	Moderate/Strong	Moderate/Strong
R120G-CryAB aa1-169	587	Moderate/Strong	Weak/Moderate
R120G-CryAB aa1-162	589	No Growth	No Growth
R120G-CryAB aa1-158	584	Strong	Moderate/Strong

Table 2.7.

Binding partners identified from the CryAB interactome are compared to other reported CryAB variants. Comparison of CryAB variants using the yeast two-hybrid system to test for clientele binding of PGM1 and ALDOA revealed altered binding protein and interaction strengths. Y2H Gold cells (Clontech) containing either empty vector or CryAB (including full-length and alleles) were transformed and streaked onto Y2H selective media (SD-Trp-Leu-His-Ade) to determine interaction strength and/or altered binding affinity. Plates were incubated at 30°C for 3-4 days until growth was apparent.

Y2H Bait CryAB Construct	pJG#	Interaction Strength with PGM1 (pJG1159)	Interaction Strength with ALDOA (pJG774)
Wild type CryAB	736	No Growth	Weak/Moderate
R120G-CryAB	581	Moderate/Strong	Moderate/Strong
R11H-CryAB	1337	No Growth	No Growth
P20S-CryAB	1269	Very Weak	Moderate/Strong
R56W-CryAB	1268	No Growth	No Growth
D109H-CryAB	1280	No Growth	No Growth/Weak
D140N-CryAB	1296	--	No Growth
G154S-CryAB	1363	No Growth	Very Weak/Weak
R157H-CryAB	1307	No Growth	No Growth/Weak
A171T-CryAB	1602	--	--

Using the Yeast Two-Hybrid to Detect Dysfunction of Human CryAB Variants

Given the altered binding affinities for CryAB and R120G clientele among other reported variants, Y2H screens were initiated using the human cardiac cDNA library (Clontech). Screens are in progress for P20S (pJG1269), D109H (pJG1280), R157H (pJG1307), R11H (pJG1337), and G154S (pJG1363). Preliminary screen transformation results show several of these variants to have an extremely low mating efficiency, similar to that of wild type CryAB. Other variants seem to behave more similar to that of R120G-CryAB, as indicated by similarities in Y2H mating efficiencies. These Y2H screens will provide valuable insight into the behavior of each mutant chaperone and may reveal unique putative clientele as was revealed for the R120G mutant.

DISCUSSION

sHSP have many important implications in maintaining proteostasis. Their roles in a variety of human diseases demonstrate the need to explore the pathways and interactions sHSP have within the cell. This study uses the powerful and highly sensitive Y2H method to detect protein-protein interactions of CryAB and the highly studied variant R120G. Our study provides the first reported protein interactome for wild type CryAB and R120G-CryAB. In support of the putative gain-of-function characteristic attributed to R120G-CryAB, this variant had an expanded clientele when compared to the wild type protein. Specific clientele in this expanded interactome may be useful in studying the unique pathways in which R120G causes disease.

Co-purification studies for the wild type protein revealed poor results with only six putative clientele. Interestingly, one of these clientele (EEF1A1) was also identified as a putative clientele in the HspB2 interactome [24]. The same construct used for the co-purification analysis of wild type CryAB was used to perform heat shock assays and

explore the chaperone function of this protein with putative clientele identified from the Y2H. In support of the poor results of the CryAB co-purification studies, this protein was unable to rescue clientele after C2C12 cells overexpressing CryAB were subjected to heat shock. We propose that this construct of CryAB protein may have decreased function and is unable to test chaperone function *in vivo*.

Using the CryAB protein interactome provided in this study, reported CryAB variants were tested for altered chaperone function in Y2H assays with CryAB and R120G clientele as well as for self-oligomerization. Interestingly, these assays revealed similarities to either wild type CryAB or R120G, suggesting gain-of-function mechanisms for other variants such as P20S. Y2H screens were initiated and will provide a basis for identifying critical interacting proteins involved in disease phenotypes associated with each variant. CryAB is a multifunctional protein involved in several critical cellular pathways. Exploring the gain and/or loss of protein-protein interactions for each variant will provide insight into the chaperone activity of each CryAB variant.

ACKNOWLEDGEMENTS

We thank BYU undergraduates Kendall Kiser, Steve Van De Graff, and Makay Chapman for their contributions to the R120G-CryAB Y2H screen. This work was supported by an NIH grant (to IJB), the BYU Cancer Grant, BYU Graduate Studies Fellowship and both BYU departments of Microbiology and Molecular Biology, and Biology

BIBLIOGRAPHY

1. Basha E, O'Neill H, Vierling E. Small heat shock proteins and α-crystallins: dynamic proteins with flexible functions. Trends Biochem Sci. 2012;37(3):106-117.
2. Mymrikov EV, Seit-Nebi AS, Gusev NB. Large potentials of small heat shock proteins. Annu Rev Physiol. 2011;91(4):1123-1159.
3. Mitra A, Basak T, Datta K, Naskar S, Sengupta S, Sarkar S. Role of α-crystallin B as a regulatory switch in modulating cardiomyocyte apoptosis by mitochondria or endoplasmic reticulum during cardiac hypertrophy and myocardial infarction. Cell Death Dis. 2013;4(4):e582.
4. Benjamin IJ, Guo Y, Srinivasan S, Boudina S, Taylor RP, Rajasekaran NS, et al. CRYAB and HSPB2 deficiency alters cardiac metabolism and paradoxically confers protection against myocardial ischemia in aging mice. Am J Physiol Heart Circ Physiol. 2007;293(5):H3201-H3209
5. Elliott JL, Perng MD, Prescott AR, Jansen KA, Koenderink GH, Quinlan RA. The specificity of the interaction between αB-crystallin and desmin filaments and its impact on filament aggregation and cell viability. Philos Trans R Soc Lond B Biol Sci. 2013;368(1617):20120375.
6. Dubińska-Magiera M, Jabłońska J, Saczko J, Kulbacka J, Jagla T, Daczewska M. Contribution of small heat shock proteins to muscle development and function. FEBS Lett. 2014;588(4):517-530.
7. Brewer AC, Mustafi SB, Murray TV, Rajasekaran NS, Benjamin IJ. Reductive stress linked to small HSPs, G6PD, and Nrf2 pathways in heart disease. Antioxid Redox Signal. 2013;18(9):1114-1127.
8. Laganowsky A, Benesch JL, Landau M, Ding L, Sawaya MR, Cascio D, et al. Crystal structures of truncated alphaA and alphaB crystallins reveal structural mechanisms of polydispersity important for eye lens function. Protein Sci. 2010;19(5):1031-1043.
9. Bakthisaran R, Akula KK, Tangirala R, Rao ChM. Phosphorylation of αB-crystallin: Role in stress, aging and patho-physiological conditions. Biochim Biophys Acta. 2016;1860(1 Pt B):167-182.
10. Pinz I, Robbins J, Rajasekaran NS, Benjamin IJ, Ingwall JS. Unmasking different mechanical and energetic roles for the small heat shock proteins CryAB and HSPB2 using genetically modified mouse hearts. FASEB J. 2008;22(1):84-92.
11. Golenhofen N, Ness W, Koob R, Htun P, Schaper W, Drenckhahn D. Ischemia-induced phosphorylation and translocation of stress protein alpha B-crystallin to Z lines of myocardium. Am J Physiol. 1998;274(5):H1457-H1464.
12. Chen Q, Ma J, Yan M, Mothobi ME, Liu Y, Zheng F. A novel mutation in CRYAB associated with autosomal dominant congenital nuclear cataract in a Chinese family. Mol Vis. 2009;15:1359-1365.
13. Liu M, Ke T, Wang Z, Yang Q, Chang W, Jiang F, et al. Identification of a CRYAB mutation associated with autosomal dominant posterior polar cataract in a Chinese family. Invest Ophthalmol Vis Sci. 2006;47(8):3461-3466.
14. Safieh LA, Khan AO, Alkuraya FS. Identification of a novel CRYAB mutation associated with autosomal recessive juvenile cataract in a Saudi family. Mol Vis. 2009;15:980-984.
15. Sacconi S, Féasson L, Antoine JC, Pécheux C, Bernard R, Cobo AM, et al. A novel CRYAB mutation resulting in multisystemic disease. Neuromuscul Disord. 2012;22(1):66-72.

16. Liu Y, Zhang X, Luo L, Wu M, Zeng R, Cheng G et al. A novel αB-crystallin mutation associated with autosomal dominant congenital lamellar cataract. Invest Ophthalmol Vis Sci. 2006;47(3):1069-1075.
17. Pilotto A, Marziliano N, Pasotti M, Grasso M, Costante AM, et al. AlphaB-crystallin mutation in dilated cardiomyopathies: low prevalence in a consecutive series of 200 unrelated probands. Biochem Biophys Res Commun. 2006;346(4):1115-1117.
18. Inagaki N, Hayashi T, Arimura T, Koga Y, Takahashi M, Shibata H, et al. αB-crystallin mutation in dilated cardiomyopathy. Biochem Biophys Res Commun. 2006;342(2):379-386.
19. Devi RR, Yao W, Vijayalakshmi P, Sergeev YV, Sundaresan P, Hejtmancik JF. Crystallin gene mutations in Indian families with inherited pediatric cataract. Mol Vis. 2008;14:1157-1170.
20. Vicart P, Caron A, Guicheney P, Li Z, Prévost MC, Faure A, et al. A missense mutation in the αB-crystallin chaperone gene causes a desmin-related myopathy. Nat Genet. 1998;20(1):92-95.
21. Rajasekaran NS, Connell P, Christians ES, Yan LJ, Taylor RP, Orosz A, et al. Human αB-crystallin mutation causes oxido-reductive stress and protein aggregation cardiomyopathy in mice. Cell. 2007;130(3):427-429.
22. Wang X, Osinska H, Klevitsky R, Gerdes AM, Nieman M, et al. Expression of R120G-alphaB-crystallin causes aberrant desmin and alphaB-crystallin aggregation and cardiomyopathy in mice. Circ Res. 2001;89(1):84-91.
23. Wilhelmus MM, Boelens WC, Otte-Höller I, Kams B, de Waal RM, Verbeek MM. Small heat shock proteins inhibit amyloid-beta protein aggregation and cerebrovascular amyloid-beta protein toxicity. Brain Res. 2006;1089(1):67-78.
24. Grose JH, Langston K, Wang X, Squires S, Mustafi SB, et al. Characterization of the cardiac overexpression of HSPB2 reveals mitochondrial and myogenic roles supported by a cardiac HspB2 interactome. PLoS One. 2015;10(10):e0133994.
25. Zhang H, Rajasekaran NS, Orosz A, Xiao X, Rechsteiner M, Benjamin IJ. Selective degradation of aggregate-prone CryAB mutants by HSPB1 is mediated by ubiquitin-proteasome pathways. J Mol Cell Cardiol. 2010;29:918-930.
26. Rajasekaran NS, Firpo MA, Milash BA, Weiss RB, Benjamin IJ. Global expression profiling identifies a novel biosignature for protein aggregation R120GCryAB cardiomyopathy in mice. Physiol Genomics. 2008;35(2):165-172.
27. Raju I, Abraham EC. Mutants of human αB-crystallin cause enhanced protein aggregation and apoptosis in mammalian cells: influence of co-expression of HspB1. Biochem Biophys Res Commun. 2013;430(1):107-112.
28. Panda AK, Nandi SK, Chakraborty A, Nagaraj RH, Biswas A. Differential role of arginine mutations on the structure and functions of α-crystallin. Biochim Biophys Acta. 2016;1860:199-210.
29. Hishiya A, Salman MN, Carra S, Kampinga HH, Takayama S. BAG3 directly interacts with mutated alphaB-crystallin to suppress its aggregation and toxicity. PLoS One. 2011;6(3):e16828.

Supplementary Table 2.1.

Plasmid	Gene	Description	Plasmid Backbone	Selection	Expression	Reference
pJG483	CryAB	WT fused to Myc	pCMV-Myc	Amp	Mammalian	[25]
pJG485	N/A	pGBKT7 Y2H bait from Clontech Y2H Gold system	pGBKT7	Kan/Trp	Yeast	Clontech
pJG549	N/A	pGADT7 Y2H prey from Clontech Y2H Gold system	pGADT7	Amp/Leu	Yeast	Clontech
pJG576	CryAB	Full-length WT CryAB	pGADT7	Amp/Leu	Yeast	This study
pJG577	CryAB	WT CryAB (aa1-169)	pGBKT7	Kan/Trp	Yeast	This study
pJG578	CryAB	WT CryAB (aa1-169)	pGADT7	Amp/Leu	Yeast	This study
pJG580	CryAB	WT CryAB (aa1-158)	pGADT7	Amp/Leu	Yeast	This study
pJG581	CryAB	Full-length R120G-CryAB	pGBKT7	Kan/Trp	Yeast	This study
pJG582	CryAB	R120G CryAB (aa1-158)	pGADT7	Amp/Leu	Yeast	This study
pJG583	CryAB	WT CryAB (aa1-158)	pGBKT7	Kan/Trp	Yeast	This study
pJG584	CryAB	R120G CryAB (aa1-158)	pGADT7	Kan/Trp	Yeast	This study
pJG585	CryAB	WT CryAB (aa1-169)	pGBKT7	Kan/Trp	Yeast	This study
pJG586	CryAB	WT CryAB (aa1-169)	pGADT7	Amp/Leu	Yeast	This study
pJG587	CryAB	R120G CryAB (aa1-169)	pGBKT7	Kan/Trp	Yeast	This study
pJG588	CryAB	R120G CryAB (aa1-169)	pGADT7	Amp/Leu	Yeast	This study
pJG589	CryAB	R120G CryAB (aa 1-162)	pGBKT7	Kan/Trp	Yeast	This study
pJG590	CryAB	R120G CryAB (aa 1-162)	pGADT7	Amp/Leu	Yeast	This study
pJG736	CryAB	Full-length WT CryAB	pGBKT7	Kan/Trp	Yeast	This study
pJG773	MYOM1	Retrieved from R120G Y2H Screen	pGADT7	Amp/Leu	Yeast	This study
pJG774	ALDOA	Retrieved from R120G Y2H Screen	pGADT7	Amp/Leu	Yeast	This study
pJG776	CRYAB	Retrieved from R120G Y2H Screen	pGADT7	Amp/Leu	Yeast	This study
pJG786	XIRP1	Retrieved from R120G Y2H Screen	pGADT7	Amp/Leu	Yeast	This study
pJG784	MYH6	Retrieved from R120G Y2H Screen	pGADT7	Amp/Leu	Yeast	This study
pJG805	MTCYB	Retrieved from R120G Y2H Screen	pGADT7	Amp/Leu	Yeast	This study
pJG825	MYH7	Retrieved from R120G Y2H Screen	pGADT7	Amp/Leu	Yeast	This study
pJG826	MARCO	Retrieved from R120G Y2H Screen	pGADT7	Amp/Leu	Yeast	This study
pJG828	TTN	Retrieved from R120G Y2H Screen	pGADT7	Amp/Leu	Yeast	This study
pJG836	MAP1B	Retrieved from R120G Y2H Screen	pGADT7	Amp/Leu	Yeast	This study
pJG906	N/A	pCMV-myc-N Empty Vector	pCMV-Myc	Amp	Mammalian	Clontech
pJG1155	ROBO2	Retrieved from R120G Y2H Screen	pGADT7	Amp/Leu	Yeast	This study

pJG1157	DCAF6	Retrieved from R120G Y2H Screen	pGADT7	Amp/Leu	Yeast	This study
pJG1159	PGM1	Retrieved from R120G Y2H Screen	pGADT7	Amp/Leu	Yeast	This study
pJG1160	GOSR1	Retrieved from R120G Y2H Screen	pGADT7	Amp/Leu	Yeast	This study
pJG1221	NBN	Retrieved from R120G Y2H Screen	pGADT7	Amp/Leu	Yeast	This study
pJG1222	KMT2C	Retrieved from R120G Y2H Screen	pGADT7	Amp/Leu	Yeast	This study
pJG1224	ARID2	Retrieved from R120G Y2H Screen	pGADT7	Amp/Leu	Yeast	This study
pJG1225	ZNF177	Retrieved from R120G Y2H Screen	pGADT7	Amp/Leu	Yeast	This study
pJG1268	CryAB	R56W-CryAB	pGBKT7	Kan/Trp	Yeast	This study
pJG1293	CryAB	R56W-CryAB	pGADT7	Amp/Leu	Yeast	This study
pJG1269	CryAB	P20S-CryAB	pGBKT7	Kan/Trp	Yeast	This study
pJG1280	CryAB	D109H-CryAB	pGBKT7	Kan/Trp	Yeast	This study
pJG1292	CryAB	R120G-CryAB	pGADT7	Amp/Leu	Yeast	This study
pJG1295	CryAB	D109H-CryAB	pGADT7	Amp/Leu	Yeast	This study
pJG1296	CryAB	D140N-CryAB	pGBKT7	Kan/Trp	Yeast	This study
pJG1307	CryAB	R157H-CryAB	pGBKT7	Kan/Trp	Yeast	This study
pJG1308	CryAB	R157H-CryAB	pGADT7	Amp/Leu	Yeast	This study
pJG1337	CryAB	R11H-CryAB	pGBKT7	Kan/Trp	Yeast	This study
pJG1339	CryAB	R11H-CryAB	pGADT7	Amp/Leu	Yeast	This study
pJG1363	CryAB	G154S-CryAB	pGBKT7	Kan/Trp	Yeast	This study
pJG1364	CryAB	G154S-CryAB	pGADT7	Amp/Leu	Yeast	This study
pJG1526	CryAB	D140N-CryAB	pGADT7	Amp/Leu	Yeast	This study
pJG1554	CryAB	WT CryAB (aa1-162)	pGBKT7	Kan/Trp	Yeast	This study
pJG1555	CryAB	WT CryAB (aa1-162)	pGADT7	Amp/Leu	Yeast	This study
pJG1585	CryAB	P20S-CryAB	pGADT7	Amp/Leu	Yeast	This study
pJG1602	CryAB	A171T-CryAB	pGBKT7	Kan/Trp	Yeast	This study

Supplementary Table 2.2.

Primer	Description	Sequence
JG2461	CryAB forward (full-length)	GGCGAATTCGACATCGCCATCCACCACCCC
JG2603	CryAB reverse (at aa158)	GGCGTCGACCTAGGTGCGCTCAGGGCCAGAG
JG2604	CryAB reverse (at aa169)	GGCGTCGACCTAGACAGCAGGCTTCTCTTCACG
JG2606	CryAB reverse (at aa162)	GGCGTCGACCTAACGGGTGATGGGAATGGTGC
JG2609	CryAB reverse (full-length)	GGCGTCGACCTATTTCTTGGGGGCTGCGGTGAC
JG2761	pGADT7 libary insert (PCR)	CTATTCGATGATGAAGATACCCCACC
JG2762	pGADT7 libary insert (PCR)	AGATGGTGCACGATGCACAG
JG2860	pGADT7 libary insert (sequencing)	CAGAGGTTACATGGCCAAGATTG
JG2877	pGADT7 libary insert (sequencing)	CTATTCGATGATGAAGATACCCCACCAAACCC
JG3157	CryAB forward (full-length)	CCGCATATGGACATCGCCATCCACCACCCC
JG3158	CryAB reverse (full-length)	GCCGGATCCCTATTTCTTGGGGGCTGCGGTGAC
JG3538	CryAB R157H for mutagenesis	GGTCTCTGGCCCTGAGCACACCATTCCCATCACCCG
JG3539	CryAB R157H for mutagenesis	CGGGTGATGGGAATGGTGTGCTCAGGGCCAGAGACC
JG3540	CryAB G154S for mutagenesis	CCAAGGAAACAGGTCTCTTCCCCTGAGCGCACCATTCC
JG3541	CryAB G154S for mutagenesis	GGAATGGTGCGCTCAGGGGAAGAGACCTGTTTCCTTGG
JG3543	CryAB P20S for mutagenesis	CTTTCCTTTCCACTCCACCAGCCGCCTCTTTGACC
JG3544	CryAB P20S for mutagenesis	GGTCAAAGAGGCGGCTGGTGGAGTGGAAAGGAAAG
JG3545	CryAB R56W for mutagenesis	GCCACCCTCCTTCCTGTGGGCACCCAGCTGGTTTG
JG3546	CryAB R56W for mutagenesis	CAAACCAGCTGGGTGCCCACAGGAAGGAGGGTGGC
JG3594	CryAB D109H for mutagenesis	CATGAAGAGCGCCAGCATGAACATGGTTTCATCTCC
JG3595	CryAB D109H for mutagenesis	GGAGATGAAACCATGTTCATGCTGGCGCTCTTCATG
JG3596	CryAB R11H for mutagenesis	CCACCACCCCTGGATCCACCGCCCCTTCTTTCCTTTCC
JG3597	CryAB R11H for mutagenesis	GGAAAGGAAAGAAGGGGCGGTGGATCCAGGGGTGGTGG
JG3598	CryAB D140N for mutagenesis	CTTCATCCCTGTCATCTAATGGGTCCTCACTGTG
JG3599	CryAB D140N for	CACAGTGAGGACCCATTAGATGACAGGGATGAAG

	mutagenesis	
JG3992	CryAB A171T for mutagenesis	GGCGCGGCCGCCTATTTCTTGGGGGCTGCGGTGAC
JG3993	CryAB A171T for mutagenesis	GAAGCCTGCTGTCACCACAGCCCCCAAGAAATAG

Supplementary Table 2.3.

Protein Name	Uniprot Accession	Gene Symbol	Cellular Localization	Function
HCLS1-associated protein X-1	O00165	HAX1	Cytoplasm	Myofibril or Cytoskeleton Structure/Regulation
Protein NipSnap homolog 2	O75323	GBAS	Cell Membrane	Small Molecule Biosynthesis
Ferritin light chain	P02792	FTL	Cytoplasm	Iron and Copper Homeostasis
Cytochrome c oxidase subunit 3	P00414	MTCO3	Mito IM	Fermentation and Respiration
Prostaglandin E2 receptor EP3 subtype	P43115	PTGER3	Cell Membrane	Signal Transduction
Periostin	Q15063	POSTN	Extracellular	Cell Adhesion
DnaJ homolog subfamily B member 6	O75190	DNAJB6	Cytoplasm	Chaperone
Integrator complex subunit 8	Q75QN2	INTS8	Nucleus	Replication
Protein kish-A	Q8TBQ9	TMEM167A	Golgi Body	Intracellular Trafficking
Ankyrin Repeat Domain 20 Family, Member A12		ANKRD20A12P	Cytoplasm	Unknown
Long intergenic non-protein coding RNA 927	Non-coding RNA	LINC00927	Not Applicable	Unknown
Long intergenic non-protein coding RNA 943	Non-coding RNA	LINC00943	Not Applicable	Unknown

CHAPTER THREE: Summary and Discussion of Findings

The knowledge provided by these studies will be foundational to understanding the basic pathways and molecular function of small Heat Shock Proteins (sHSP). Their contributions to the regulation and structure of cardiac muscle are critical to maintaining proteostasis. These small molecular chaperones are unique in their ability to form heteroligomeric complexes and prevent misfolded proteins from forming cytoplasmic aggregates. Their ability to refold proteins and prevent their denaturation enables protein clientele to remain functional within the cell. It has been suggested that sHSP protein interaction is non-specific and redundant in function, with sHSP interacting with any unstable protein. This idea was supported by the proposed theory of gene devolution by duplication, in the case of CryAB and HspB2 due to their sharing of promoter and regulatory transcription elements. However, the conservation of both sHSP throughout mammals suggests evolutionary selection, and hence some independent function. This function may be due to differential specificity for substrates, or alternative expression, localization, regulation, etc. Thus, an in depth study of these related sHSP may provide evidence for or against the non-specific nature of sHSP.

Both CryAB and HspB2 are expressed predominantly in skeletal and cardiac muscle, however CryAB is expressed ubiquitously. The chaperone role of CryAB is of clear importance due to over nine reported dominant and recessive human mutations resulting in a wide variety of severe, human disease-associated alleles. CryAB has been highly studied, with the aberrant mutation R120G-CryAB being of primary focus due to its direct cause of multisystemic disease. Interestingly, studies have not pursued the characterization of *in vivo* CryAB clientele. We have recently published the interactome of HspB2, suggesting over a hundred clientele. This research is the first study aimed to investigate and characterize the protein clientele and chaperone activity of CryAB,

which was compared to HspB2 to provide evidence for the differential function of CryAB and HspB2 at the molecular level. In addition, the CryAB interactome allowed us to characterize several CryAB alleles associated with human mutation including R120G-CryAB. Thus, this research also supports a mechanism for the dysfunction of R120G-CryAB and other reported disease-causing alleles at the molecular level, which may guide future research in understanding the mechanisms of such disparate diseases.

The binding partners of CryAB identified via yeast two-hybrid shared roles in muscle maintenance and central metabolism. In response to physiological stress, CryAB has been shown to bind the cytoskeletal structure and modulate remodeling of the cytoskeletal network through direct interactions with desmin, actin and titin. CryAB has been found to play a key role in the development of several disparate human diseases as a direct result in over nine reported autosomal dominant and recessive variants. This study provides evidence for the differential binding of wild type CryAB when compared to various disease-causing alleles. R120G-CryAB remains the most studied sHSP variants it its contributions to the development of cardiomyopathy and cataract, replicated both in human and mice studies. The yeast two-hybrid analysis provided herein identified three binding partners that demonstrated binding specificity for R120G-CryAB in comparison to the wild type chaperone. This supports a hypothesis of chaperone dysfunction of R120G binding to otherwise fully functional proteins and forming aggregates throughout the cell and "gaining" a larger span of protein clientele in comparison to wild type.

Using the protein clientele retrieved via yeast two-hybrid screening for CryAB and R120G-CryAB, changes in chaperone activity were characterized for other missense alleles of CryAB. Yeast two-hybrid analysis reveals changes in self-oligomerization as well as changes in protein clientele for disease-reported variants. The R120G mutant

protein has been shown to have reduced chaperone activity under heat stress conditions which results in increased aggregate formation. This hyper-binding activity may be the change in chaperone function that results in disease. This chaperone model provides the basis for studying other missense CryAB mutants and to characterize the change in chaperone activity for other reported alleles. Changes in ability to bind to wild type clientele as well as self-oligomerization are the beginning steps to understand the changes in sHSP activity. This protein-interaction analysis can help to elucidate the change in molecular mechanisms associated with different disease-causing alleles.

The unique protein clientele of each sHSP, including CryAB, is a novel approach to reveal the key pathways and molecular function of these chaperones. The yeast two-hybrid interactome comparison provided herein for CryAB and HspB2 demonstrate that even these closely related sHSPs share non-redundant molecular roles and harbor specificity in their protein-protein interactions. In addition, a different subset of clientele for R120G-CryAB and several other disease-causing mutants was revealed, containing both shared and chaperone-specific interaction when assessed via yeast two-hybrid. This study is the first analysis to identify protein clientele specificity and altered binding ability for such reported variants. The interactome of CryAB not only provides insight for the molecular involvement of CryAB in specific metabolic and cardiac maintenance pathways, but also serves as a basis for studying all reported alleles for CryAB and their change in mechanisms of action. This research provides a foundation to identify key pathways critical to the maintenance of cardiac muscle structure and function.

COMPLETE BIBLIOGRAPHY

1. Basha E, O'Neill H, Vierling E. Small heat shock proteins and α-crystallins: dynamic proteins with flexible functions. Trends Biochem Sci. 2012;37(3):106-117.
2. Mymrikov EV, Seit-Nebi AS, Gusev NB. Large potentials of small heat shock proteins. Annu Rev Physiol. 2011;91(4):1123-1159.
3. Wang X, Su H, Ranek MJ. Protein quality control and degradation in cardiomyocytes. J Mol Cell Cardiol. 2008;45:11-27.
4. Velotta JB, Kimura N, Chang SH, Chung J, Itoh S, Rothbard J, et al. B-crystallin improves murine cardiac function and attenuates apoptosis in human endothelial cells exposed to ischemia-reperfusion. Ann Thorac Surg. 2011;91:1907-1913.
5. Benjamin IJ, McMillan DR. Stress (heat shock) proteins: molecular chaperones in cardiovascular biology and disease. Circ Res. 1998;83(2):117-132.
6. Acunzo J, Katsogiannou M, Rocchi P. Small heat shock proteins HSP27 (HspB1), αB-crystallin (HspB5) and Hsp22 (HspB8) as regulators of cell death. Int J Biochem Cell Biol. 2012;44(10):1622-1631.
7. Garrido C, Paul C, Seigneuric R, Kampinga HH. The small heat shock proteins family: the long forgotten chaperones. Int J Biochem Cell Biol. 2012;44(10):1588-1592.
8. Golenhofen N, Ness W, Koob R, Htun P, Schaper W, Drenckhahn D. Ischemia-induced phosphorylation and translocation of stress protein alpha B-crystallin to Z lines of myocardium. Am J Physiol. 1998;274(5):H1457-H1464.
9. Morrison LE, Hoover HE, Thuerauf DJ, Glembotski CC. Mimicking Phosphorylation of αB-crystallin on Serine-59 Is Necessary and Sufficient to Provide Maximal Protection of Cardiac Myocytes From Apoptosis. Circ Res. 2003;92:203-211.
10. Hilton GR, Lioe H, Stengel F, Baldwin AJ, Benesch JLP. Small heat-shock proteins: paramedics of the cell. Top Curr Chem. 2013;328:69-98.
11. Pinz I, Robbins J, Rajasekaran NS, Benjamin IJ, Ingwall JS. Unmasking different mechanical and energetic roles for the small heat shock proteins CryAB and HSPB2 using genetically modified mouse hearts. FASEB J. 2008;22(1):84-92.
12. Oshita SE, Chen F, Kwan T, Yehiely F, Cryns VL. The small heat shock protein HspB2 is a novel anti-apoptotic protein that inhibits apical caspase activation in the extrinsic apoptotic pathway. Breast Cancer Res Treat. 2010;124(2):307-315.
13. Grose JH, Langston K, Wang X, Squires S, Mustafi SB, et al. Characterization of the cardiac overexpression of HSPB2 reveals mitochondrial and myogenic roles supported by a cardiac HspB2 interactome. PLoS One. 2015;10(10):e0133994.
14. Dubińska-Magiera M, Jablońska J, Saczko J, Kulbacka J, Jagla T, Daczewska M. Contribution of small heat shock proteins to muscle development and function. FEBS Lett. 2014;588(4):517-530.
15. Kato K, Shinohara H, Kurobe N, Inaguma Y, Shimizu K, et al. Tissue distribution and developmental profiles of immunoreactive alpha B crystallin in the rat determined with a sensitive immunoassay system. Biochim Biophys Acta. 1991;1074:201-208.
16. Horwitz J. Alpha-crystallin can function as a molecular chaperone. Proc Natl Acad Sci U S A. 1992;89(21):10449-10453.

17. Wettstein G, Bellaye PS, Micheau O, Bonniaud P. Small heat shock proteins and the cytoskeleton: an essential interplay for cell integrity? Int J Biochem Cell Biol. 2012;44(10):1680-1686.
18. Arrigo AP. Human small heat shock proteins: protein interactomes of homo- and hetero-oligomeric complexes: an update. FEBS Lett. 2013;587(13):1959-1969.
19. Ray PS, Martin JL, Swanson EA, Otani H, Dillman WH, et al. Transgene overexpression of αB crystallin confers simultaneous protection against cardiomyocyte apoptosis and necrosis during myocardial ischemia and reperfusion. FASEB J. 2001;15(2):393-402.
20. Vicart P, Caron A, Guicheney P, Li Z, Prévost MC, Faure A, et al. A missense mutation in the αB-crystallin chaperone gene causes a desmin-related myopathy. Nat Genet. 1998;20(1):92-95.
21. Barbato R, Menabò R, Dainese P, Carafoli E, Schiaffino S, Di Lisa F. Binding of cytosolic proteins to myofibrils in ischemic rat hearts. Circ Res. 1996;78(5):821-828.
22. Parcellier A, Gurbuxani S, Schmitt E, Solary E, Garrido C. Heat shock proteins, cellular chaperones that modulate mitochondrial cell death pathways. Biochem Biophys Res Commun. 2003;304(3):505-512.
23. Kamradt MC, Chen F, Cryns VL. The small heat shock protein alpha B-crystallin negatively regulates cytochrome c- and caspase-8-dependent activation of caspase-3 by inhibiting its autoproteolytic maturation. J Biol Chem. 2001;276(19):16059-16063.
24. Rajasekaran NS, Firpo MA, Milash BA, Weiss RB, Benjamin IJ. Global expression profiling identifies a novel biosignature for protein aggregation R120GCryAB cardiomyopathy in mice. Physiol Genomics. 2008;35(2):165-172.
25. Wang X, Osinska H, Klevitsky R, Gerdes AM, Nieman M, et al. Expression of R120G-alphaB-crystallin causes aberrant desmin and alphaB-crystallin aggregation and cardiomyopathy in mice. Circ Res. 2001;89(1):84-91.
26. Kumar LV, Ramakrishna T, Rao CM. Structural and functional consequences of the mutation of a conserved arginine residue in alphaA and alphaB crystallins. J Biol Chem. 1999;274(34):24137-24141.
27. Bova MP, Yaron O, Huang O, Ding L, Haley DA, Stewart PL, et al. Mutation R120G in alphaB-crystallin, which is linked to a desmin-related myopathy, results in an irregular structure and defective chaperone-like function. Proc Natl Acad Sci U S A. 1999;96(11):6137-6142.
28. Perng MD, Muchowski PJ, van Den IJssel P, Wu GJ, Hutcheson AM, Clark JI, et al. The cardiomyopathy and lens cataract mutation in alphaB-crystallin alters its protein structure, chaperone activity, and interaction with intermediate filaments in vitro. J Biol Chem. 1999;274(47):33235-33243.
29. Treweek TM, Rekas A, Lindner RA, Walker MH, Aquilina JA, et al. R120G alphaB-crystallin promotes the unfolding of reduced alpha-lactalbumin and is inherently unstable. FEBS J. 2005;272(3):711-724.
30. Rajasekaran NS, Connell P, Christians ES, Yan LJ, Taylor RP, Orosz A, et al. Human αB-crystallin mutation causes oxido-reductive stress and protein aggregation cardiomyopathy in mice. Cell. 2007;130(3):427-429.
31. Zhang H, Rajasekaran NS, Orosz A, Xiao X, Rechsteiner M, Benjamin IJ. Selective degradation of aggregate-prone CryAB mutants by HSPB1 is mediated by ubiquitin-proteasome pathways. J Mol Cell Cardiol. 2010;29:918-930.

32. Préville X, Salvemini F, Giraud S, Chaufour S, Paul C, Stepien G, et al. Mammalian small stress proteins protect against oxidative stress through their ability to increase glucose-6-phosphate dehydrogenase activity and by maintaining optimal cellular detoxifying machinery. Exp Cell Res. 1999;247(1):61-78.
33. Maloyan A, Sanbe A, Osinska H, Westfall M, Robinson D, Imahashi K, et al. Mitochondrial dysfunction and apoptosis underlie the pathogenic process in αB-crystallin desmin-related cardiomyopathy. Circulation. 2005;112(22):3451-3461.
34. Chen Q, Ma J, Yan M, Mothobi ME, Liu Y, Zheng F. A novel mutation in CRYAB associated with autosomal dominant congenital nuclear cataract in a Chinese family. Mol Vis. 2009;15:1359-1365.
35. Liu M, Ke T, Wang Z, Yang Q, Chang W, Jiang F, et al. Identification of a CRYAB mutation associated with autosomal dominant posterior polar cataract in a Chinese family. Invest Ophthalmol Vis Sci. 2006;47(8):3461-3466.
36. Safieh LA, Khan AO, Alkuraya FS. Identification of a novel CRYAB mutation associated with autosomal recessive juvenile cataract in a Saudi family. Mol Vis. 2009;15:980-984.
37. Sacconi S, Féasson L, Antoine JC, Pécheux C, Bernard R, Cobo AM, et al. A novel CRYAB mutation resulting in multisystemic disease. Neuromuscul Disord. 2012;22(1):66-72.
38. Liu Y, Zhang X, Luo L, Wu M, Zeng R, Cheng G et al. A novel αB-crystallin mutation associated with autosomal dominant congenital lamellar cataract. Invest Ophthalmol Vis Sci. 2006;47(3):1069-1075.
39. Pilotto A, Marziliano N, Pasotti M, Grasso M, Costante AM, et al. AlphaB-crystallin mutation in dilated cardiomyopathies: low prevalence in a consecutive series of 200 unrelated probands. Biochem Biophys Res Commun. 2006;346(4):1115-1117.
40. Inagaki N, Hayashi T, Arimura T, Koga Y, Takahashi M, Shibata H, et al. αB-crystallin mutation in dilated cardiomyopathy. Biochem Biophys Res Commun. 2006;342(2):379-386.
41. Devi RR, Yao W, Vijayalakshmi P, Sergeev YV, Sundaresan P, Hejtmancik JF. Crystallin gene mutations in Indian families with inherited pediatric cataract. Mol Vis. 2008;14:1157-1170.
42. Volkmann J, Reuning U, Rudelius M, Häfner N, Schuster T, Becker V Ros A, et al. High expression of crystallin αB represents an independent molecular marker for unfavourable ovarian cancer patient outcome and impairs TRAIL- and cisplatin-induced apoptosis in human ovarian cancer cells. Int J Cancer. 2013;132(12):2820-2832.
43. Stronach EA, Sellar GC, Blenkiron, et al. Identification of Clinically Relevant Genes on Chromosome 11 in a Functional Model of Ovarian Cancer Tumor Suppression. Cancer Res. 2003;63:8648-8655.
44. Ruan Q, Han S, Jiang WG, Boulton ME, Chen ZJ, Law BK, et al. αB-crystallin, an effector of unfolded protein response, confers anti-VEGF resistance to breast cancer via maintenance of intracrine VEGF in endothelial cells. Mol Cancer Res. 2011;9(12): 1632-1643.
45. Raju I, Abraham EC. Mutants of human αB-crystallin cause enhanced protein aggregation and apoptosis in mammalian cells: influence of co-expression of HspB1. Biochem Biophys Res Commun. 2013;430(1):107-112.

46. Aguzzi A, O'Connor T. Protein aggregation diseases: pathogenicity and therapeutic perspectives. Nat Rev Drug Discov. 2010;9:237-248.
47. Bakthisaran R, Akula KK, Tangirala R, Rao ChM. Phosphorylation of αB-crystallin: Role in stress, aging and patho-physiological conditions. Biochim Biophys Acta. 2016;1860(1 Pt B):167-182.
48. Huang Z, Cheng Y, Chiu PM, Cheung FM, Nicholls JM, Kwong DL, et al. Tumor suppressor Alpha B-crystallin (CRYAB) associates with the cadherin/catenin adherens junction and impairs NPC progression-associated properties. Oncogene. 2012;31(32):3709-3720.
49. Mitra A, Basak T, Datta K, Naskar S, Sengupta S, Sarkar S. Role of α-crystallin B as a regulatory switch in modulating cardiomyocyte apoptosis by mitochondria or endoplasmic reticulum during cardiac hypertrophy and myocardial infarction. Cell Death Dis. 2013;4(4):e582.
50. Préville X, Gaestel M, Arrigo AP. Phosphorylation is not essential for protection of L929 cells by Hsp25 against H202-mediated disruption actin cytoskeleton, a protection which appears related to the redox changed mediated by Hsp25. Cell Stress Chaperones. 1998;3(3):177-187.
51. Dammer EB, Lee AK, Duong DM, Gearing M, Lah JJ, Levey AI, et a. Quantitative phosphoproteomics of Alzheimer's disease reveals cross-talk between kinases and small heat shock proteins. Proteomics. 2015;15:508-519.
52. Sanbe A, Osinska H, Villa C, Gulick J, Klevitsky R, Glabe CG, et al. Reversal of amyloid-induced heart disease in desmin-related cardiomyopathy. Proc Natl Acad Sci U S A. 2005;102(38):13592-13597.
53. Reilich P, Schoser B, Schramm N, Krause S, Schessl J, Kress W, et al. The p.G154S mutation of the alpha-B crystallin gene (CRYAB) causes late-onset distal myopathy. Neuromuscul Disord. 2010;20(4):255-259.
54. Chen Q, Yan M, Xiang F, Zhou X, Liu Y, Zheng F. Characterization of a mutant R11H αB-crystallin associated with human inherited cataract. Biol Chem. 2010;391(12):1391-1400.
55. Selcen D, Engel AG. Myofibrillar myopathy caused by novel dominant negative alpha B-crystallin mutations. Ann Neurol. 2003;54(6):804-810.
56. Panda AK, Nandi SK, Chakraborty A, Nagaraj RH, Biswas A. Differential role of arginine mutations on the structure and functions of α-crystallin. Biochim Biophys Acta. 2016;1860:199-210.
57. Zheng Q, Su H, Ranek MJ, Wang X. Autophagy and p62 in cardiac proteinopathy. Circ Res. 2011;109(3):296-308.
58. Mymrikov EV, Seit-Nebi AS, Gusev NB. Heterooligomeric complexes of human small heat shock proteins. Cell Stress Chaperones. 2012;17(2):157-169.
59. Clark AR, Naylor CE, Bagnéris C, Keep NH, Slingsby C. Crystal structure of R120G disease mutant of human αB-crystallin domain dimer shows closure of a groove. J Mol Biol. 2011;408:118-134.
60. Campbell-Lloyd AJ, Mundy J, Deva R, Lampe G, Hawley C, Boyle G, et al. Is alpha-B crystallin an independent marker for prognosis in lung cancer? Heart Lung Circ. 2013;22(9):759-766.
61. Andley UP, Hamilton PD, Ravi N, Weihl CC. A knock-in mouse model for the R120G mutation of αB-crystallin recapitulates human hereditary myopathy and cataracts. PLoS One. 2011;6(3):e17671.
62. Mehlen P, Kretz-Remy C, Préville X, Arrigo AP. Human hsp27, Drosophila hsp27 and human αB-crystallin expression-mediated increase in glutathione is essential

for the protective activity of these proteins against TNFα-induced cell death. EMBO J. 1996;15(11):2695-2706.
63. Feder ME, Hofmann GE. Heat-shock proteins, molecular chaperones, and the stress response: evolutionary and ecological physiology. Annu Rev Physiol. 1999:61:243-282.
64. Elliott JL, Perng MD, Prescott AR, Jansen KA, Koenderink GH, Quinlan RA. The specificity of the interaction between αB-crystallin and desmin filaments and its impact on filament aggregation and cell viability. Philos Trans R Soc Lond B Biol Sci. 2013;368(1617):20120375.
65. Kamradt MC, Chen F, Sam S, Cryns VL. The small heat shock protein alpha B-crystallin negatively regulates apoptosis during myogenic differentiation by inhibiting caspase-3 activation. J Biol Chem. 2002;277(41):38731-38736.
66. Arrigo AP, Simon S, Gibert B, Kretz-Remy C, Nivon M, Czekalla A, et al. Hsp27 (HspB1) and αB-crystallin (HspB5) as therapeutic targets. FEBS Lett. 2007;581(19):3665-3674.
67. Benndorf R, Martin JL, Kosakovsky Pond SL, Wertheim JO. Neuropathy- and myopathy-associated mutations in human small heat shock proteins: Characteristics and evolutionary history of the mutation sites. Mutat Res Rev Mutat Res. 2014;761:15-30.
68. Benjamin IJ, Guo Y, Srinivasan S, Boudina S, Taylor RP, Rajasekaran NS, et al. CRYAB and HSPB2 deficiency alters cardiac metabolism and paradoxically confers protection against myocardial ischemia in aging mice. Am J Physiol Heart Circ Physiol. 2007;293(5):H3201-H3209.
69. Tannous P, Zhu H, Johnstone JL, Shelton JM, Rajasekaran NS, Benjamin IJ, et al. Autophagy is an adaptive response in desmin-related cardiomyopathy. Proc Natl Acad Sci U S A. 2008;105(28):9745-9750.
70. Zhang X, Min X, Li C, Benjamin IJ, Qian B, Zhang X, et al. Involvement of reductive stress in the cardiomyopathy in transgenic mice with cardiac-specific overexpression of heat shock protein 27. Hypertension. 2010;55(6):1412-1417.
71. Jiaox X, Khan SY, Irum B, Khan AO, Wang Q, Kabir F, et al. Missense mutations in CRYAB are liable for recessive congenital cataracts. PLoS One. 2015;10(9):e0137973.
72. Dou G, Sreekumar PG, Spee C, He S, Ryan SJ, Kannan R, et al. Deficiency of αB-crystallin augments ER stress-induced apoptosis by enhancing mitochondrial dysfunction. Free Radic Biol Med. 2012; 53:1111-1122.
73. Laganowsky A, Benesch JL, Landau M, Ding L, Sawaya MR, Cascio D, et al. Crystal structures of truncated alphaA and alphaB crystallins reveal structural mechanisms of polydispersity important for eye lens function. Protein Sci. 2010;19(5):1031-1043.
74. Brewer AC, Mustafi SB, Murray TV, Rajasekaran NS, Benjamin IJ. Reductive stress linked to small HSPs, G6PD, and Nrf2 pathways in heart disease. Antioxid Redox Signal. 2013;18(9):1114-1127.
75. Zeng L, Tan J, Lu W, Lu T, Hu Z. The potential role of small heat shock proteins in mitochondria. Cell Signal. 2013;25(11):2312-2319.
76. Ganguly S. Mitra A, Sarkar S. Role of α-crystallin B in regulation of stress induced cardiomyocyte apoptosis. Cardiovasc Hematol Agents Med Chem. 2014;12(2):60-65.

77. Kötter S, Unger A, Hamdani N, Lang P, Vorgerd M, Nagel-Steger L, et al. Human myocytes are protected from titin aggregation-induced stiffening by small heat shock proteins. J Cell Biol. 2014;204(2):187-202.
78. Lutsch G, Vetter R, Offhauss U, Wieske M, Gröne HJ, Klemenz R et al. Abundance and location of the small heat shock proteins HSP25 and αB-crystallin in rat and human heart. Circulation. 1997;96(10):3466-3476.
79. Maloyan A, Sayegh J, Osinska H, Chua BHL, Robbins J. Manipulation of death pathways in desmin-related cardiomyopathy. Circ Res. 2010;106:1524-1532.
80. Wilhelmus MM, Boelens WC, Otte-Höller I, Kams B, de Waal RM, Verbeek MM. Small heat shock proteins inhibit amyloid-beta protein aggregation and cerebrovascular amyloid-beta protein toxicity. Brain Res. 2006;1089(1):67-78.
81. van de Klundert FA, Gijsen ML, van de IJssel PR, Snoeckx LH, de John WW. alpha B-crystallin and hsp25 in neonatal cardiac cells -- differences in cellular localization under stress conditions. Eur J Cell Biol. 1998;75(1):38-45.
82. Christopher KL, Pedler MG, Shieh B, Ammar DA, Petrash JM, Mueller NH. Alpha-crystallin-mediated protection of lens cells against heat and oxidative stress-induced cell death. Biochim Biophys Acta. 2014;1843(2):309-315.
83. Wistow G. The human crystallin gene families. Hum Genomics. 2012;6:2.6
84. Su H, Wang X. The ubiquitin-proteasome system in cardiac proteinopathy: a quality control perspective. Cardiovas Res. 2010;85:253-262.
85. Kamradt MC, Chen F, Sam S, Cryns VL. The small heat shock protein alpha B-crystallin negatively regulates apoptosis during myogenic differentiation by inhibiting caspase-3 activation. J Biol Chem. 2002;277(41):38731-38736.
86. Yan LJ, Christians ES, Liu L, Xiao X, Sohal RS, Benjamin IJ. Mouse heat shock transcription factor 1 deficiency alters cardiac redox homeostasis and increases mitochondrial oxidative damage. EMBO J. 2002;21(19):5164-5172.
87. Hishiya A, Salman MN, Carra S, Kampinga HH, Takayama S. BAG3 directly interacts with mutated alphaB-crystallin to suppress its aggregation and toxicity. PLoS One. 2011;6(3):e16828.

APPENDIX A: Characterization of the Cardiac Overexpression of HSPB2 Reveals Mitochondrial and Myogenic Roles Supported by a Cardiac HspB2 Interactome

CONTRIBUTIONS

In addition to my contributions to the CryAB interactome, I also contributed to the following study on the related protein chaperone HspB2. My contributions to this publication included the following:

Table 2: Dependency test transformations for the HspB2 Y2H screen and sequence analysis of HspB2 protein clientele to determine truncations within library plasmid constructs.

Table 3: Performed and verified Y2H assay data to demonstrate non-redundancy in HspB2 vs. CryAB protein clientele.

Figure 6: Created the HspB2 interactome network for all dependent HspB2 Y2H putative clientele.

Figure 7C: Performed *in vivo* heat shock assays to provide evidence for GAPDH as a putative binding partner for HspB2, identified in the Y2H screen.

PLOS | ONE

RESEARCH ARTICLE

Characterization of the Cardiac Overexpression of *HSPB2* Reveals Mitochondrial and Myogenic Roles Supported by a Cardiac HspB2 Interactome

Julianne H. Grose[1]*, Kelsey Langston[1], Xiaohui Wang[2], Shayne Squires[2,3], Soumyajit Banerjee Mustafi[2], Whitney Hayes[1], Jonathan Neubert[1], Susan K. Fischer[4], Matthew Fasano[4], Gina Moore Saunders[2], Qiang Dai[3], Elisabeth Christians[2], E. Douglas Lewandowski[4], Peipei Ping[5], Ivor J. Benjamin[2,3]*

1 Microbiology and Molecular Biology Department, Brigham Young University, Provo, UT, 84602, United States of America, **2** Laboratory of Cardiac Disease, Redox Signaling and Cell Regeneration, Division of Cardiology, University of Utah School of Medicine, Salt Lake City, UT, 84132, United States of America, **3** Division of Cardiovascular Medicine, Dept. of Medicine, Medical College of Wisconsin, Milwaukee, WI, 53226, United States of America, **4** Program in Integrative Cardiac Metabolism, Center for Cardiovascular Research, University of Illinois at Chicago College of Medicine, Chicago, IL, 60612, United States of America, **5** UCLA Departments of Physiology, Medicine, and Cardiology, Los Angeles, CA, 90095, United States of America

* julianne_grose@byu.edu (JHG); ibenjamin@mcw.edu (IJB)

OPEN ACCESS

Citation: Grose JH, Langston K, Wang X, Squires S, Mustafi SB, Hayes W, et al. (2015) Characterization of the Cardiac Overexpression of *HSPB2* Reveals Mitochondrial and Myogenic Roles Supported by a Cardiac HspB2 Interactome. PLoS ONE 10(10): e0133994. doi:10.1371/journal.pone.0133994

Editor: Harm H Kampinga, UMCG, NETHERLANDS

Received: October 3, 2014

Accepted: July 3, 2015

Published: October 14, 2015

Data Availability Statement: All HspB2 interactome data are available from the Biological General Repository for Interaction Datasets database (BioGrid, thebiogrid.org). Data can be accessed using the PubMED ID.

Funding: This work was supported by the National Institute of Health (NIH): 2R01 HL063834-06, 5R01HL074370-03, and NIH 5DP1OD006438-03 to I. J.B, and the Leducq Transatlantic Network "Redox and Nitrosative Regulation of Cardiac Remodeling: Novel Therapeutic Approaches for Heart Failure" to I. J.B.

Abstract

Small Heat Shock Proteins (sHSPs) are molecular chaperones that transiently interact with other proteins, thereby assisting with quality control of proper protein folding and/or degradation. They are also recruited to protect cells from a variety of stresses in response to extreme heat, heavy metals, and oxidative-reductive stress. Although ten human sHSPs have been identified, their likely diverse biological functions remain an enigma in health and disease, and much less is known about non-redundant roles in selective cells and tissues. Herein, we set out to comprehensively characterize the cardiac-restricted Heat Shock Protein B-2 (HspB2), which exhibited ischemic cardioprotection in transgenic overexpressing mice including reduced infarct size and maintenance of ATP levels. Global yeast two-hybrid analysis using HspB2 (bait) and a human cardiac library (prey) coupled with co-immunoprecipitation studies for mitochondrial target validation revealed the first HspB2 "cardiac interactome" to contain many myofibril and mitochondrial-binding partners consistent with the overexpression phenotype. This interactome has been submitted to the Biological General Repository for Interaction Datasets (BioGRID). A related sHSP chaperone HspB5 had only partially overlapping binding partners, supporting specificity of the interactome as well as non-redundant roles reported for these sHSPs. Evidence that the cardiac yeast two-hybrid HspB2 interactome targets resident mitochondrial client proteins is consistent with the role of HspB2 in maintaining ATP levels and suggests new chaperone-dependent functions for metabolic homeostasis. One of the HspB2 targets, glyceraldehyde 3-phosphate dehydrogenase (GAPDH), has reported roles in HspB2 associated phenotypes including cardiac

Competing Interests: The authors have declared that no competing interests exist.

ATP production, mitochondrial function, and apoptosis, and was validated as a potential client protein of HspB2 through chaperone assays. From the clientele and phenotypes identified herein, it is tempting to speculate that small molecule activators of HspB2 might be deployed to mitigate mitochondrial related diseases such as cardiomyopathy and neurodegenerative disease.

Introduction

Studies of molecular chaperones and their regulatory pathways are among the most challenging and illuminating ones for understanding the hierarchical integration among genotype-phenotype relationships, biological systems and cellular networks [1–3]. Among their multifaceted functions, molecular chaperones transiently interact with other proteins to facilitate protein folding, translocation, and degradation, all of which contribute to the quality control requirements for maintaining homeostasis of the proteome (termed "proteostasis"). In parallel, systems biology has emerged as a powerful organizing principle for integrating biophysical properties, creating biological functions of complex webs of macromolecular interactions (termed the "interactome" network). How molecular (HSP) chaperones might be inextricably linked to interactome networks and interrelated organelles in cardiac health and disease remain poorly defined.

In recent decades, attempts to understand genotype-phenotype relationships have been significantly aided by the characterization of inheritable Mendelian traits and experimental genetic maneuvers such as transgenesis and gene targeting in model organisms. In the present context, owing to the head-to-tail genomic organization of the genes encoding HspB2 (also known as Myotonic Dystrophy Protein Kinase Binding Protein, MKBP [4]) and HspB5 (also known as alpha-B crystallin, CryAB), Brady and collaborators had originally set out to create the single *HSPB5* knockout but inadvertently eliminated both genes resulting in double knockout (DKO) mice [5]. Because DKO mice survived into adulthood, these initial studies were the first to illustrate that both *HSPB2* and *HSPB5* deficiency was dispensable for early and postnatal development with relative mild effects of cardiac hypertrophy (~10% heart weight) in adult hearts, perhaps due to redundancy among sHSPs [5, 6].

Further characterization of DKO hearts by Morrison et al. (2004) revealed severely diminished levels of total reduced glutathione (GSH, 56%) and increased oxidized glutathione (GSSG) when compared with wild type (WT) mice, suggesting that DKO hearts are under higher levels of oxidative stress. Evidence of sHSPs in redox state regulation is based on our earlier work that showed that knockout of heat shock transcription factor 1 (HSF1) in mice not only lowered basal levels of HspB5 expression but also decreased GSH content [7]. Whereas *HSPB5* deficiency could contribute to the lower GSH in the DKO mice, these findings could not exclude a role for HspB2, which not only interacts with the outer membrane of mitochondria [8] but has been hypothesized to regulate mitochondria energetics [9]. Taken together, these studies support the general notion that genotype-phenotype relationships are governed by higher order complexities, which, in part, are related to variable expressivity, genetic modifiers, incomplete penetrance, redundancy, and age-related conditions.

In an attempt to unmask tissue-specific roles of HspB2, which can be hidden by overlapping sHSP function, we report here on the phenotypes of cardiac *HSPB2* overexpression (OE) as well as a large-scale cardiac HspB2 protein interactome. HspB2 OE mice (HSPB2cTg) protected cells from ischemia/reperfusion (I/R) and enhanced mitochondrial recovery with improved ATP levels at reperfusion. These results were supported by a cardiac protein

interactome for HspB2 achieved through Y2H and co-immunoprecipitation (co-IP) approaches. A combined total of 149 HspB2 binding partners are reported, many of which are mitochondrial. This interacome showed specificity for HspB2 in that HspB5 binds only a subset of HspB2 binding partners. The HspB2 interactome was further supported by preliminary validation of an HspB2 target, glyceraldehyde 3-phosphate dehydrogenase (GAPDH) as an *in vivo* client. Many of these newly discovered HspB2 binding partners are linked to myopathies or neurodegenerative disease, suggesting a role for HspB2 in these debilitating human conditions.

Materials and Methods

HSPB2cTg mouse line and controls

Human cDNA of *HSPB2* was amplified and inserted under the control of the α-myosin heavy chain (α-MHC) (Fig 1A) [10]. Transgenic [11] mice were generated by microinjection of fertilized embryos and maintained in a mixed genetic background of the C57Bl/6J and 129S6 strains. Genotyping of the HSPB2cTg mice was performed by PCR using the following primers: forward AGGCAGGGAAGTGGTGGTGTAGG and reverse GGCCTTCTCCGAAGCGCTGC, respectively. Mice overexpressing cardiac *HSPB2* are referred to as HSPB2cTg and their corresponding Flox wild type control littermates as HSPB2NTg, whereas the cardiac *HSPB2* KO and littermate control are HSPB2cKO and HSPB2wt, respectively.

Western blot analysis of heart tissue

Mouse hearts were removed and rinsed with ice cold PBS as previously described from our laboratory [9]. The tissue was minced into small pieces and homogenized in 0.25 ml of 50 mM Tris–HCl, pH 7.4, 150 mM NaCl, 1 mM EDTA, 1% Triton X-100. Following incubation on ice for 30 m, the lysates were clarified by centrifugation at 12,000 rpm for 10 m at 4°C. The supernatants were used as detergent-soluble fractions. The resulting pellet fractions were washed twice and sonicated in 100 μl 1× SDS buffer (50 mM Tris–HCl, pH 6.8, 2% SDS, 100 mM DTT, 10% Glycerol) for 30 s as detergent-insoluble fractions. Protein concentration was determined and western blots were performed using anti-sHSP (HspB1, HspB2, HspB5, HspB6 and HspB8) with anti-histone3 and anti-GAPDH as loading controls as previously described [9]. All antibodies were commercially available as described [9], with the exception of the HspB2 antibody which we purchased through 21st Century Biochemicals using the following peptide sequence: CPATAEYEFANPSRLGEQ-amide. In addition, anti-HspB3 antibodies were obtained from StressMarq Biosciences Inc. and HspB3 levels were determined on a separate western blot.

Ischemia reperfusion *in vivo*

Age-matched male mice (10–12 week-old) selected for the study were bred according to approved guidelines of Institutional Animal Care and Use Committee (IACUC) at the University of Utah. Animals were anesthetized with a ketamine (100mg/kg) and xylazine (0.5mg/kg) cocktail administered intraperitoneally. Following tracheal intubation of the trachea, the mouse was placed on a small rodent ventilator at a respiratory rate of 120 breaths per m and 0.25 ml tidal volume. To maintain temperature control, animals were placed on a water-heated surgical bed (E-Z Anesthesia, US State) with temperature setting at 37°C. Under sterile conditions, the heart was exposed through the 4th intercostal space and a 7–0 suture, attached to a balloon, was applied around left descending coronary artery [12]. The cardiac ischemia was introduced by inflating the balloon while using continuous electrocardiographic (ECG)

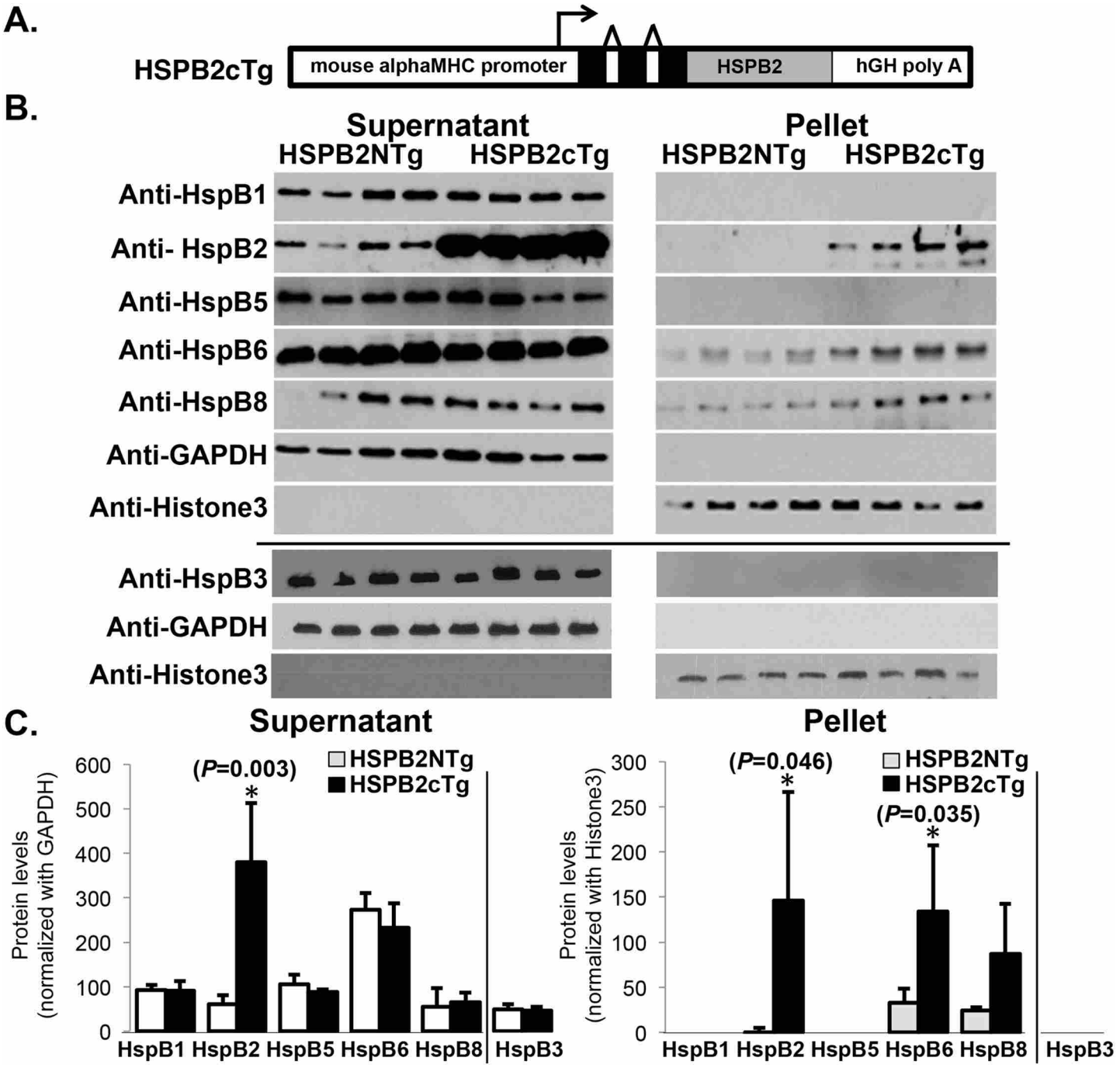

Fig 1. Generation of *HSPB2* cardiac specific overexpressors and effects on sHSP expression in transgenic mice (HSPB2cTg). (A) A schematic diagram illustrates the human heat shock protein B2 (HSPB2) under the control of the α-myosin heavy chain (α-MyHC) promoter: the 3 black boxes in the promoter represent noncoding exons in the 5'-untranslated region [10] and polyA splicing is provided by the human growth hormone sequences downstream of the inserted cDNA (hGH). **(B)** Representative Western blots of cardiac samples of transgenic (HSPB2cTg) mice and non-transgenic (HSPB2NTg) littermates (n = 4 animals per group) prepared as detergent soluble (supernatant) and non-soluble (pellet) portions, respectively. Protein levels of HSPB2 expression is markedly elevated (~4 x fold) in the HSPB2cTg hearts compared with non-transgenic (HSPB2NTg) littermates when assessed by western blot using anti-HspB2 antibodies [9]. Representative small heat shock proteins (sHSPs—HspB1, HspB3, HspB5, HspB6 and HspB8) exhibit similar levels in detergent soluble extracts, while HspB6 is significantly elevated in detergent insoluble fractions. Protein concentration was determined and western blots were performed using anti-sHSP (HspB1, HspB2, HspB5, HspB6 and HspB8) with anti-histone3 and anti-GAPDH as loading controls as previously described [9]. In addition, anti-HSPB3 antibodies were obtained from StressMarq Biosciences Inc and HspB3 levels were determined separately, which is indicated by a black line. **(C)** Densitometry-based quantification of the levels of protein in the immunoblots in Fig 1B. * $P<0.05$ when compared with corresponding HSPB2NTg group.

doi:10.1371/journal.pone.0133994.g001

monitoring. Myocardial ischemia was monitored by the appearance of pale color of the lateral myocardial wall to the apex, S-T segment elevation, widening of the QRS, and/or ventricular arrhythmias on continuous ECG. The duration of ischemia lasted 45 m before the balloon was deflated and suture tie removed to initiate reperfusion. The chest cavity was closed before extubation of the animal.

Assessment of infarction size

Twenty-four hours (h) after reperfusion start, the mice were euthanized, the hearts were excised and cannulated with a 20-gauge needle through the aorta, and then the hearts were perfused with Krebs-Henseleit solution [13]. The LAD was sutured and tied at the site of previous occlusion to permit perfusion of the aorta with 5% Evans Blue, which stains the non-risk area dark blue. The hearts were trimmed to leave only the left ventricle, which was frozen and sliced into 6–7 pieces. Staining in a 1% solution of 2,3,5-triphenyltetrazolium chloride (TTC) at 37°C for 30 m resulted in viable tissue and infarct tissue appearing in red and white colors, respectively. Each piece of heart was photographed (Dino-Lite) on both sides and images were processed with ImagePro Plus 7.0 software. The infarction mass of each piece was calculated as white (infarcted) average of both sides, divided by the sum of red plus white [14] average of both sides, then multiplied by the mass of that piece. Total infarction was calculated by the sum of the mass of infarction divided by the sum of the mass of risk as previously described from our laboratory [13].

Troponin I measurement

Mouse blood samples were set for clotting before centrifugation for 15 m at 800g. The serum was collected, diluted in series from 1:10 to 1:1000, and then loaded into a 96-well sample plate from the High Sensitive Mouse Cardiac Troponin-I kit (Life Diagnostics, Inc.). Troponin I level was measured at 450 nm by following the manufacturers recommendations.

Mitochondria swelling assay

Mitochondria were isolated from mouse hearts as previously described [9] and diluted to 250 ug/ml in mitochondria swelling buffer containing 120 mM KCl, 10 mM Tris, 5 mM KH_2PO_4. The mitochondria were equilibrated for 5 m at room temperature and 250 uM $CaCl_2$ was loaded to induce swelling. Data was read at 540 nm.

Bioenergetics consequences

For isolated heart studies and ^{31}P NMR data collection, mice were heparizined (50 U/10 g, i.p.) and anesthetized (ketamine, 80 mg/kg, plus xylazine, 12 mg/kg, i.p.). Excised hearts were retrogradely perfused (60 mm Hg) with modified Krebs–Henseleit buffer (118.5 mM NaCl, 4.7 mM KCl, 1.5 mM $CaCl_2$,1.2 mM$MgSO_4$ and 1.2 mMKH_2PO_4) equilibrated with 95% O_2/5% CO_2, at 37°C, and containing 0.4 mM palmitate/fatty acid free albumin complex (3:1 molar ratio) and 10 mM glucose [15]. A water-filled latex balloon was placed into the left ventricle and set to a diastolic pressure of 5 mm Hg to provide a physiological load.

The isolated perfused hearts were placed inside a 10 mm broadband NMR radiofrequency probe within a 14.1 T NMR magnet (Bruker Biospin, Billerica, MA) for collection of sequential, ^{31}P NMR spectra. ^{31}P NMR data provided detection of high-energy phosphate content, including phosphocreatine (PCr) and ATP throughout an I/R protocol. Following collection of baseline, pre-ischemic baseline NMR data, perfused hearts were subjected to 16 m of global ischemia at 37°C, followed by 32 m of reperfusion. Relative ATP content in each heart during

the pre-ischemic, ischemic, and reperfusion periods was determined from the signal intensity of the β-phosphate resonance signal at -16 ppm. Time-averaged spectra were collected at 243 MHz from the intact beating hearts in 4 m time blocks using 64 scans with a 45° flip angle and 2 s interpulse interval, using previously described data collection and processing/analysis schemes for high-energy phosphate levels and intracellular pH [15–17].

Y2H screen and HspB2 dependency tests

Yeast harboring a human cardiac cDNA Y2H library (Clontech) were mated by the standard Matchmaker mating protocol (Clontech) to yeast harboring a full-length human *HSPB2* plasmid (pJG591). The bait plasmid (pJG591) was constructed by standard cloning techniques in which *HSPB2* was amplified by PCR from a human template using primers GGCGAATTCT CGGGCCGCTCAGTGCCAC and GGCGGATCCTCAGGGCTCAACTATGGCTGCC and cloned into the EcoR1/BamHI sites of pGBKT7 (Clontech) for fusion to the Gal4 DNA binding domain at the N-terminus; the C-terminus is native. Over 22 million yeasts were mated, from which 10,000 colonies arose on SD-Trp-Leu plus Aureobasidin (Clontech) selection plates. Colonies were then patched to alternate Y2H selection plates (SD-Trp-Leu-His-Ade) for phenotype validation through alternate transcriptional reporters (HIS and ADE). The plasmid inserts of the library were identified for over 1,000 colonies arising on the SD-Trp-Leu-His-Ade plates by colony PCR (primer AGATGGTGCACGATGCACAG and CTATTCGATGATGAAGATACCCCA CC) followed by sequencing and NCBI BLASTN [18] analysis. A subset of library plasmids were purified and secondarily subjected to false positive analysis. Briefly, plasmids were retransformed into yeast harboring the *HSPB2*-bait plasmid or empty bait plasmid, selected on SD-Trp-Leu and streaked to SD-Trp-Leu-His-Ade to test for an *HSPB2*-dependent interaction. For HspB2 specificity testing, *HSPB5* was PCR amplified from a human template and cloned into the EcoRI/SalI sites of pGBKT7 (Clontech) using primers GGCGAATTCGACATCGCCA TC CACCACCCC and GGCGTCGACCTATTTCTTGGGGGCTGCGGTGAC. The *HSPB5* bait plasmid was then co-transformed with a library plasmid into yeast, selected on SD-Trp-Leu and streaked to SD-Trp-Leu-His-Ade to test for an *HSPB5*-dependent interaction.

Mitochondrial co-IP proteomics

Mitochondrial HspB2 was immunopurified from mice harboring either the wild type *HSPB2* (HSPB2wt), transgenic cardiac *HSPB2* (HSPB2cTg), or an *HSPB2* cardiac knockout (HSPB2cKO, [9]). For each group, mitochondria from four mouse hearts were combined, lysed in 0.1% NP-40 homogenization buffer, and 2 mg was incubated with anti-HspB2 antibodies [9]. The IP eluates were then fractionated on SDS-PAGE, excised and analyzed by LC-MS/MS. Samples had one biological replicate and two technical replicates. Technical replicates showed greater than 90% overlap. The raw data were analyzed by BioWorks (ThermoFisher Scientific, version 3.3.1 SP1) and proteins were identified using SEQUEST (ThermoFisher Scientific, version 3.3.1) and Scaffold (Proteome Software, version 3.3.3). At least two peptides and 99.0% protein confidence were required for protein algorithms; the global false discovery rate was approximately 0.1%.

Bioinformatic analysis of the HspB2 interactome

Cytoscape version 3.2.1 [19] was used to construct protein-protein interaction networks by retrieving previously identified interactions from the *mentha*, Reactome-Fls, Reactome, IntAct and MINT databases (partners reported for either human or mouse proteins) and mapping them into a single merged network. Gene Ontology analysis for the resulting networks was done using the Cytoscape ClueGO plugin [20]. Associated diseases were obtained using the

Online Mendelian Inheritance in Man (OMIM) database (McKusick-Nathans Institute of Genetic Medicine, Johns Hopkins University (Baltimore, MD). World Wide Web URL: http://omim.org/).

Protein purification and *in vitro* chaperone assays

GAPDH and *HSPB2* were cloned into pet15b (Novagen) for expression and purification. *GAPDH* was amplified from Origene plasmids SC118869 (accession number NM_002046) using the following primers, GGCCATATGGGGAAGGTGAAGGTCGGAGTC and GGCGG ATCCTTACTCCTTGGAGGCCATGTGGGC, and cloned into pet15b at the NdeI/BamHI sites. *HSPB2* was PCR amplified from pJG591 (using primers GGCCATATGTCGGGCCGCT CAGTGCC and GGCGGATCCTCAGGGCTCAACTATGGCTGCC) and cloned into pet15b at the NdeI/BamHI sites. Expression vectors were transformed into BL21 (DE3) *E. coli* (Novagen). Overnight cultures of transformants were diluted 1:500 into LB-AMP and grown for 3 h at 37°C. Expression was induced by 0.5 mM ITPG for 5 h at 37°C. Pelleted bacteria were then resuspended in 20 mL XWA lysis buffer (20 mM HEPES pH 7.4, 10 mM KCl, 1.5 mM $MgCl_2$, 1 mM EDTA pH 8.0, 1 mM EGTA, 300 mM NaCl, 1 mM beta-mercaptoethanol, pH 7.4, and Roche Complete Protease Inhibitor Cocktail). Cells were lysed using the Microfluidics M-110P homogenizer and debris pelleted at 15,000 rpm for 60 m. The supernatants were incubated with 250 μL of Ni-NTA agarose (Qiagen) for 2–3 h, beads were washed twice with 15–25 mL of XWA lysis buffer and then transferred to a column to be washed with 50 mL of lysis buffer containing 25 mM imidazole. Protein was eluted three times per sample with 0.3 mL of lysis buffer containing 250 mM imidazole and only 100 mM NaCl. The control, porcine citrate synthase was purchased from Sigma-Aldrich. Proteins were dialyzed into 40 mM HEPES-KOH buffer (pH 7.5) prior to *in vitro* chaperone assays. *In vitro* chaperone assays were conducted as previously described [21] by incubating 0.015 mM GAPDH with and without 0.105 mM HspB2 at high temperature (43°C) for 30 m in 40 mM HEPES-KOH buffer (pH 7.5). Seven-fold excess of chaperone compared to substrate is used because oligomerization is required for activity. Aggregates were then pelleted by centrifugation (13,000 rpm for 10 m in a microcentrifuge). For chaperone assays, both supernatant and pellet were analyzed by SDS-PAGE. Bands of the SDS-PAGE gel were analyzed using ImageJ software [22], and pellet to supernatant ratios calculated. Samples were run in triplicate and averaged.

In vivo chaperone assays

In vivo GAPDH chaperone activity assays were performed by transfecting plasmids bearing human HspB2 fused to myc peptide or the empty plasmid control (pCMV-myc) into C2C12 cells in a 6-well plate using 6.5 μL lipofectamine 2000 (Life Technologies) and manufacturers protocol. After 48 h at 37°C, cells were shifted to 45°C for 30 m and then placed back at 37°C for three h prior to lysis. Cells were resuspended in 300 μL lysis buffer (20 mM HEPES (pH 7.8), 10 mM KCl, 100 mM NaCl, 1 mM EDTA, 1 mM EGTA, 1% NP-40 and 10% glycerol), homogenized in a Dounce homogenizer ten times for five seconds on ice, and debris pelleted at 13,000 rpm for 5 m. The pellet was resuspended in 100 μL of 2X SDS buffer (125 mM Tris-Cl, pH 6.8, 0.01% (w/v) bromophenol blue, 100 mM fresh dithiothreitol, 2.5% (w/v) SDS, 25% glycerol) while 6X SDS buffer was added to the supernatant for a final concentration of 1X. Samples were boiled 2 m, analyzed by 12% SDS-PAGE and transferred to nitrocellulose paper. Proteins were visualized using anti-GAPDH antibody, anti-beta-Tubulin antibody, and anti-Myc antibody (all antibodies are from Cell Signaling Technologies). Protein bands were analyzed using ImageJ software [22] and pellet to supernatant ratios were calculated.

Data analysis, statistics and repository

Data are expressed as average ± standard deviation with student's *t*-test used for statistical analysis using two-tailed distribution and two-sample equal/unequal variance for all experiments with the exception of the NMR experiments, which were analyzed by ANOVA with Student-Newman Keuls post test [23]. Statistical significance was set at $p<0.05$. The HspB2 interactome described herein has been deposited in the Biological General Repository for Interaction Datasets (BioGrid, [24]) where it may be identified by PubMed ID.

Ethics statement

This study was carried out in strict accordance with the Guide for the Care and Use of Laboratory Animals of the National Institutes of Health. The protocol was approved by the Institutional Animal Care and Use Committee (IACUC) at the University of Utah (Permit Number: 10–05006). All surgery was performed under ketamine and xylazine cocktail anesthesia administered intraperitoneally, and all efforts were made to minimize suffering.

Results

Cardiac HSPB2 OE does not alter levels of other sHSPs

Cardiac-specific *HSPB2* overexpressor mice (HSPB2cTg) were generated using human *HSPB2* under the control of α-myosin heavy chain (α-MyHC) promoter as schematically shown in Fig 1A. Neither early lethality nor age-related cardiomyopathy was observed in these HSPB2cTg mice (data not shown). In detergent soluble extracts, protein levels of HSPB2 were markedly elevated (~4 fold) in hearts of HSPB2cTg mice (n = 4 animals per group) compared with non-transgenic littermates (HSPB2NTg) (Fig 1B, quantification in Fig 1C). To determine the effects of HSPB2cTg OE, the expression patterns of several other sHSPs were analyzed by western blot. The previously reported sHSP binding partners of HspB2 are HspB3 [25, 26], HspB5 [27] and HspB8 [28]. Protein levels of HspB1, HspB3, HspB5, HspB6 and HspB8 were all found to be unaltered in the soluble fractions, whereas HspB6 was modestly ($P = 0.035$) and HspB8 was non-statistically significantly elevated ($P = 0.064$) in the detergent insoluble fraction, respectively (Fig 1B and 1C). In contrast, protein levels of HspB1, HspB3 and HspB5 were unaffected by cardiac-specific *HSPB2* OE in intact mouse hearts.

HSPB2 OE protects mouse hearts from I/R injury

We have reported paradoxical effects of either *HSPB2* KO and/or *HSPB2*/*HSPB5* DKO in I/R studies [13, 29]. To investigate the specific role of HSPB2 in I/R injury, transgenic mice overexpressing cardiac *HSPB2* (HSPB2cTg) were compared with cardiac *HSPB2* KO mice (HSPB2cKO) and their littermate controls (HSPB2NTg and HSPB2wt respectively, n = 9–11 per group). Mouse hearts of HSPB2cTg (n = 11), HSPB2cKO (n = 9) and their corresponding controls underwent 45 m of ischemia followed by 24 h of reperfusion *in situ*. The size of infarction in each mouse heart was analyzed as described in Materials and Methods. An infarction area of 35.4 ± 5.6% was significantly lower in HSPB2cTg mouse hearts compared with the infarction area of 48.7 ± 10.0% for the HSPB2NTg controls ($p< 0.0006$, Fig 2A and 2B). Both HSPB2cKO and the corresponding Flox control animals (HSPB2wt) developed similar sizes of heart infarction upon I/R *in situ*, 49.4 ± 12.1% vs. 48.8 ± 13.5% respectively. Of all cardiac markers, cardiac specific troponin-I is the most sensitive indicator for cardiomyocyte injury, and its amount in the blood correlates well with heart infarction size after microvascular obstruction [30]. In agreement with the smaller cardiac infarction size, HSPB2cTg animals had significantly lower troponin-I levels after I/R stress compared with HSPB2NTg controls (Fig

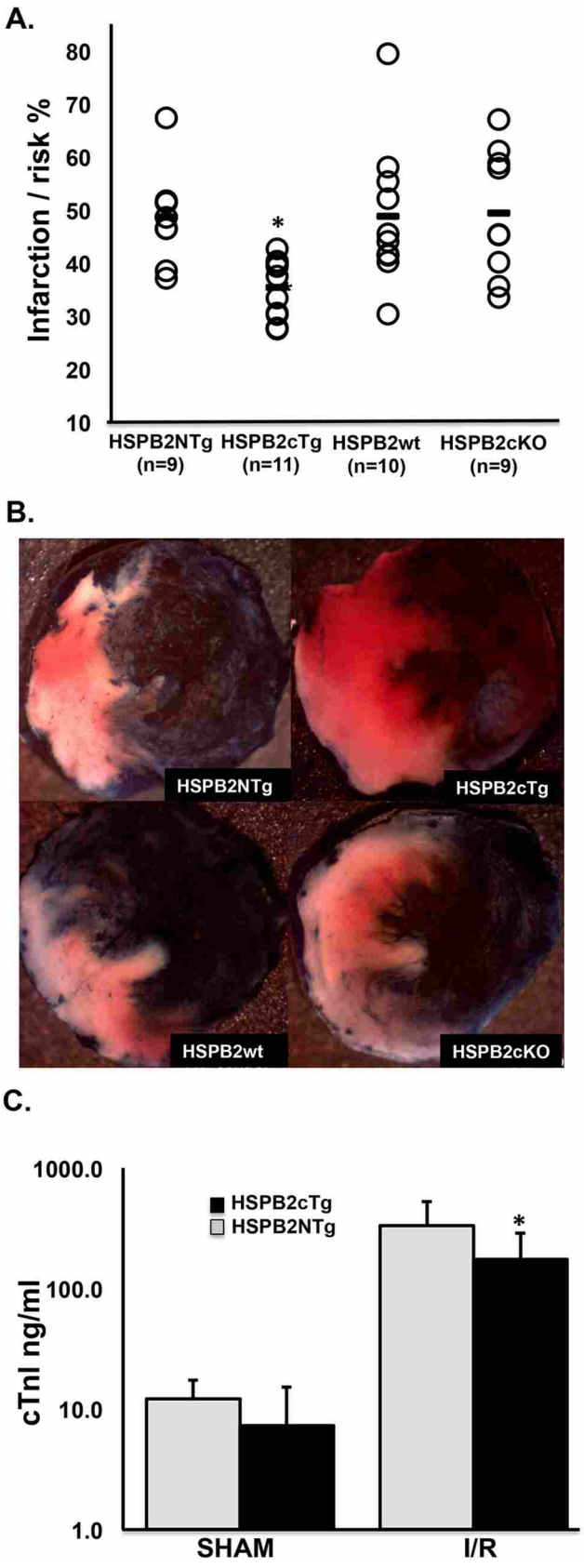
A.
Infarction / risk %
80
70
60
50
40
30
20
10
*
HSPB2NTg (n=9)
HSPB2cTg (n=11)
HSPB2wt (n=10)
HSPB2cKO (n=9)
B.
HSPB2NTg
HSPB2cTg
HSPB2wt
HSPB2cKO
C.
cTnI ng/ml
1000.0
100.0
10.0
1.0
HSPB2cTg
HSPB2NTg
*
SHAM
I/R

Fig 2. *HSPB2* OE protects mouse hearts from ischemia/reperfusion (I/R) injury *in vivo*. (A) Quantification of mouse cardiac infarction/risk size 24 h post I/R surgery. Each circle represents one animal from the transgenic cardiac overexpressor (HSPB2cTg), the cardiac knockout (HSPB2cKO), or control groups (HSPB2NTg and HSPB2wt, respectively). The number of animals in each group is labeled in the figure. **(B)** Representative staining images of mouse cardiac infarction post I/R surgery indicating the decreased infarct size in HSPB2cTg animals compared to controls. The same groups of animals as A are shown. Non-risk, live, and infarction tissue stained dark blue, red and white respectively. I/R surgery and infarction size measurements were performed as described in *Material and Methods*. The duration of ischemia lasted 45 m before deflation of the balloon and suture tie to initiate reperfusion. Hearts were excised 24 h after reperfusion start, cannulized, and the aorta was perfused with 5% Evans Blue, which stained the non-risk area dark blue. **(C)** Cardiac specific troponin-I levels in mouse serum 24 h post I/R surgery indicate HSPB2 OE is cardioprotective. Mouse serum was diluted in series from 1:10 to 1:1000, and loaded into a 96-well sample plate from the High Sensitive Mouse Cardiac Troponin-I kit (Life Diagnostics, Inc.). Troponin I level was measured at 450 nm by following the manufacturers recommendations. * $P<0.05$ when compared with corresponding HSPB2NTg group.

doi:10.1371/journal.pone.0133994.g002

2C). Troponin-I levels were similar between HSPB2cTg and HSPB2NTg after sham surgery in these animals.

In addition to infarct size, the cardiac function of these animals was assessed with both echocardiography and left ventricle catheter (Table 1). Interestingly, echocardiographic studies revealed wall motion abnormality at 24-h time points post I/R in HSPB2NTg but not in HSPB2cTg animals, in support of smaller infarction size in the HSPB2cTg animals. In addition, cardiac ejection fraction appeared to be reduced only in the HSPB2NTg group, although the data did not achieve statistical significance. The hemodynamic data acquired by left ventricle catheter did not show any difference among groups.

Mitochondria function in HSPB2cTg mouse heart with I/R injury

We previously reported a deficit in the recovery of phosphocreatine (PCr) and ATP levels in the *HSPB2*-deficient mice following I/R stress, suggesting HspB2 protects mitochondrial function during I/R [9]. The ability of *HSPB2* OE to protect ATP synthesis was formally determined throughout the I/R protocol for each experimental group (HSPB2cTg, n = 7, HSPB2NTg, n = 5, HSPB2cKO, n = 7, and HSPB2wt, n = 6). Fig 3A–3C displays representative changes in NMR-detected high-energy phosphate compounds and comparisons of ATP content among

Table 1. Heart function in HSPB2cTg mouse with ischemia/reperfusion injury *in vivo*. Hemodynamic data is acquired by left ventricle catheter and analyzed by LabChart 7. Echocardiography is acquired with VisualSonics Vevo2100 imaging system. LV, left ventricle; SP, systolic pressure; DP, diastolic pressure; EDP, end diastolic pressure; HR, heart rate; LVEF, left ventricle ejection fraction; IR, ischemia/reperfusion. Each experiment group acquired by LV catheter contains at least 6 mice. Statistics and calculation of +dp/dt, -dp/dt and LVEF are described in *Materials and Methods*.

Groups	Sham		I/R	
	HSPB2NTg	HSPB2cTg	HSPB2NTg	HSBP2cTg
LV catheter				
Aorta SP	88.57 ± 23.28	76.41 ± 13.03	73.85 ± 6.38	72.35 ± 6.57
Aorta DP	61.90 ± 11.84	49.25 ± 20.21	50.43 ± 8.53	48.94 ± 9.36
LV SP	89.56 ± 19.61	78.74 ± 12.74	76.79 ± 6.12 *	72.89 ± 5.75
LV EDP	1.96 ± 2.17	2.15 ± 1.75	5.89 ± 2.61	4.97 ± 2.52
HR	328.37 ± 45.02	347.14 ± 39.60	335.02 ± 44.87	345.13 ± 59.35
+dp/dt	5834.53 ± 1650.23	6159.39 ± 2848.88	5196.99 ± 606.56	4785.15 ± 1140.38
-dp/dt	-4867.77 ± 1716.10	-5475.04 ± 1873.88	-4169.81 ± 565.11	-4220.02 ± 1011.12
Echo				
LVEF	0.700342461	0.78	0.66 ± 0.15	0.81 ± 0.12
Wall motion abnormality	0/1	0/1	3/8	0/4

doi:10.1371/journal.pone.0133994.t001

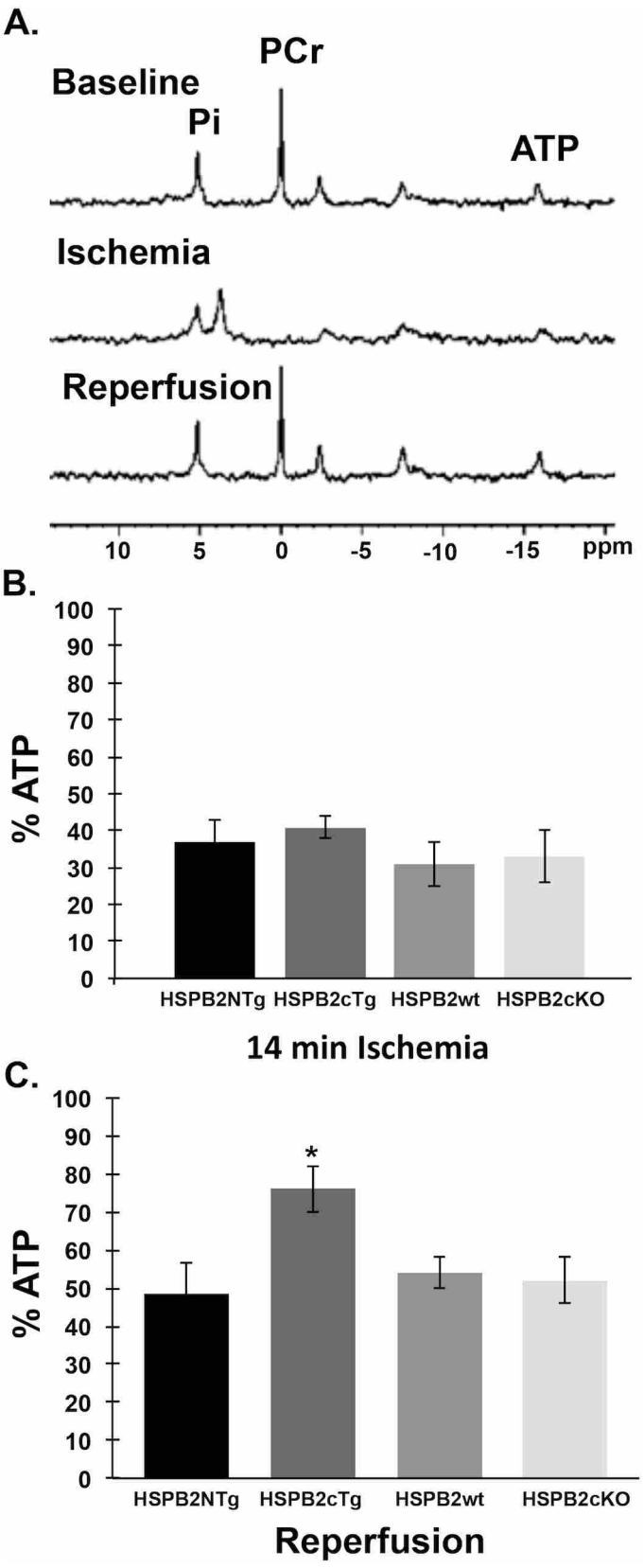
A.
PCr
Baseline
Pi
ATP
Ischemia
Reperfusion
10
5
0
-5
-10
-15
ppm
B.
% ATP
100
90
80
70
60
50
40
30
20
10
0
HSPB2NTg
HSPB2cTg
HSPB2wt
HSPB2cKO
14 min Ischemia
C.
% ATP
*
HSPB2NTg
HSPB2cTg
HSPB2wt
HSPB2cKO
Reperfusion

Fig 3. Mitochondrial protection in HSPB2cTg mouse heart with ischemia/reperfusion (I/R) injury. (A) Representative ^{31}P NMR spectra of a transgenic HSPB2 overexpressor (HSPB2cTg) heart taken at baseline before ischemia, at 14 m of ischemia, and at 32 m of reperfusion. Phosphocreatine (PCr) was depleted during ischemia but rapidly recovered upon reperfusion in all groups. Note loss and recovery of ATP content, as represented by the only resonance that is uncontaminated from signal from ADP and AMP, which is the β-phosphate group at -16 ppm. The peak at 3.5 ppm is signal from the intracellular inorganic phosphate (Pi), which shifts to lower values due to the increasing concentration of diprotonated Pi versus mono-protonated Pi as the pH becomes increasingly acidic during ischemia. The peak at 5 ppm is a combined signal from both extracellular pH and residual buffer surrounding and in the isolated perfused heart, which also contains inorganic phosphate and reflects neutral pH. **(B)** ATP content after 14 m of ischemia was reduced similarly in all groups, as shown as a percentage of pre-ischemic content at 100%. (C) Recovery of ATP content upon reperfusion was greater in HSPB2cTg hearts than in the knockout hearts (HSPB2KO) or control groups (HSPB2NTg or HSPB2wt, respectively). Values shown are at 2 min reperfusion and did not change significantly from these over the remaining duration of the reperfusion period. * $P<0.05$ when compared with corresponding HSPB2NTg group.

doi:10.1371/journal.pone.0133994.g003

groups at the end of ischemia and upon reperfusion. Although no difference in PCr content occurred among experimental heart groups at any time throughout the protocol, consistent with the role of PCr as a phosphagen that responds to reoxygenation of viable mitochondria following non-lethal ischemia, we did observe a difference in ATP content in the HSPB2cTg mice.

As shown in Fig 3B, there was no significant difference in ATP loss during the ischemic period, demonstrating that all groups held similar susceptibility to impaired energy production during zero flow ischemia. Since oxidative mitochondrial energy production was essentially shut down during ischemia, the presence or absence of HSPB2 did not affect ATP levels during ischemia. ATP depletion was required to support the same energy demands for residual cell function during the ischemic insult among all experimental groups. The similar levels of ATP hydrolysis ($ATP + H_2O \rightarrow ADP + Pi + H^+$) that occurred during ischemia among all groups is consistent with the similar reduction in intracellular pH among the groups, from a preischemic baseline of 7.1 to the final pH range observed at the end of ischemia of 6.2–6.1. The peak at 3.5 ppm is signal from the intracellular inorganic phosphate (Pi), which shifts to lower values due to the increasing concentration of diprotonated Pi versus mono-protonated Pi as the pH becomes increasingly acidic during ischemia. The peak at 5 ppm is a combined signal from both extracellular pH and residual buffer surrounding and in the isolated perfused heart, which also contains inorganic phosphate and reflects neutral pH.

In contrast to the similarities observed during ischemia, ATP content and recovery was augmented in HSPB2cTg hearts upon early reperfusion in comparison to all other groups (Fig 3C, ANOVA with Student-Newman Keuls post test). These data show a 41% to 57% increase in the postischemic mean ATP content of the HSP2cTg hearts over the other groups. The initial ATP content seen upon reperfusion persisted throughout the entire assay period in all groups, with no significant change over time (Repeated Measures ANOVA). These results strongly support a role for *HSPB2* alone via cardioprotection during ischemia and sustained mitochondrial function upon reperfusion.

Kadono et al. suggests that the lack of *HSPB2* and *HSPB5* preconditions myocytes for damage due to increased calcium sequestration by the mitochondria, a known step in the inducement of mitochondria permeability transition [31, 32]. Mitochondrial swelling assays were performed in the HSPB2cTg and HSPB2NTg mice to determine if this calcium response is dependent on HspB2. Although mitochondria isolated from HSPB2cTg hearts (n = 4) trended toward lower levels of swelling in response to calcium, the differences were not significant when analyzed by student's t-test (S1 Fig).

An unbiased Y2H screen for HspB2 substrates reveals surprising specificity for mitochondrial binding partners

The foregoing findings for HspB2-associated phenotypes predicts protective roles for HspB2 activators and strongly suggest that HspB2 has hitherto unknown molecular clientele critical to mitochondrial health, however mitochondrial HspB2 clientele are unreported. To identify these client proteins, we performed an unbiased, large-scale Y2H screen using a human heart cDNA Y2H library (Clontech) as prey and human *HSPB2* as bait. From over 22 million mated yeasts, approximately 10,000 putative interactions were detected indicating only one of every ~2,000 mattings resulted in a positive Y2H interaction, suggesting a high degree of specificity of *HSPB2* targets. Over 1,000 library plasmids were re-plated for phenotypic verification and subsequently sequenced to identify the compendium of interacting partners. As expected for a molecular chaperone, such sequencing revealed a large number of interacting partners (437 unique hits). These binding partners were further grouped by their frequencies, depending on if they were retrieved only once (S1 Table, "single-hit" list) or multiple times (Table 2, "multi-hit" list) in the Y2H screen.

The advantage of high sensitivity in the Y2H method comes at the expense of specificity (i.e., high false positive rates) [12, 33, 34]. To test the overall reliability of the Y2H, a subset of the putative binding partners were tested for *HSPB2*-dependence. Briefly, prey plasmids encoding 90 of the putative HspB2 binding partners (49 from the multi-hit list and 41 from the single-hit list) were purified from yeast and reintroduced into naïve yeast harboring either the empty bait plasmid or the *HSPB2* bait plasmid. A remarkable 81.6% of the 49 multi-hit library plasmids tested showed a positive Y2H result that was dependent on *HSPB2* (i.e., growth with only the *HSPB2* bait, not the empty bait plasmid), 10.2% were false positives (i.e., growth either with or without HspB2), and 8.2% were true negatives (i.e., no growth with either HspB2 or the empty bait plasmid). In contrast, we found that only 51.2% of the 41 single hit plasmids harbored HspB2 dependent-binding partners, 12.2% were false positives, and another 36.6% were true negatives. The multi-hit binding partners with an 82% rate for validation were then sequenced to determine frame, and are used for all subsequent studies and analysis due to its reliability.

The Y2H screen identifies non-redundant client proteins of cytosolic HspB2 and HspB5

In order to test the specificity of the HspB2 Y2H interactome, the interactome was compared to the recently published HspB1 (Hsp27) interactome in which 228 binding partners were identified by Katsogiannou et al. from large-scale Y2H screens of testis and Hela cancer cell libraries [35]. Of the 84 proteins on the high confidence multi-hit HspB2 Y2H list, only two were identified as HspB1 binding partners (EIF4A2 and GARS), suggesting specificity of the HspB2 and HspB1 interactomes. However, different Y2H libraries were used in these studies that could also account for the variances. To further verify specificity of HspB2, a subset of HspB2 binding partners were tested for their ability to interact with a more closely related HSP, HspB5 (Fig 4A, Table 3). Remarkably, HspB2 was specific for a majority of the binding partners tested (eight of the 12 binding partners, or 67%), with only four displaying both HspB2 and HspB5 binding (including HspB5 itself, which was used as a positive control). In addition, two of these four HspB2 and HspB5 binding partners gave a much stronger Y2H result with HspB2 than HspB5. These findings validate the specificity of HspB2 in the large-scale Y2H screen and provide further *in vivo* support for non-redundant clientele among sHSPs, consistent with expression and phenotypic analyses that have revealed unique functions for HspB5 and HspB2 chaperones [6].

Table 2. Putative HspB2 binding partners retrieved from the Y2H screen reveal a role in muscle and mitochondrial maintenance. Proteins retrieved multiple times from a Y2H screen for HspB2 binding partners (84 hits) are given along with the following information: protein name, UniProt [73, 74] protein accession number (hyperlink), gene symbol, primary cellular localization reported on HPRD [76] or UniProt, the number of times it was retrieved from the screen (# hits) and the amino acids corresponding to the library construct from the n-terminal amino acid to the c-terminal amino acid (if the terminal amino acid is not reached the total amino acids are given in parenthesis). In some cases the nucleotide fusion occurred before the initiating ATG and is indicated by the number of amino acids upstream of the start (for example, -12–136 for LGALS1 denotes 22 amino acids upstream of the ATG start to amino acid 136). Hits that did not correspond to a coding sequence are not listed and include the 3' region of ABLIM1, AXIN1, DYRK1A, FHL1, GPX3, HIPK2, NCAM1, PPAPDC3, PLXNA4, LRP10, SCN1B, SEC62, SGSM2, SLC25A4, SNTA1, SYNPO, TNIP1, USP28, and XIRP1 mRNA. The proteins are functionally categorized by their description on UniProt [73, 74] and/or GeneCards [73]. See supplementary S1 Table for a complete list of putative HspB2 binding partners retrieved from the Y2H screen only once.

Protein Name	UniProt Accession	Gene Symbol	Cellular Localization**	# hits	aa
Myofibril or Cytoskeleton Structure/Regulation					
Actin, alpha 1, skeletal muscle*	P68133	ACTA1	Cytoskeleton	8	253–377
Actin, beta	P60709	ACTB	Cytoskeleton	2	267–375
Actin, alpha, cardiac muscle 1	P68032	ACTC1	Cytoskeleton	37	84–377
Actin, gamma 1	P63261	ACTG1	Cytoskeleton	5	195–375
Capping protein (actin filament) muscle Z-line, alpha 2	P47755	CAPZA2	Cytoskeleton	3	117–286
Cardiomyopathy associated*	Q8N3K9	CMYA5	Cytoskeleton	4	3972–4069
Biglycan	P21810	BGN	Extracellular	2	191–368
Dynactin 1*	Q14203	DCTN1	Cytoskeleton	3	910–1144
Beta-enolase 3 (beta, muscle)*	P13929	ENO3	Cytoskeleton	7	85–434
Filamin C, gamma	Q14315	FLNC	Cytoskeleton	2	2608–2692
Myosin binding protein C, cardiac*	Q14896	MYBPC3	Cytoskeleton	11	945–1274
Myosin, heavy chain 6, cardiac muscle, alpha*	P13533	MYH6	Cytoskeleton	3	846–958
Myosin, heavy chain 7, cardiac muscle, beta*	A5YM51	MYH7	Cytoskeleton	14	1865–1935
Myomesin (M-protein) 2*	P54296	MYOM2	Cytoskeleton	6	1283–1465
Ryanodine receptor 2 (cardiac)	Q92736	RYR2	SR	3	1864–2359(4968)#
Titin-cap (telethonin)	O15273	TCAP	Cytoskeleton	6	92–167
Titin*	Q8WZ42	TTN	Cytoskeleton	5	1493–1890(5605)
Troponin I type 3*	Q6FGX2	TNNI3	Cytoskeleton	5	-17–210
WD repeat domain 1	O75083	WDR1	Cytoskeleton	3	221–466#
Fermentation/Respiration					
Acetyl-CoA acyltransferase 2*	P42765	ACAA2	Mito IM	5	208–397
Aldehyde dehydrogenase, mitochondrial	P05091	ALDH2	Mito Matrix		266–470#
Aldolase A, fructose-bisphosphate*	P04075	ALDOA	Cytoplasm	15	159–418
ATP synthase subunit alpha, mitochondrial, F1*	P25705	ATP5A1	Mito IM/Matrix	11	137–503
Cytochrome P450, family 1, subfamily B, polypeptide1	Q16678	CYP1B1	ER	4	436–543
Enolase 1, alpha-enolase	P06733	ENO1	Cytoskeleton	4	-36–341#
Electron-transfer-flavoprotein, alpha subunit*	P13804	ETFA	Mito Matrix	15	108–284
Glyceraldehyde 3-phosphate dehydro.*	P04406	GAPDH	Cytoplasm	19	21–293
Hydroxyacyl-CoA dehydro./3-ketoacyl-CoA thiolase*	P55084	HADHB	Mito IM/OM	5	205–452#
Methylcrotonoyl-CoA carboxylase beta chain	Q9HCC0	MCCC2	Mito Matrix	2	42–563
Malate dehydro. 1, NAD (soluble)	P40925	MDH1	Mito, Cytoplasm	2	68–352#
Cytochrome c oxidase subunit 1	P00395	MT-CO1	Mito IM	12	222–512
Cytochrome c oxidase subunit 2	P00403	MT-CO2	Mito IM	2	67–227
Cytochrome c oxidase subunit 3	P00414	MT-CO3	Mito IM	2	1–260
NADH dehydro. (ubiquinone) 1 alpha subcomplex 6*	P56556	NDUFA6	Mito IM	2	66–154
NADH dehydro. (ubiquinone) 1 alpha subcomplex, 13	Q9P0J0	NDUFA13	Mito IM	2	-5–144
Oxoglutarate (alpha-ketoglutarate) dehydro.*	A2VCT2	OGDH	Mito	2	907–1019
Phosphoglucomutase 1	P36871	PGM1	Cytoplasm	2	250–365#
Succinate dehydro. complex, subunit A*	D6RFM5	SDHA	Mito IM	5	351–654

(*Continued*)

Table 2. (*Continued*)

Protein Name	UniProt Accession	Gene Symbol	Cellular Localization**	# hits	aa
Signal Transduction					
Ankyrin repeat & GTPase Arf activating protein 11	Q8TF27	AGAP11	Cytoplasm	2	19–550#
DNA-damage-inducible transcript 4	Q9NX09	DDIT4	Cytoplasm	2	167–232
Dual specific phosphatase 1	P28562	DUSP1	Nucleus	2	158–367
Four and a half LIM domains 2*	Q14192	FHL2	Nucleus	10	47–279
Myozenin 2	Q9NPC6	MYOZ2	Cytoplasm	2	31–264#
Parvin, alpha	Q9NVD7	PARVA	PM	2	181–412
Prosaposin*	Q5BJH1	PSAP	Lysosome	14	425–526
Zinc finger protein 335*	Q8IW09	ZNF335	Nucleus	2	610–1342#
Gene/Protein Expression					
Brain expressed X-linked 4	Q9NWD9	BEX4	Cytoplasm	2	1–120
Eukaryotic translation elongation factor 1 alpha 1*	P68104	EEF1A1	Ribosome, Nucleus	13	213–462#
Eukaryotic translation elongation factor 2	Q6PK56	EEF2	Ribosome	2	685–858
Eukaryotic translation initiation factor 4A2	Q14240	EIF4A2	Ribosome	3	360–407
Glycine-tRNA synthetase	P41250	GARS	Cytoplasm	2	254–739#
Asparagine-tRNA ligase	O43776	NARS	Cytoplasm	2	379–548
NHP2 non-histone chromosome protein 2-like 1	P55769	NHP2L1	Nucleus	2	41–123#
Ribosomal protein L11, 60S*	P62913	RPL11	Ribosome	10	83–177
Ribosomal protein L36a, 60S*	J3KQN4	RPL36A	Ribosome	13	81–142
Ribosomal protein L36a-like, 60S	Q969Q0	RPL36AL	Ribosome	2	45–106
Ribosomal protein S11, 40S	P62280	RPS11	Ribosome	4	90–158
THUMP domain-containing 2	Q9BTF0	THUMPD2	Cytoplasm	2	11–503#
Transport					
ATP-binding cassette, sub-family C, member 9	O60706	ABCC9	PM	2	1263–1549#
ATP-binding cassette, sub-family D, member 4	O14678	ABCD4	Peroxisome	2	204–606
ATPase, H+ transporting, V1 subunit E1	Q53Y06	ATP6V1E1	Lysosome	2	165–196#
Myoglobin	P02144	MB	Cytoplasm	3	9–154
Protein phosphatase, IK	Q8N3J5	PPM1K	Mito Matrix	2	260–372
Stromal cell-derived factor 2	Q99470	SDF2	Extracellular	2	(-9)–211
Solute carrier family 2, member 1	P11166	SLC2A1	PM	3	369–492
Protein Degradation					
Alpha-2-macroglobulin	P01023	A2M	Extracellular	3	1184–1474#
Cathepsin B	P07858	CTSB	Lysosome	4	238–339
Cathepsin D*	P07339	CTSD	Lysosome	4	229–413
Nucleotide Metabolism					
Creatine kinase, muscle	P06732	CKM	Cytoplasm	3	133–381#
Guanylate kinase 1*	Q96IN2	GUK1	Cytoplasm	3	11–197
Putative deoxyribonuclease 1	Q6P1N9	TATDN1	Nucleus	2	-6–298#
Immune					
Beta-2-microglobulin*	P61769	B2M	Extracellular	8	-11–119
Complement component 1, q subcomponent, A chain	P02745	C1QA	Extracellular	2	134–245
Thymocyte selection associated family member 2	Q5TEJ8	THEMIS2	Cytoplasm	2	246–447
Cell Adhesion					
Lectin, galactoside-binding, soluble, 1 (Galectin-1)*	P09382	LGALS1	Extracellular	9	-22–135
Plakophilin 2	Q99959	PKP2	Cytoskeleton'PM	3	619–837
Osmoregulation					
ATPase, Na+/K+ transporting, beta 1	Q6LEU2	ATP1B1	PM	2	101–303

(*Continued*)

Table 2. (*Continued*)

Protein Name	UniProt Accession	Gene Symbol	Cellular Localization**	# hits	aa
Small Molecule Biosynthesis					
N-acylsphingosine amidohydrolase 1	Q13510	ASAH1	Lysosome	2	290–389
Oxidoreductive Stress					
Thioredoxin-interacting protein	Q9H3M7	TXNIP	Cytoplasm	6	175–391
Chaperone					
Heat Shock Protein 2 (HspB2)	Q16082	HSPB2	Cytoplasm	6	-66–175
Crystallin, alpha B*	P02511	HSPB5	Cytoskeleton	34	-3–175
Unknown					
Dynactin 6	O00399	DCTN6	Mito	3	82–190
Myeloid leukemia factor 2	Q15773	MLF2	Nucleus	2	98–248#
Nucleotidase domain containing 2	Q9H857	NT5DC2	unknown	2	302–462

* Indicates the 30 proteins shown to be HspB2 dependent in the Y2H binding assay. All others were not tested for dependency. Of the total 49 plasmids tested for dependency from the multi-hitter list, 10 did not appear in frame from sequence analysis, 81.6% showed a positive Y2H result that was dependent on HspB2 (indicating a HspB2/prey interaction), 10.2% were false positives (they grew with either HspB2 or the empty bait plasmid), and 8.2% were true negatives (they did not grow with either HspB2 or the empty bait). Out of frame fusions, false positives and true negatives revealed through this analysis are not listed.

** Abbreviations include Endoplasmic Reticulum (ER), Mitochondrial (Mito), Mitochondrial Inner Membrane (Mito IM), Mitochondrial Outer Membrane (Mito OM), Mitochondrial Matrix (Mito Matrix), Plasma Membrane (PM) and Sarcoplasmic Reticulum (SR).]

Indicates that the final amino acid listed is the C-terminal amino acid of the native protein.

Indicates that there is extra DNA from the mitochondrial chromosome on the 3' end of this construct in addition to the MYH6 DNA which adds an extra 82 aa.

# Indicates that the sequence quality was too poor to unambiguously tell the N-terminal fusion (WDR1, NHP2L, ATP6V1E1, TATDN1, MLF2) or the C-terminal end (RYR2, WDR1, ALDH2, ENO1, HADHB, MDH1, PGM1, AGAP11, MYOZ2, ANF335, GARS, CKM, ABCC9, EEF1A1, THUMPD2, A2M).

doi:10.1371/journal.pone.0133994.t002

The Y2H screen identifies mitochondrial clients for HspB2

The 84 high confidence binding partners identified by Y2H were further analyzed for their cellular localization and molecular functions. The majority of the binding partners have been reported to primarily localize to the mitochondria (19%), the cytoskeleton (24%) and the cytoplasm (19%) (Fig 4B). The functional classes to which the most interacting partners belong are those of fermentation/respiration (23%, including 13 targets directly involved in oxidative phosphorylation) and myofibril or cytoskeletal function (23%), consistent with the previously reported roles of HspB2 in ATP production [6, 9, 13] and muscle fiber maintenance [4, 6, 26, 29, 36, 37]. The high proportion of mitochondrial proteins identified by Y2H may, in part, be due to the abundance of mitochondria in cardiac tissue, yet there is interest in this subset of mitochondrial proteins when considering the total mitochondrial proteome, with over 1,000 mitochondrial proteins estimated in studies of both human [38] and rat [14] cardiac tissues.

Coaffinity proteomics of HspB2 validates mitochondrial targets of HspB2

The identification of multiple mitochondrial binding partners poses a novel hypothesis that HspB2, a resident cytosolic molecular chaperone, might also have distinct mitochondrial clientele. Such clientele would be consistent with the transient association with the outer mitochondrial membrane reported by Nakagawa et al. from tissue culture studies [8]. To test this hypothesis, co-purification studies were performed followed by quantitative mass spectroscopy to identify both HspB2 mitochondrial localization as well as native mitochondrial binding partners [39, 40]. Anti-HspB2 antibodies [9] were used to IP protein from cardiac muscle

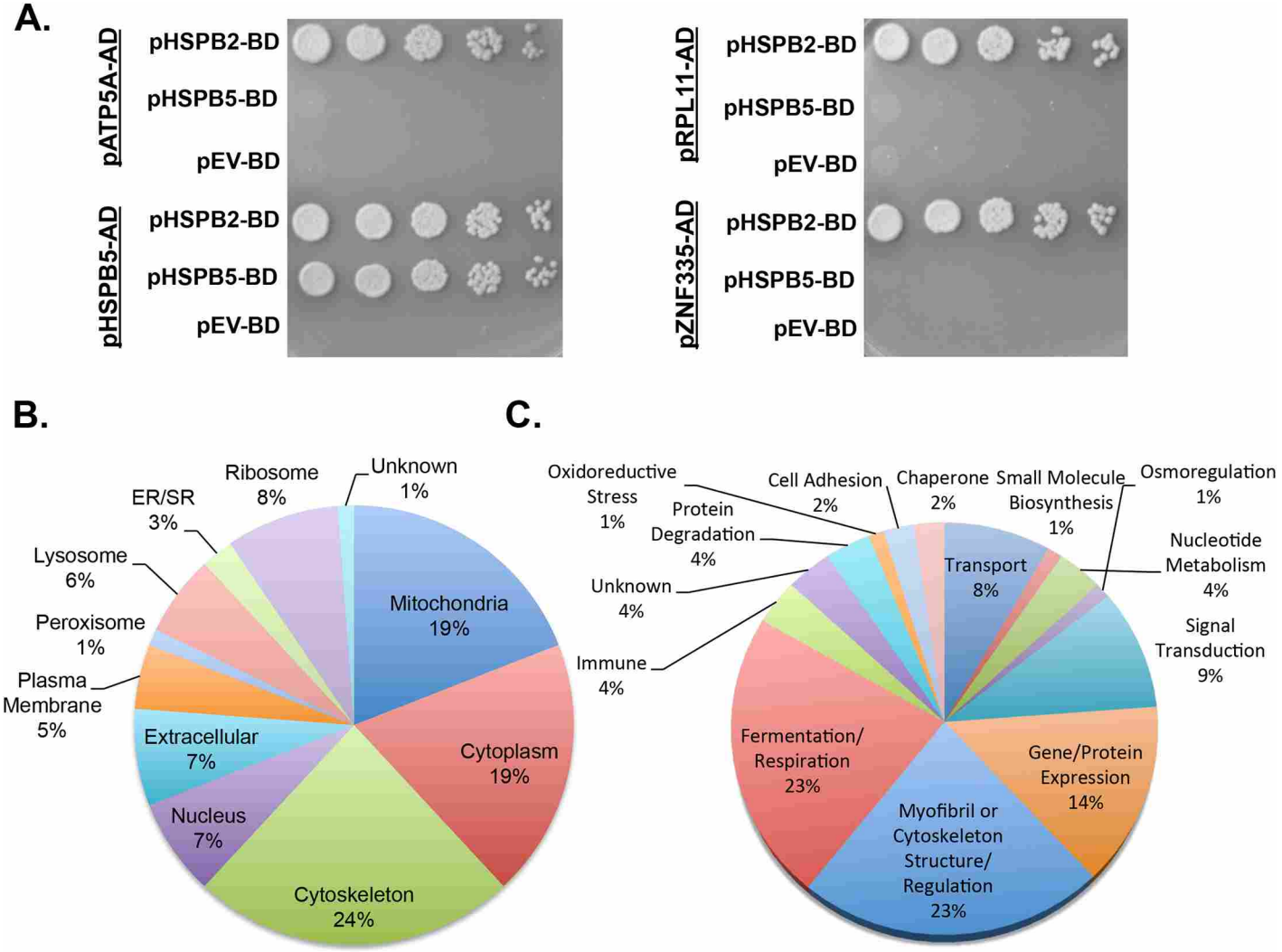

Fig 4. A large-scale HspB2 yeast two-hybrid (Y2H) screen reveals specificity in sHSP binding partners and identifies putative myofibril and mitochondrial clientele. (A) Y2H assays for direct binding between HspB2 or HspB5 baits and four putative HspB2 binding partner preys reveals non-redundant binding. Y2H prey plasmids (pGADT7, Clontech) retrieved from the HspB2 Y2H screen were transformed into Y2HGold cells (Clontech) containing bait plasmids (pGBKT7, Clontech) with either HSPB2 (pHSPB2-BD) or HSPB5 (pHSPB5-BD) fused to the Gal4 DNA binding domain (BD), or the empty vector (pEV-BD). Overnight cultures were grown for 48 h in SD-Trp-Leu to select for plasmids, then serially diluted 1:5 and plated on SD-Trp-Leu-His-Ade plates to select for protein-protein interaction. These four (ATP synthase alpha subunit (ATP5A1), alphaB-crystallin (HspB5), ribosomal protein L11 (RPL11), and zinc finger protein 335 (ZNF335) are representative. Results of all 12 binding partners are given in Table 3. **(B)** Pie charts summarizing the reported localization of the putative HspB2 binding partners revealed that a majority are localized to the cytoplasm, cytoskeleton or mitochondria. **(C)** Pie charts summarizing the reported function for putative cardiac HspB2 binding partners reveals two major categories of myofibril or mitochondrial function. Function and localization was assigned by basic description on GeneCards [73], UniProt [73, 74] or literature searches when necessary.

doi:10.1371/journal.pone.0133994.g004

mitochondrial lysate derived from either the HSPB2NTg control, heart-specific transgenic (HSPB2cTg), or heart-specific KO (HSPB2cKO) mice. Co-purified proteins were run on SDS-PAGE for fractionation and then identified by quantitative LC/MS/MS in two technical replicates. HspB2 was identified in the HSPB2cTg samples confirming mitochondrial association, but it was not identified either in the samples from littermate control (HSPB2NTg) or HSPB2cKO mice, presumably due to low or no HSPB2 expression, respectively. This restricted detection of HspB2 in only the OE lysates is consistent with previous assays for mitochondrial association of HspB2 and is thought to be due to low HspB2 expression [9].

Table 3. HspB2 is highly specific for its targets as revealed by a comparison of HspB2 and HspB5 binding partners. Twelve binding partners from the HspB2 Y2H screen were tested for their ability to bind HspB2 or HspB5. The columns are as follows: gene (the name of the gene encoded on the library 'prey' plasmid retrieved from the Y2H screen), plasmid (the pJG number of the purified plasmid), HspB2 (the Y2H protein-protein interaction result using HspB2 as bait), HspB5 (the Y2H protein-protein interaction result using HspB5 as bait), and EV (the Y2H result using an empty vector control). Strong, medium or weak indicates apparent strength of the interaction as determined by growth on selective media (SD–Trp–Leu–His–Ade); NG means no detectable growth. HspB5 was used as a positive control and was also retrieved from the yeast two-hybrid screen.

Gene	Plasmid	HspB2	HspB5	EV
HSPB5	pJG933	Strong	Strong	NG
ALDOA	pJG774	Strong	Weak	NG
ATP5A1	pJG745	Strong	NG	NG
DCTN1	pJG885	Strong	Weak	NG
ENO3	pJG877	Strong	NG	NG
EEF1A1	pJG882	Strong	NG	NG
MYH6	pJG785	Strong	NG	NG
OGDH	pJG988	Strong	NG	NG
PSAP	pJG878	Strong	Strong	NG
RPL11	pJG903	Strong	NG	NG
SDHA	pJG871	Strong	NG	NG
ZNF335	pJG944	Strong	NG	NG

doi:10.1371/journal.pone.0133994.t003

A total of 68 proteins (Table 4) were uniquely identified in the HSPB2cTg samples (Fig 5A). An additional 127 proteins were identified in both the HSPB2cTg and HSPB2cKO samples, suggesting they bind nonspecifically to the resins used in purification. The 68 HSPB2cTg-specific proteins compared with 12 HSPB2cKO-specific suggest HspB2-specific binding. In addition, the 68 HSPB2cTg-specific proteins were enriched for membrane bound proteins involved in oxidative phosphorylation, transport and metabolism (65%, Fig 5B), consistent with the Y2H results.

When combined, the 84 high confidence targets from the Y2H screen and 68 from co-IP studies identify 149 unique proteins as putative HspB2 clientele. Three proteins were identified by both methods (HspB2, OGDH, and MCCC2). The low level of overlap between the two independent screens is due to the difference in using whole-cell verses mitochondrial extract and is also consistent with previous reports on differences due to the diverse strengths of each approach [41]. Of note, if all of the proteins identified in the HSPB2cTg co-IP samples are analyzed (including the 127 that also occur in the HSPB2cKO control), there are 39 proteins that overlap between the Y2H and co-IP samples. These additional proteins interacted with the purification resin itself and may represent proteins that naturally aggregate easily, prime targets for chaperones. This aggregation, however, makes it difficult to show protein-protein association by co-IP and these proteins are not included in the 68 retrieved from co-IP.

Network analysis of the combined HspB2 cardiac interactome reveals functional links to myopathies and neurodegenerative disease

HspB2 is one of only a few sHSP to date (including HspB9 and HspB10) without identified disease-associated human alleles. Therefore, the combined high confidence Y2H and co-IP interactome (a total of 149 unique proteins) was analyzed for diseases associated with the putative HspB2 binding partners. There were 35 Y2H and 14 co-IP HspB2 binding partners associated with disease, and of these, 28 (57%) were associated with myopathies and neurodegenerative

Table 4. Unique proteins identified from HSPB2 co-immunoprecipitation from HSPB2cTg heart tissue when compared to the HSPB2cKO heart tissue. This table lists information on all 68 uniquely identified proteins from the HSPB2cTg samples when compared with those identified from the HSPB2cKO samples by quantitative mass spectroscopy. It contains the following information sequentially: protein name, UniProt [73, 74] protein accession number, gene name, primary cellular localization from HPRD [76] or UniProt, molecular weight (MW), and protein length (# of amino acids). The proteins are functionally categorized by their description on UniProt and/or GeneCards.

Protein Name	UniProt Accession	Gene Symbol	Cellular Localization**	MW	Protein Length [67]
Fermentation/Respiration					
Protein Acad12	D3Z2B3	ACAD12	Mito	41332	373
ATP synthase subunit e, mitochondrial	P56385	ATP5I	Mito IM	8218	71
ATP synthase subunit g, mitochondrial	O75964	ATP5L	Mito IM	11407	103
CDGSH iron-sulfur domain-containing protein 1	Q9NZ45	CISD1	Mito OM	12079	108
Carnitine O-palmitoyltransferase 1, muscle isoform	A5PLL0	CPT1B	Mito,OM	88202	772
Carnitine palmitoyltransferase 2	P23786	CPT2	Mito IM	24889	223
Carnitine O-acetyltransferase	P43155	CRAT	Mito IM, ER, Perox	70823	626
Cytochrome c oxidase subunit 7A-related protein	Q6FGA0	COX7A2L	Mito IM	14913	134
Dihydrolipoyl dehydrogenase, mitochondrial	P09622	DLD	Mito Matrix	54254	509
Dihydrolipoyllysine-residue succinyltransferase	Q6IBS5	DLST	Mito, Nucleus	22212	454
Methylcrotonoyl-Coenzyme A carboxylase 2 (Beta)	Q9HCC0	MCCC2	Mito	61362	563
Novel protein GN = Mtfp1	Q9UDX5	MTFP1	Mito	18314	166
NADH-ubiquinone oxidoreductase chain 1	P03886	MT-ND1	Mito IM	36012	318
NADH-ubiquinone oxidoreductase chain 4	P03905	MT-ND4	Mito IM	51869	459
NADH-ubiquinone oxidoreductase chain 5	P03915	MT-ND5	Mito IM	68441	607
NADH dehydrogenase 1 alpha subcomplex subunit 11	Q86Y39	NDUFA11	Mito IM	14965	141
NADH dehydrogenase 1 beta subcomplex subunit 3	O43676	NDUFB3	Mito IM	11674	104
NADH dehydrogenase 1 beta subcomplex, 5	O43674	NDUFB5	Mito IM	14038	119
NADH dehydrogenase 1 beta subcomplex, 6	O95139	NDUFB6	Mito IM	15498	128
NADH dehydrogenase 1 beta subcomplex subunit 8	O95169	NDUFB8	Mito IM	21858	186
NADH dehydrogenase 1 beta subcomplex subunit 9	Q9Y6M9	NDUFB9	Mito IM	21966	179
NADH dehydrogenase 1 beta subcomplex, 11	Q9NX14	NDUFB11	Mito	17426	151
NADH dehydrogenase 1 subunit C2	O95298	NDUFC2	Mito IM	14146	120
NAD(P) transhydrogenase, mitochondrial	Q13423	NNT	Mito IM	113823	1086
2-oxoglutarate dehydrogenase, mitochondrial	Q02218	OGDH	Mito	117741	214
Ubiquinol-cytochrome c reductase hinge protein	P07919	UQCRH	Mito IM	10417	89
Cytochrome b-c1 complex subunit 8	O14949	UQCRQ	Mito IM	9751	82
Transport					
Platelet glycoprotein 4	P16671	CD36	Golgi, PM	52681	472
Mitochondrial carrier homolog 2	Q9Y6C9	MTCH2	Mito IM	32328	294
Metaxin 2	O75431	MTX2	Mito OM	29740	263
ADP/ATP translocase 2	Q6NVC0	SLC25A5	Mito IM	32915	298
Calcium-binding mitochondrial carrier protein Aralar1	O75746	SLC25A12	Mito IM	74554	677
Mitochondrial carnitine/acylcarnitine carrier protein	O43772	SLC25A20	Mito IM	33010	301
Solute carrier family 25 member 42	Q86VD7	SLC25A42	Mito IM	35241	318
Cell Adhesion					
Perlecan (Heparan sulfate proteoglycan 2)	Q2VPA1	HSPG2	Extracellular	469023	4735
Laminin subunit alpha-2	P24043	LAMA2	Extracellular	342761	3105
Laminin subunit gamma-1	P11047	LAMC1	Extracellular	177298	1607
Nidogen-1	P14543	NID1	Extracellular	136519	1245
Vinculin	P18206	VCL	Cytoplasm	116717	1066
Small Molecule Biosynthesis and Catabolism					

(*Continued*)

Table 4. (*Continued*)

Protein Name	UniProt Accession	Gene Symbol	Cellular Localization**	MW	Protein Length [67]
Apolipoprotein O	Q9BUR5	APOO	Mito	22587	198
Ferrochelatase (EC 4.99.1.1)	P22830	FECH	Mito, IM	44667	399
Amine oxidase [flavin-containing] B	P27338	MAOB	Mito OM	58541	520
Methylcrotonoyl-CoA carboxylase subunit alpha	Q96RQ3	MCCC1	Mito IM/Matrix	79327	717
Isoform 2 of Perilipin-4	Q96Q06	PLIN4	Cytoplasm,PM	139415	1403
Gene/Protein Expression					
Crip2 protein	P52943	CRIP2	Nucleus,Cortex	22709	208
Methylglutaconyl-CoA hydratase, mitochondrial	Q13825	AUH	Mito	22898	219
39S ribosomal protein L12, mitochondrial	P52815	MRPL12	Mito	21691	201
Nascent polypeptide-associated complex subunit alpha	Q13765	NACA	Cytoplasm,Nucleus	220499	2187
Sorting and assembly machinery component 50 homolog	Q9Y512	SAMM50	Mito, OM	51847	469
Myofibril or Cytoskeleton Structure/Regulation					
Alpha actinin 1a	P12814	ACTN1	Cytoplasm, Z-disk	102706	887
Spectrin alpha 2	A3KGU5	SPNA2	Cytoskeleton	282895	2457
Isoform 2 of Spectrin beta chain, brain 1	Q62261	SPNB2	Cytoskeleton	274223	2363
Troponin C, slow skeletal and cardiac muscles	P63316	TNNC1	Cytoskeleton	18421	161
Uncharacterized protein GN = Vim	P08670	VIM	PM	52185	453
Intracellular Trafficking					
AP-3 complex subunit delta-1	O14617	AP3D1	Cytoplasm,PM	135081	1199
EH-domain containing 4	Q9H223	EHD4	ER,PM	61481	541
Ras-related protein Rab-7a	P51149	RAB7A	Lysosome	23472	207
Chaperone					
Heat shock cognate 71 kDa protein	Q96IS6	HSPA8	Cytoplasm	70871	646
Heat shock protein beta-2	Q16082	HSPB2	Cytoplasm	20357	182
Cell Death					
Dynamin-like 120 kDa protein, mitochondrial	O60313	OPA1	Mito IM	78918	692
Immune					
Complement component 1 Q subcomponent-binding protein	Q07021	C1QBP	Mito Matrix	31013	278
Oxidoreductive Stress					
Apoptosis-inducing factor, mitochondrion-associated 1	O95831	AIFM1	Mito IM/OM	66748	612
Unknown					
Apolipoprotein O-like	Q6UXV4	APOOL	Mito IM	29244	265
Mitochondrial pyruvate carrier	Q9D023	MPC2	Mito IM	14269	127
ES1 protein homolog, mitochondrial	Q9D172	D10JHU81E	Mito	28072	266
Uncharacterized protein GN = Ogdhl	Q9ULD0	OGDHL	Cytoplasm	116584	1029
Prohibitin	P35232	PHB	Mito IM	29803	272
Translocase of inner mitochondrial membrane domain containing 1	Q9NPL8	TIMMDC1	Mito IM	31774	285

**Abbreviations include Endoplasmic Reticulum (ER), Mitochondrial (Mito), Mitochondrial Inner Membrane (Mito IM), Mitochondrial Outer Membrane (Mito OM), Mitochondrial Matrix (Mito Matrix), Peroxisome (Perox), Plasma Membrane (PM)

doi:10.1371/journal.pone.0133994.t004

diseases such as Alzheimer's disease (AD) (Fig 5C). These results predict that alterations in HspB2 function may contribute to these diseases.

Although the high confidence Y2H and co-IP HspB2 interactome revealed proteins with a wide range of biological functions, it was apparent that many of these proteins overlap in their

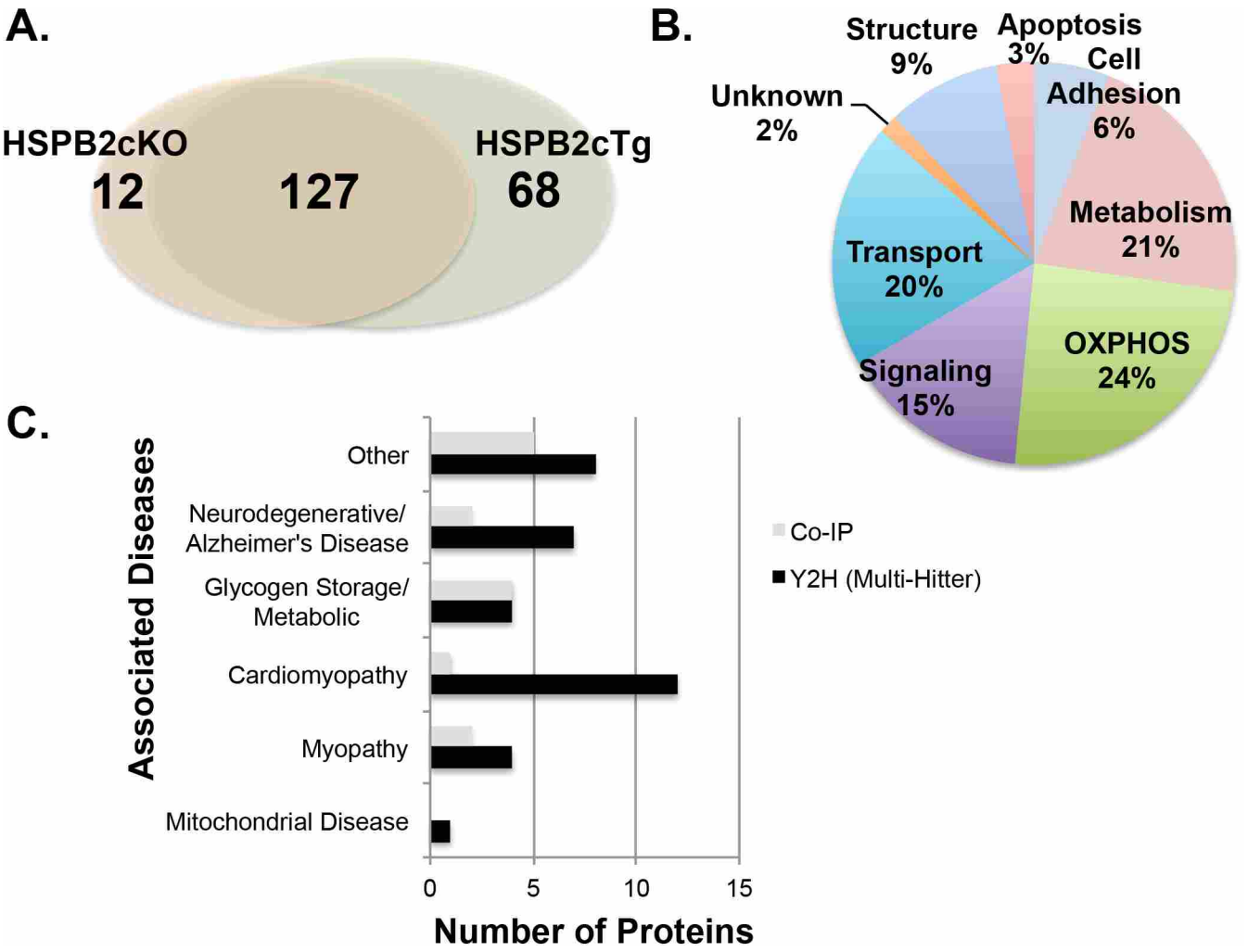

Fig 5. Co-purification of mitochondrial HspB2 binding partners supports the mitochondrial role predicted by Y2H and mouse data and identifies associations with disease. (A) Analysis of 207 proteins retrieved via co-immunoprecipitation (IP) from mouse cardiac mitochondria lysate with anti-HSPB2 antibodies reveals 68 proteins unique to the HSPB2cTg samples, 12 unique to the HSPB2cKO control and 127 that overlap. Mitochondrial HspB2 was immunopurified from mice harboring either transgenic cardiac HSPB2 (HSPB2cTg) or an HSPB2 cardiac knockout (HSPB2cKO). In each group, mitochondria were combined from four mouse hearts, lysed in 0.1% NP-40 homogenization buffer and 2 mg was incubated with anti-HspB2 antibodies. The IP eluates were then fractionated on SDS-PAGE, excised and analyzed by LC-MS/MS. Samples had one biological replicate and two technical replicates. **(B)** The unique proteins retrieved only from HSPB2cTg tissue (68 total) are enriched in oxidative phosphorylation functions. Predicted protein function was inferred by Gene Ontology [75]. **(C)** Diseases associated with proteins in the combined HspB2 Y2H and IP interactomes predict a role for HspB2 in neurodegenerative diseases and myopathies. Of the 149 HspB2 binding partners, 49 are associated with diseases and 57% of these are associated with myopathies and neurodegenerative diseases including cardiomyopathy and Alzheimer's disease. Associated diseases were identified by the Online Mendelian Inheritance in Man (OMIM) database (McKusick-Nathans Institute of Genetic Medicine, Johns Hopkins University (Baltimore, MD). World Wide Web URL: http://omim.org/).

doi:10.1371/journal.pone.0133994.g005

biological pathways. In order to identify key pathways influenced by HspB2, the combined Y2H and co-IP interactome (149 proteins) was analyzed using protein-protein interaction and functional annotation datasets in Cytoscape [42]. Detailed analysis of the interactome using Cytoscape revealed a large network with 69 of the interactome proteins having 365 reported protein-protein interactions (Fig 6). The remaining 80 proteins not included in this larger network have one or zero known binding partners. There are two major clusters of this large network, one that contains primarily myofibril proteins and the other primarily fermentation/respiration proteins, consistent with the functional analysis of these targets (Figs 4C and 5B).

Amid the 64 mitochondria-associated protein partners of HspB2 (19 from Y2H, 48 from co-IP and 3 that overlap), 32 (50%) are in this large Cytoscape network, with 200 of the 365 total interactions (55%) reported occurring with these 32 mitochondria-associated proteins. The fact that many (50%) of the mitochondrial proteins from both screens are previously reported binding partners suggests that HspB2 is targeting related proteins or specific pathways.

Gyceraldehyde 3-phosphate dehydrogenase (GAPDH) is a central protein in the network (indicated in orange) with many connections to the major protein cluster with myofibril functions. GAPDH catalyzes the sixth step of glycolysis and is a key metabolic switch for partitioning glucose to TCA for respiration [43], and has recently been implicated in a wide variety of pathways including mitochondrial functions (for recent reviews see [44–48]). The pivotal position of GAPDH within the cluster and its connection to mitochondrial function suggested GAPDH as an important HspB2 target central to these pathways, and it was investigated further.

HspB2 protects GAPDH from heat inactivation

GAPDH was chosen to validate by further characterization because it was a central node in the bioinformatic analysis of the HspB2 interactome, it is a soluble protein (facilitating its characterization as chaperone target), and it has been associated with all of the HspB2-related cardiac phenotypes including maintaining ATP levels (Fig 3 and [9]), mitochondrial outer membrane potential ([31, 32]) and protection from I/R-induced infarction (Fig 2, Table 1). Specifically, GAPDH has recently shown to maintain cellular ATP levels during mitochondrial crisis [49], and to localize to mitochondria where it regulates respiratory complex I cytochrome C-oxidase [49], mitochondrial outer membrane permeability (MOMP) [50] and mitochondrial-based apoptosis [50, 51] in cardiomyocytes. These roles for GAPDH in MOMP and apoptosis have also been established in other tissues and cell lines [52–55]. In addition, GAPDH enhances aggregation and cytotoxicity in models of Huntington and Amytrophic Lateral Sclerosis [43, 56] as well as Alzheimer's disease [57–59].

We tested directly the ability of HspB2 to prevent heat-induced aggregation of GAPDH through *in vivo* and in vitro chaperone assays (Fig 7). To assess the effects of HspB2 on GAPDH *in vivo*, GAPDH expression in cardiac protein lysates from HSPB2cTg mice was compared with the littermate controls (HSPB2NTg). No significant differences in soluble GAPDH were observed when compared with β-Tubulin and GAPDH was not observed in the pellet of homogenized mouse cardiac tissue (Fig 7A and 7B). These results suggest that HspB2 may only be important for GAPDH solubility or folding during stress states. To test this hypothesis, the effects of HspB2 expression on GAPDH heat aggregation were investigated in mammalian cells. In C2C12 cells, HspB2 was overexpressed prior to heat stress (30 m at 45°C) and cell lysates examined for levels of GAPDH contained in the supernatant and pellet fractions. When compared with control cells, forced HspB2 expression significantly prevented aggregation and increased solubilized GAPDH protein (~92% vs 62%, $P < 0.005$), whereas just over one-third (38%) aggregated, rescuing 30% of the total GAPDH protein (Fig 7C and 7D). In contrast, HspB2 did not recognize β-Tubulin as a binding partner in either the Y2H or co-IP interactomes; accordingly, HspB2 did not confer protection of β-Tubulin when used as a control under these conditions. These results offer for the first time evidence for HspB2-dependent stabilization of GAPDH, a key protein in the regulation of ATP levels and apoptosis.

In addition to *in vivo* assays, the ability of HspB2 to prevent GAPDH aggregation was investigated in vitro. HspB2 was able to prevent *in vitro* aggregation of almost three quarters (~73%) of the GAPDH where ~50% of GAPDH aggregated without HSPB2 (increasing solubility by about half, Fig 7E and 7F). However, HspB2 also prevented aggregation of other proteins tested

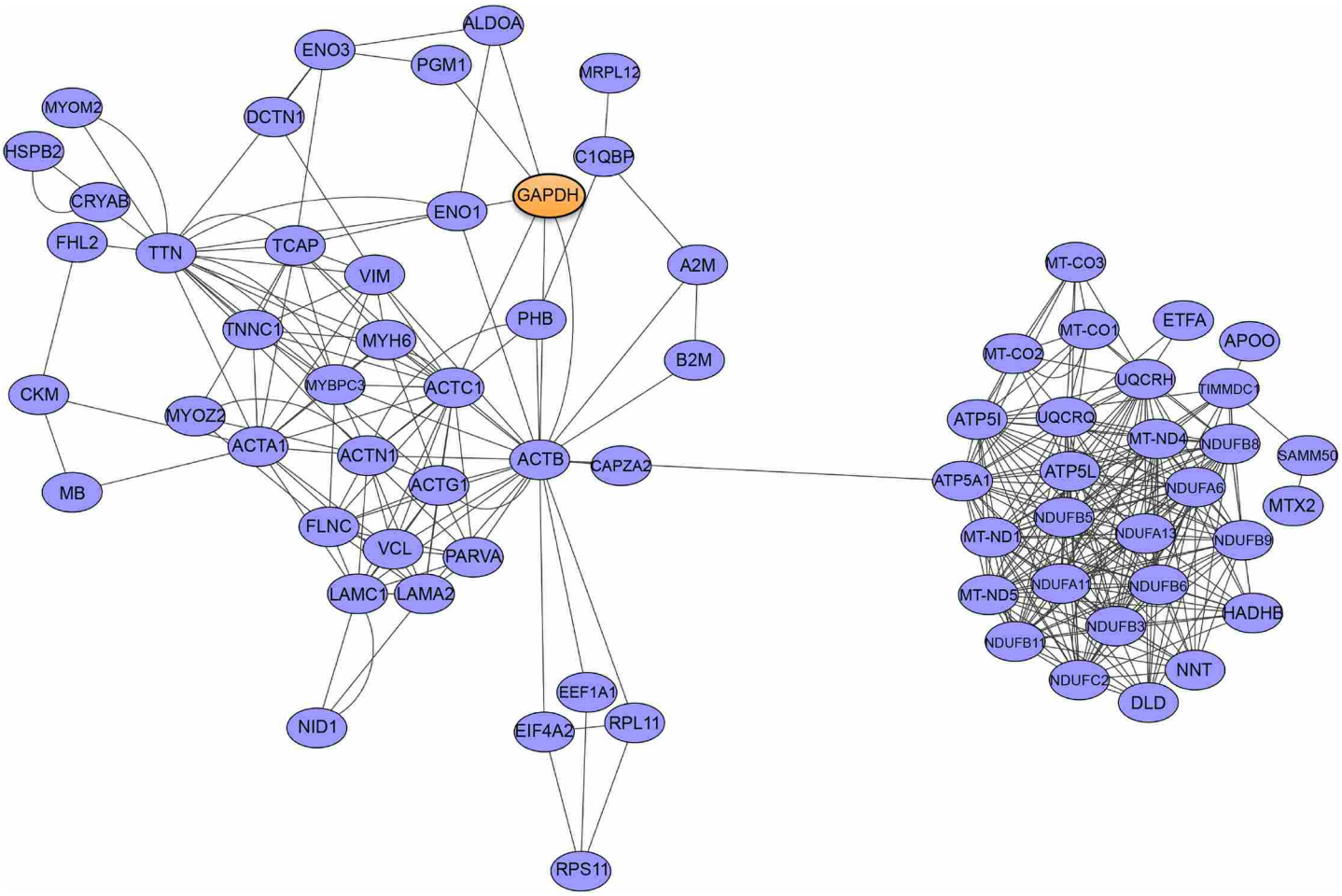

Fig 6. Analysis of the HspB2 interactome confirms the related nature of the binding partners and identified two major networks involved in mitochondrial metabolism and myofibril maintenance. Analysis of known protein-protein interactions among the 149 HspB2 binding partners reveals a tight network of 69 proteins. Glyceraldehyde 3-phosphate dehydrogenase (GAPDH) (indicated by orange coloring) is investigated further in this study. Cytoscape version 3.2.1 [19] was used to construct each of the protein-protein interaction networks by retrieving previously identified interactions from the *mentha*, Reactome-FIs, Reactome, IntAct and MINT databases (partners reported for either human or mouse proteins) and mapping them into a single merged network.

doi:10.1371/journal.pone.0133994.g006

that were not identified in this study, including citrate synthase (CS). Citrate synthase was reported as a weak client, with HspB2 providing only partial protection in a previous study [21], however these results suggest non-specificity of HspB2 binding *in vitro* with HspB2 rescuing both heat denatured GAPDH and CS.

Discussion

The physiological importance of the family of sHSPs in human disease has been well established, however the unique roles of the ten members are just beginning to be unveiled due to the complexity of overlapping function [1, 2, 60]. This study utilized the power of OE to reveal cardiac HspB2-associated phenotypes that are not seen with gene KO, most likely due to overlapping sHSP function. In addition, a system's biology approach was taken to identify specific molecular functions of HspB2 via a cardiac HspB2 interactome, which supports the observed phenotypes and provides key targets for future investigation.

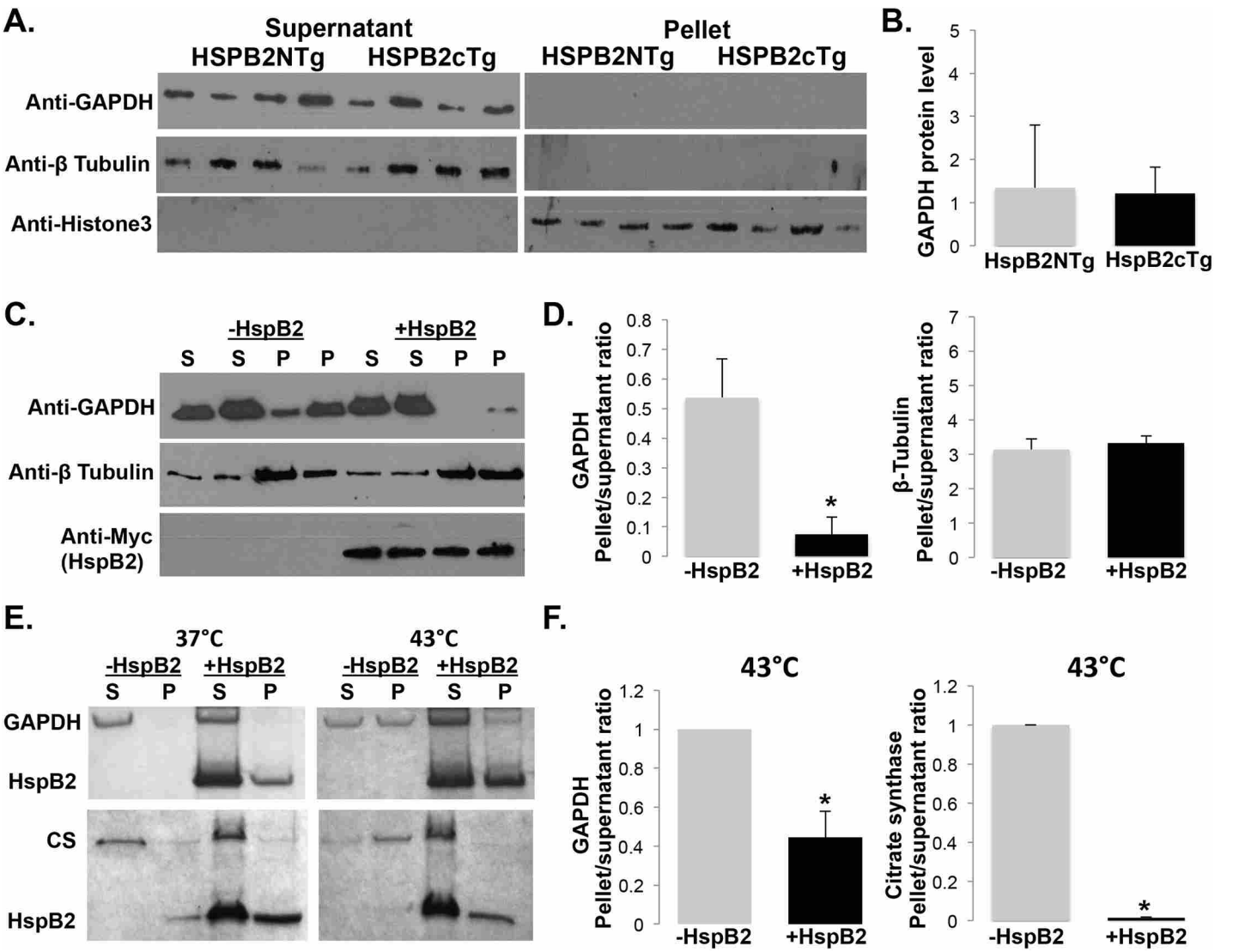

Fig 7. HspB2 protects glyceraldehyde 3-phosphate dehydrogenase (GAPDH) from heat stress. (A) Overexpression of HspB2 does not alter GAPDH levels in mouse cardiac lysates. Total protein concentration was determined and western blots were performed using anti-GAPDH with anti-beta Tubulin and anti-histone3 as loading controls as previously described [9]. **(B)** Quantification of A using ImageJ software [22]. **(C)** Overexpression of HspB2 protects GADPH from denaturation in mammalian C2C12 cells subjected to heat shock. Plasmids bearing human HspB2 fused to myc or the empty plasmid control (pCMV-myc) were transfected into C2C12 cells in a 6-well plate using 6.5-μl lipofectamine 2000 (Life Technologies) and manufacturers protocol. After 48 h at 37°C, cells were shifted to 45°C for 30 m and then placed back at 37°C for 3 h prior to lysis. Debris was pelleted at 13,000 rpm for 5 m, and pellet (P) and supernatant (S) were resuspended in 1X SDS buffer. Samples were boiled 2 m, analyzed by SDS-PAGE and transferred to nitrocellulose paper for visualization using anti-GAPDH antibody, anti-beta Tubulin antibody, and anti-Myc antibody (all antibodies are from Cell Signaling Technologies). **(D)** Protein bands from C were quantified using ImageJ software [22]. **(E)** *In vitro* chaperone assay reveals HspB2-dependent protection of GAPDH aggregation, however HspB2 appears to be non-specific in vitro. GAPDH or citrate synthase (control) was incubated with or without HspB2 at 37°C and 43°C and aggregated protein was pelleted by centrifugation. Pellets (P) and supernatants (S) were assayed for protein by SDS-PAGE analysis **(E)** and quantified **(F)**. Briefly, 0.015 mM GAPDH or citrate synthase was incubated at 37°C or 43°C with or without 0.105 mM HspB2 in 40 mM HEPES-KOH buffer (pH 7.5). Aggregates were then pelleted by centrifugation (13,000 rpm for 10 m in a microcentrifuge), run on SDS-PAGE, quantified using ImageJ software [22] and normalized to the no HspB2 pellet to supernatant ratio for each run. Samples were run in triplicate. * $P<0.05$ when compared with corresponding control group.

doi:10.1371/journal.pone.0133994.g007

The HspB2 protein was overexpressed in cardiac tissue (HSPB2cTg) where it reduced I/R stress-induced infarct size (Fig 2A and 2B). In support of this finding, the HSPB2cTg animals also had a lower troponin-1 level post surgery (Fig 2C) and were resistant to wall motion

abnormality as observed at 24-hour time points post I/R (Table 1). These findings demonstrate the power of OE in the study of complex, overlapping functions, as no difference in infarct size was seen between the wild type (HSPB2wt) and HSPB2cKO mice, which may be due to functional overlap of HSPs. This study of cardiac OE also confirmed the *HSPB2*-dependent preservation of cellular ATP levels seen in the study of HSPB2cKO mice [9], with ATP content following reperfusion significantly greater in the HSPB2cTg mice when compared to the control (Fig 3). These results mimic the function of putative HspB2 activators and suggest them as cardioprotectant agents. In addition, they suggest a mitochondrial role for HspB2 that may explain the protection of cardiac muscle from I/R stress, however a lack of reported mitochondrial HspB2 clientele prohibited molecular analysis.

Complex cellular protein networks underlie most genotype/phenotype relationships, making detailed analysis of protein interactomes essential in functional analysis, particularly with a protein chaperone [61]. Two widely used strategies were employed for determining the HspB2 cardiac interacome; namely, large-scale Y2H screens and co-IP studies. The large-scale cardiac Y2H screen retrieved 84 high confidence *in vivo* binding partners, whereas only four prior HspB2 clientele binding partners were reported to date (DMPK [4], insulin, alcohol dehydrogenase and α-synuclein [21]). Interactions with three other sHSPs (HspB3 [25, 26], HspB5 [27] and HspB8 [28]) have also been previously reported, however, we only retrieved HspB5 from the screen. This may be due to low levels of HspB3 or HspB8 constructs in the Y2H library, or nonfunctional Y2H fusion constructs. The later is highly probable as we were unable to detect an interaction between HspB3 and HspB2 when HspB3 was cloned directly into the Y2H prey (data not shown). The screen would also fail to uncover HspB2 targets that result only from formation of sHSP heterocomplexes (such as an HspB2/HspB5 complex) because only HspB2 was expressed in yeast.

The 84 HspB2 binding partners identified by Y2H are supported by the fact that the HspB2 bait interacted with less than 0.05% of the cardiac cDNA library and was specific for HspB2 when compared to other sHSPs. The HspB2 interactome was compared to the recently published HspB1 (Hsp27) Y2H interactome of 228 binding partners [35], and only two partners were in common (EIF4A2 and GARS). Specificity was also supported by a comparison of HspB2 and HspB5 binding where ten of 12 HspB2 binding partners tested preferentially interacted with HspB2 (see Table 3 and Fig 4A). HspB5 and HspB2, having 43% amino acid identity, are ohnologous [62] proteins in that they are divergently transcribed on human chromosome 11 and appear to have arisen by gene duplication [63]. Differences in function have been attributed to differences in their expression levels and tissue-type patterns, however, the non-redundant clientele-specificity reported herein suggests differential function and supports the unique structure reported for HspB2 when compared with HspB5 [21] as well as the non-redundant cardiac phenotypes [9].

In order to identify key pathways of HspB2 function from among the binding partners, a systems biology approach was used to map previously known protein-protein interactions, protein localization patterns, and related diseases. Such approaches have proven fruitful in identifying key pathways involved in protein function as well as human disease [61]. Functional analysis of the 84 Y2H binding partners revealed an abundance of proteins involved in myofibril and mitochondrial function (Fig 4C). Small HSPs have long been known for stabilizing myofibril structure in both skeletal and cardiac sarcomeres and HspB2 is no exception [6, 36], however this is the first report of putative mitochondrial clientele for HspB2.

The abundance of putative mitochondrial clientele posit HspB2 as a key factor in maintaining cardiac mitochondrial function, particularly when combined with the increased ability to maintain ATP seen in the HSPB2cTg mice (Fig 3). Several of the mitochondrial proteins are reported to localize to the inner membrane and matrix (Table 2) while HspB2 has been

associated with the outer mitochondrial membrane, therefore, HspB2 may function as a chaperone for these proteins by helping refold exported, denatured proteins during stress or it may be involved in the import and folding of naïve proteins. In support of a mitochondrial role for HspB2, HspB2 and/or HspB5 have recently been shown to regulate ROS generation and respiration [64]. Cardiac muscle has evolved to be highly resistant to fatigue due to the high proportion of mitochondria within each cardiomyocyte, which is estimated at 40% weight compared with 2% in skeletal muscle [65]. Unlike other muscle, cardiac muscle is almost completely dependent on oxygen with only 1% of energy being derived from anaerobic respiration. Mitochondrial damage is prevalent under growth conditions that stimulate high respiration, making protein chaperones of utmost importance in the heart. We, therefore, set out to validate mitochondrial clientele for HspB2 through co-IP.

The mitochondrial HspB2 clientele obtained by Y2H were supported by 68 proteins retrieved from co-IP with cardiac, mitochondrial HspB2 (Fig 5), with three proteins identified by both methods (HspB2, OGDH, and MCCC2). The low level of overlap between the two independent screens is consistent with previous reports and is due to the differences in whole-cell verses mitochondrial extract as well as the diverse strengths of each approach; co-IP is likely to retrieve large protein complexes while the Y2H primarily identifies direct protein interactions occurring in non-mammalian cells [41]. Although we have only been able to detect HspB2 in mitochondrial fractions when overexpressed in both this study and our previous study [9], HspB2 has also been shown to localize to the mitochondrial membrane in tissue culture studies [8]. This inability to detect HspB2 in mitochondrial fractions under normal cellular conditions has been attributed to its low level of de novo expression as well as its loose association with the mitochondria [9]. The precise role of HspB2 remains to be determined, but the combined phenotypic and interactome results herein strongly argue for a mitochondrial role for HspB2 and identify 64 putative mitochondria-associated clientele to guide future study.

To test the *in vivo* significance of the interactome and analysis, GAPDH was studied in more detail due to its identification as a central hub in the protein-protein interaction network (Fig 6). In addition, GAPDH is soluble, which facilitates chaperone assays and has previously reported roles in each of the HspB2-related phenotypes (namely maintenance of ATP levels and reduced infarct size [49, 50, 52–55]). GAPDH was identified herein as a client through chaperone assays (Fig 7), providing support for the interactome and analysis. Although multiple clienteles are likely to be involved in these phenotypes, GAPDH emerges as a key HspB2 target for further analysis due to its association with mitochondrial ATP production and reduced infarct size.

Although many other sHSPs (including HspB5) have been found to play a role in various diseases including neurodegenerative and muscular disease, disease-associated alleles of HspB2 have not been identified. The systems biology analysis herein, however, posits HspB2 as a player in neurodegenerative, mitochondrial, and muscular disease (Fig 5C). In support of this analysis, a dual KO of *HSPB5* and *HSPB2* was recently shown to enhance Alzheimer's phenotypes when crossed with AD model mice, including the loss of synapses and the build-up of amyloid beta-peptide (AB) plaques [66]. In addition, HspB2 has recently been found in the senile plaques of AD [67]. This is not surprising given the recently discovered similarities between proteotoxicity in cardiac dysfunction and in AD [68]. Both neurodegenerative and muscular diseases have also been associated with mitochondrial dysfunction [48, 69, 70]. Since the mitochondria of neuronal cells are the main organelle affected during AD [71, 72], mitochondrial dysfunction becomes a primary target for drug development. This analysis of the cardiac HspB2 interactome and cardiac HspB2 OE mice provides insight into the possible effects of treatment with HspB2 activators, including protection from I/R stress and mitochondrial

maintenance. The results herein suggest these activators may not only be useful in cardioprotection, but in the treatment of neurodegenerative disease.

Supporting Information

S1 Fig. Mitochondrial permeability assays suggest protection by HspB2 overexpression, however, the data is not statistically significant. Mitochondria were isolated from HSPB2 overexpressors (HSPB2cTg) or control hearts (HSPB2NTg), equilibrated for 5 m at room temperature and 250uM $CaCl_2$ was loaded to induce swelling. Data was read at 540nm.
(TIF)

S1 Table. Putative HspB2 binding partners retrieved from the Y2H screen only once. Proteins retrieved a single time from a Y2H screen for HspB2 binding partners are given along with the following information: protein name, UniProt [73] protein accession number (hyperlink), gene symbol, and cellular localization reported on UniProt, HPRD or GeneCards [73]. The proteins are functionally categorized by their description on UniProt and/or GeneCards. See Table 2 for a complete list of putative HspB2 binding partners retrieved from the Y2H screen multiple times.
(PDF)

Acknowledgments

The authors are grateful to undergraduates Kendall Kiser, John Collins, Jonathan Wood and Fred Nelson for aiding with the large-scale Y2H screen and for the support from the Microbiology and Molecular Biology department at Brigham Young University.

Author Contributions

Conceived and designed the experiments: JHG KL XW SS SBM QD EC EDL PP IJB. Performed the experiments: JHG KL XW SS SBM WH JN SKF MF GMS EC QD. Analyzed the data: JHG KL XW SS SBM WH JN SKF MF EC EDL PP IJB. Contributed reagents/materials/analysis tools: JHG GMS QD EC EDL PP IJB. Wrote the paper: JHG KL XW EC EDL PP IJB.

References

1. Christians ES, Ishiwata T, Benjamin IJ. Small heat shock proteins in redox metabolism: implications for cardiovascular diseases. The international journal of biochemistry & cell biology. 2012; 44(10):1632–45. doi: 10.1016/j.biocel.2012.06.006 PMID: 22710345; PubMed Central PMCID: PMC3412898.
2. Kampinga HH, Garrido C. HSPBs: small proteins with big implications in human disease. The international journal of biochemistry & cell biology. 2012; 44(10):1706–10. doi: 10.1016/j.biocel.2012.06.005 PMID: 22721753.
3. Kumarapeli AR, Horak K, Wang X. Protein quality control in protection against systolic overload cardiomyopathy: the long term role of small heat shock proteins. American journal of translational research. 2010; 2(4):390–401. PMID: 20733949; PubMed Central PMCID: PMC2923863.
4. Suzuki A, Sugiyama Y, Hayashi Y, Nyu-i N, Yoshida M, Nonaka I, et al. MKBP, a novel member of the small heat shock protein family, binds and activates the myotonic dystrophy protein kinase. The Journal of cell biology. 1998; 140(5):1113–24. PMID: 9490724; PubMed Central PMCID: PMC2132705.
5. Brady JP, Garland DL, Green DE, Tamm ER, Giblin FJ, Wawrousek EF. AlphaB-crystallin in lens development and muscle integrity: a gene knockout approach. Investigative ophthalmology & visual science. 2001; 42(12):2924–34. PMID: 11687538.
6. Pinz I, Robbins J, Rajasekaran NS, Benjamin IJ, Ingwall JS. Unmasking different mechanical and energetic roles for the small heat shock proteins CryAB and HSPB2 using genetically modified mouse hearts. FASEB journal: official publication of the Federation of American Societies for Experimental Biology. 2008; 22(1):84–92. doi: 10.1096/fj.07-8130com PMID: 17846079.

7. Yan LJ, Christians ES, Liu L, Xiao X, Sohal RS, Benjamin IJ. Mouse heat shock transcription factor 1 deficiency alters cardiac redox homeostasis and increases mitochondrial oxidative damage. The EMBO journal. 2002; 21(19):5164–72. PMID: 12356732; PubMed Central PMCID: PMC129050.
8. Nakagawa M, Tsujimoto N, Nakagawa H, Iwaki T, Fukumaki Y, Iwaki A. Association of HSPB2, a member of the small heat shock protein family, with mitochondria. Experimental cell research. 2001; 271 (1):161–8. doi: 10.1006/excr.2001.5362 PMID: 11697892.
9. Ishiwata T, Orosz A, Wang X, Mustafi SB, Pratt GW, Christians ES, et al. HSPB2 is dispensable for the cardiac hypertrophic response but reduces mitochondrial energetics following pressure overload in mice. PloS one. 2012; 7(8):e42118. doi: 10.1371/journal.pone.0042118 PMID: 22870288; PubMed Central PMCID: PMC3411653.
10. Gulick J, Hewett TE, Klevitsky R, Buck SH, Moss RL, Robbins J. Transgenic remodeling of the regulatory myosin light chains in the mammalian heart. Circulation research. 1997; 80(5):655–64. PMID: 9130446.
11. Rual JF, Venkatesan K, Hao T, Hirozane-Kishikawa T, Dricot A, Li N, et al. Towards a proteome-scale map of the human protein-protein interaction network. Nature. 2005; 437(7062):1173–8. doi: 10.1038/nature04209 PMID: 16189514.
12. James P, Halladay J, Craig EA. Genomic libraries and a host strain designed for highly efficient two-hybrid selection in yeast. Genetics. 1996; 144(4):1425–36. PMID: 8978031; PubMed Central PMCID: PMC1207695.
13. Benjamin IJ, Guo Y, Srinivasan S, Boudina S, Taylor RP, Rajasekaran NS, et al. CRYAB and HSPB2 deficiency alters cardiac metabolism and paradoxically confers protection against myocardial ischemia in aging mice. American journal of physiology Heart and circulatory physiology. 2007; 293(5):H3201–9. doi: 10.1152/ajpheart.01363.2006 PMID: 17873008.
14. Zhang J, Li X, Mueller M, Wang Y, Zong C, Deng N, et al. Systematic characterization of the murine mitochondrial proteome using functionally validated cardiac mitochondria. Proteomics. 2008; 8 (8):1564–75. doi: 10.1002/pmic.200700851 PMID: 18348319; PubMed Central PMCID: PMC2799225.
15. Pound KM, Arteaga GM, Fasano M, Wilder T, Fischer SK, Warren CM, et al. Expression of slow skeletal TnI in adult mouse hearts confers metabolic protection to ischemia. Journal of molecular and cellular cardiology. 2011; 51(2):236–43. doi: 10.1016/j.yjmcc.2011.05.014 PMID: 21640727; PubMed Central PMCID: PMC3124599.
16. Griffin JL, White LT, Lewandowski ED. Substrate-dependent proton load and recovery of stunned hearts during pyruvate dehydrogenase stimulation. American journal of physiology Heart and circulatory physiology. 2000; 279(1):H361–7. PMID: 10899076.
17. Lewandowski ED, Johnston DL, Roberts R. Effects of inosine on glycolysis and contracture during myocardial ischemia. Circulation research. 1991; 68(2):578–87. PMID: 1991356.
18. Johnson M, Zaretskaya I, Raytselis Y, Merezhuk Y, McGinnis S, Madden TL. NCBI BLAST: a better web interface. Nucleic acids research. 2008; 36(Web Server issue):W5–9. doi: 10.1093/nar/gkn201 PMID: 18440982; PubMed Central PMCID: PMC2447716.
19. Kohl M, Wiese S, Warscheid B. Cytoscape: software for visualization and analysis of biological networks. Methods in molecular biology. 2011; 696:291–303. doi: 10.1007/978-1-60761-987-1_18 PMID: 21063955.
20. Bindea G, Mlecnik B, Hackl H, Charoentong P, Tosolini M, Kirilovsky A, et al. ClueGO: a Cytoscape plug-in to decipher functionally grouped gene ontology and pathway annotation networks. Bioinformatics. 2009; 25(8):1091–3. doi: 10.1093/bioinformatics/btp101 PMID: 19237447; PubMed Central PMCID: PMC2666812.
21. Prabhu S, Raman B, Ramakrishna T, Rao Ch M. HspB2/myotonic dystrophy protein kinase binding protein (MKBP) as a novel molecular chaperone: structural and functional aspects. PloS one. 2012; 7(1): e29810. doi: 10.1371/journal.pone.0029810 PMID: 22272249; PubMed Central PMCID: PMC3260166.
22. Girish V, Vijayalakshmi A. Affordable image analysis using NIH Image/ImageJ. Indian journal of cancer. 2004; 41(1):47. PMID: 15105580.
23. Muth JE. Basic Statistics and Pharmaceutical Statistical Applications: Boca Raton, FL: Chapman and Hall/CRC; 2006. 229–59 p.
24. Stark C, Breitkreutz BJ, Reguly T, Boucher L, Breitkreutz A, Tyers M. BioGRID: a general repository for interaction datasets. Nucleic acids research. 2006; 34(Database issue):D535–9. doi: 10.1093/nar/gkj109 PMID: 16381927; PubMed Central PMCID: PMC1347471.
25. den Engelsman J, Boros S, Dankers PY, Kamps B, Vree Egberts WT, Bode CS, et al. The small heat-shock proteins HSPB2 and HSPB3 form well-defined heterooligomers in a unique 3 to 1 subunit ratio. Journal of molecular biology. 2009; 393(5):1022–32. doi: 10.1016/j.jmb.2009.08.052 PMID: 19715703.

26. Sugiyama Y, Suzuki A, Kishikawa M, Akutsu R, Hirose T, Waye MM, et al. Muscle develops a specific form of small heat shock protein complex composed of MKBP/HSPB2 and HSPB3 during myogenic differentiation. The Journal of biological chemistry. 2000; 275(2):1095–104. PMID: 10625651.

27. Vos MJ, Kanon B, Kampinga HH. HSPB7 is a SC35 speckle resident small heat shock protein. Biochimica et biophysica acta. 2009; 1793(8):1343–53. doi: 10.1016/j.bbamcr.2009.05.005 PMID: 19464326.

28. Sun X, Fontaine JM, Rest JS, Shelden EA, Welsh MJ, Benndorf R. Interaction of human HSP22 (HSPB8) with other small heat shock proteins. The Journal of biological chemistry. 2004; 279(4):2394–402. doi: 10.1074/jbc.M311324200 PMID: 14594798.

29. Morrison LE, Whittaker RJ, Klepper RE, Wawrousek EF, Glembotski CC. Roles for alphaB-crystallin and HSPB2 in protecting the myocardium from ischemia-reperfusion-induced damage in a KO mouse model. American journal of physiology Heart and circulatory physiology. 2004; 286(3):H847–55. doi: 10.1152/ajpheart.00715.2003 PMID: 14592939.

30. Younger JF, Plein S, Barth J, Ridgway JP, Ball SG, Greenwood JP. Troponin-I concentration 72 h after myocardial infarction correlates with infarct size and presence of microvascular obstruction. Heart. 2007; 93(12):1547–51. doi: 10.1136/hrt.2006.109249 PMID: 17540686; PubMed Central PMCID: PMC2095742.

31. Kadono T, Zhang XQ, Srinivasan S, Ishida H, Barry WH, Benjamin IJ. CRYAB and HSPB2 deficiency increases myocyte mitochondrial permeability transition and mitochondrial calcium uptake. J Mol Cell Cardiol. 2006; 40(6):783–9. PMID: 16678848.

32. Toda T, Kadono T, Hoshiai M, Eguchi Y, Nakazawa S, Nakazawa H, et al. Na+/H+ exchanger inhibitor cariporide attenuates the mitochondrial Ca2+ overload and PTP opening. American journal of physiology Heart and circulatory physiology. 2007; 293(6):H3517–23. doi: 10.1152/ajpheart.00483.2006 PMID: 17906113.

33. Fields S, Song O. A novel genetic system to detect protein-protein interactions. Nature. 1989; 340 (6230):245–6. doi: 10.1038/340245a0 PMID: 2547163.

34. Luban J, Goff SP. The yeast two-hybrid system for studying protein-protein interactions. Current opinion in biotechnology. 1995; 6(1):59–64. PMID: 7894083.

35. Katsogiannou M, Andrieu C, Baylot V, Baudot A, Dusetti NJ, Gayet O, et al. The functional landscape of Hsp27 reveals new cellular processes such as DNA repair and alternative splicing and proposes novel anticancer targets. Molecular & cellular proteomics: MCP. 2014; 13(12):3585–601. doi: 10.1074/mcp.M114.041228 PMID: 25277244; PubMed Central PMCID: PMC4256507.

36. Yoshida K, Aki T, Harada K, Shama KM, Kamoda Y, Suzuki A, et al. Translocation of HSP27 and MKBP in ischemic heart. Cell structure and function. 1999; 24(4):181–5. PMID: 10532352.

37. Golenhofen N, Redel A, Wawrousek EF, Drenckhahn D. Ischemia-induced increase of stiffness of alphaB-crystallin/HSPB2-deficient myocardium. Pflugers Archiv: European journal of physiology. 2006; 451(4):518–25. doi: 10.1007/s00424-005-1488-1 PMID: 16217658.

38. Pohjoismaki JL, Kruger M, Al-Furoukh N, Lagerstedt A, Karhunen PJ, Braun T. Postnatal cardiomyocyte growth and mitochondrial reorganization cause multiple changes in the proteome of human cardiomyocytes. Molecular bioSystems. 2013; 9(6):1210–9. doi: 10.1039/c3mb25556e PMID: 23459711.

39. Cravatt BF, Simon GM, Yates JR, 3rd. The biological impact of mass-spectrometry-based proteomics. Nature. 2007; 450(7172):991–1000. doi: 10.1038/nature06525 PMID: 18075578.

40. Gavin AC, Maeda K, Kuhner S. Recent advances in charting protein-protein interaction: mass spectrometry-based approaches. Current opinion in biotechnology. 2011; 22(1):42–9. doi: 10.1016/j.copbio.2010.09.007 PMID: 20934865.

41. Rajagopala SV, Sikorski P, Caufield JH, Tovchigrechko A, Uetz P. Studying protein complexes by the yeast two-hybrid system. Methods. 2012; 58(4):392–9. doi: 10.1016/j.ymeth.2012.07.015 PMID: 22841565; PubMed Central PMCID: PMC3517932.

42. Praneenararat T, Takagi T, Iwasaki W. Integration of interactive, multi-scale network navigation approach with Cytoscape for functional genomics in the big data era. BMC genomics. 2012; 13 Suppl 7:S24. doi: 10.1186/1471-2164-13-S7-S24 PMID: 23281970; PubMed Central PMCID: PMC3521214.

43. Ralser M, Wamelink MM, Kowald A, Gerisch B, Heeren G, Struys EA, et al. Dynamic rerouting of the carbohydrate flux is key to counteracting oxidative stress. Journal of biology. 2007; 6(4):10. doi: 10.1186/jbiol61 PMID: 18154684; PubMed Central PMCID: PMC2373902.

44. Cerella C, Dicato M, Diederich M. Modulatory roles of glycolytic enzymes in cell death. Biochemical pharmacology. 2014. doi: 10.1016/j.bcp.2014.07.005 PMID: 25034412.

45. Tristan C, Shahani N, Sedlak TW, Sawa A. The diverse functions of GAPDH: views from different subcellular compartments. Cellular signalling. 2011; 23(2):317–23. doi: 10.1016/j.cellsig.2010.08.003 PMID: 20727968; PubMed Central PMCID: PMC3084531.

46. Nicholls C, Li H, Liu JP. GAPDH: a common enzyme with uncommon functions. Clinical and experimental pharmacology & physiology. 2012; 39(8):674–9. doi: 10.1111/j.1440-1681.2011.05599.x PMID: 21895736.

47. Guo C, Liu S, Sun MZ. Novel insight into the role of GAPDH playing in tumor. Clinical & translational oncology: official publication of the Federation of Spanish Oncology Societies and of the National Cancer Institute of Mexico. 2013; 15(3):167–72. doi: 10.1007/s12094-012-0924-x PMID: 22911551.

48. Guo X, Disatnik MH, Monbureau M, Shamloo M, Mochly-Rosen D, Qi X. Inhibition of mitochondrial fragmentation diminishes Huntington's disease-associated neurodegeneration. The Journal of clinical investigation. 2013; 123(12):5371–88. doi: 10.1172/JCI70911 PMID: 24231356; PubMed Central PMCID: PMC3859413.

49. Ramzan R, Weber P, Linne U, Vogt S. GAPDH: the missing link between glycolysis and mitochondrial oxidative phosphorylation? Biochemical Society transactions. 2013; 41(5):1294–7. doi: 10.1042/BST20130067 PMID: 24059522.

50. Yao LL, Wang YG, Liu XJ, Zhou Y, Li N, Liu J, et al. Phenylephrine protects cardiomyocytes from starvation-induced apoptosis by increasing glyceraldehyde-3-phosphate dehydrogenase (GAPDH) activity. Journal of cellular physiology. 2012; 227(10):3518–27. doi: 10.1002/jcp.24053 PMID: 22252379.

51. Liang S, Figtree G, Aiqun M, Ping Z. GAPDH-knockdown reduce rotenone-induced H9C2 cells death via autophagy and anti-oxidative stress pathway. Toxicology letters. 2015; 234(3):162–71. doi: 10.1016/j.toxlet.2015.02.017 PMID: 25725130.

52. Colell A, Ricci JE, Tait S, Milasta S, Maurer U, Bouchier-Hayes L, et al. GAPDH and autophagy preserve survival after apoptotic cytochrome c release in the absence of caspase activation. Cell. 2007; 129(5):983–97. doi: 10.1016/j.cell.2007.03.045 PMID: 17540177.

53. Colell A, Green DR, Ricci JE. Novel roles for GAPDH in cell death and carcinogenesis. Cell death and differentiation. 2009; 16(12):1573–81. doi: 10.1038/cdd.2009.137 PMID: 19779498.

54. Tarze A, Deniaud A, Le Bras M, Maillier E, Molle D, Larochette N, et al. GAPDH, a novel regulator of the pro-apoptotic mitochondrial membrane permeabilization. Oncogene. 2007; 26(18):2606–20. doi: 10.1038/sj.onc.1210074 PMID: 17072346.

55. Jang M, Kang HJ, Lee SY, Chung SJ, Kang S, Chi SW, et al. Glyceraldehyde-3-phosphate, a glycolytic intermediate, plays a key role in controlling cell fate via inhibition of caspase activity. Molecules and cells. 2009; 28(6):559–63. doi: 10.1007/s10059-009-0151-7 PMID: 19937139.

56. Lazarev VF, Sverchinskyi DV, Ippolitova MV, Stepanova AV, Guzhova IV, Margulis BA. Factors Affecting Aggregate Formation in Cell Models of Huntington's Disease and Amyotrophic Lateral Sclerosis. Acta naturae. 2013; 5(2):81–9. PMID: 23819039; PubMed Central PMCID: PMC3695356.

57. Bertram L, McQueen MB, Mullin K, Blacker D, Tanzi RE. Systematic meta-analyses of Alzheimer disease genetic association studies: the AlzGene database. Nature genetics. 2007; 39(1):17–23. doi: 10.1038/ng1934 PMID: 17192785.

58. Butterfield DA, Hardas SS, Lange ML. Oxidatively modified glyceraldehyde-3-phosphate dehydrogenase (GAPDH) and Alzheimer's disease: many pathways to neurodegeneration. Journal of Alzheimer's disease: JAD. 2010; 20(2):369–93. doi: 10.3233/JAD-2010-1375 PMID: 20164570; PubMed Central PMCID: PMC2922983.

59. Sunaga K, Takahashi H, Chuang DM, Ishitani R. Glyceraldehyde-3-phosphate dehydrogenase is overexpressed during apoptotic death of neuronal cultures and is recognized by a monoclonal antibody against amyloid plaques from Alzheimer's brain. Neuroscience letters. 1995; 200(2):133–6. PMID: 8614562.

60. Garrido C, Paul C, Seigneuric R, Kampinga HH. The small heat shock proteins family: the long forgotten chaperones. Int J Biochem Cell Biol. 2012; 44(10):1588–92. doi: 10.1016/j.biocel.2012.02.022 PMID: 22449631.

61. Vidal M, Cusick ME, Barabasi AL. Interactome networks and human disease. Cell. 2011; 144(6):986–98. doi: 10.1016/j.cell.2011.02.016 PMID: 21414488; PubMed Central PMCID: PMC3102045.

62. Wolfe K. Robustness—it's not where you think it is. Nature genetics. 2000; 25(1):3–4. doi: 10.1038/75560 PMID: 10802639.

63. Franck E, Madsen O, van Rheede T, Ricard G, Huynen MA, de Jong WW. Evolutionary diversity of vertebrate small heat shock proteins. Journal of molecular evolution. 2004; 59(6):792–805. doi: 10.1007/s00239-004-0013-z PMID: 15599511.

64. Liu S, Yan B, Lai W, Chen L, Xiao D, Xi S, et al. As a novel p53 direct target, bidirectional gene HspB2/alphaB-crystallin regulates the ROS level and Warburg effect. Biochimica et biophysica acta. 2014; 1839(7):592–603. doi: 10.1016/j.bbagrm.2014.05.017 PMID: 24859470.

65. Ganong WF. Review of medical physiology. 13th ed. Norwalk, Conn.: Appleton & Lange; 1987. 665 p. p.

66. Ojha J, Karmegam RV, Masilamoni JG, Terry AV, Cashikar AG. Behavioral defects in chaperone-deficient Alzheimer's disease model mice. PloS one. 2011; 6(2):e16550. doi: 10.1371/journal.pone.0016550 PMID: 21379584; PubMed Central PMCID: PMC3040748.

67. Wilhelmus MM, Otte-Holler I, Wesseling P, de Waal RM, Boelens WC, Verbeek MM. Specific association of small heat shock proteins with the pathological hallmarks of Alzheimer's disease brains. Neuropathology and applied neurobiology. 2006; 32(2):119–30. doi: 10.1111/j.1365-2990.2006.00689.x PMID: 16599941.

68. Willis MS, Patterson C. Proteotoxicity and cardiac dysfunction—Alzheimer's disease of the heart? The New England journal of medicine. 2013; 368(5):455–64. doi: 10.1056/NEJMra1106180 PMID: 23363499.

69. Hroudova J, Singh N, Fisar Z. Mitochondrial dysfunctions in neurodegenerative diseases: relevance to Alzheimer's disease. BioMed research international. 2014; 2014:175062. doi: 10.1155/2014/175062 PMID: 24900954; PubMed Central PMCID: PMC4036420.

70. Tan W, Pasinelli P, Trotti D. Role of mitochondria in mutant SOD1 linked amyotrophic lateral sclerosis. Biochimica et biophysica acta. 2014; 1842(8):1295–301. doi: 10.1016/j.bbadis.2014.02.009 PMID: 24568860; PubMed Central PMCID: PMC4074562.

71. Bobba A, Amadoro G, Valenti D, Corsetti V, Lassandro R, Atlante A. Mitochondrial respiratory chain Complexes I and IV are impaired by beta-amyloid via direct interaction and through Complex I-dependent ROS production, respectively. Mitochondrion. 2013; 13(4):298–311. doi: 10.1016/j.mito.2013.03.008 PMID: 23562762.

72. Jiao Y, Zhang Y, Wei Y, Liu Z, An W, Guo M. Direct observation of internalization and ROS generation of amyloid beta-peptide in neuronal cells at subcellular resolution. Chembiochem: a European journal of chemical biology. 2012; 13(16):2335–8. doi: 10.1002/cbic.201200465 PMID: 23060092.

73. Stelzer G, Dalah I, Stein TI, Satanower Y, Rosen N, Nativ N, et al. In-silico human genomics with GeneCards. Hum Genomics. 2011; 5(6):709–17. PMID: 22155609; PubMed Central PMCID: PMC3525253.

74. Magrane M, Consortium U. UniProt Knowledgebase: a hub of integrated protein data. Database: the journal of biological databases and curation. 2011; 2011:bar009. doi: 10.1093/database/bar009 PMID: 21447597; PubMed Central PMCID: PMC3070428.

75. Ashburner M, Ball CA, Blake JA, Botstein D, Butler H, Cherry JM, et al. Gene ontology: tool for the unification of biology. The Gene Ontology Consortium. Nature genetics. 2000; 25(1):25–9. doi: 10.1038/75556 PMID: 10802651; PubMed Central PMCID: PMC3037419.

76. Prasad TS, Kandasamy K, Pandey A. Human Protein Reference Database and Human Proteinpedia as discovery tools for systems biology. Methods in molecular biology. 2009; 577:67–79. doi: 10.1007/978-1-60761-232-2_6 PMID: 19718509.